SIMULATION NOTES EUROPE
SNE

SNE Special Issue
EUROSIM Congress 2019

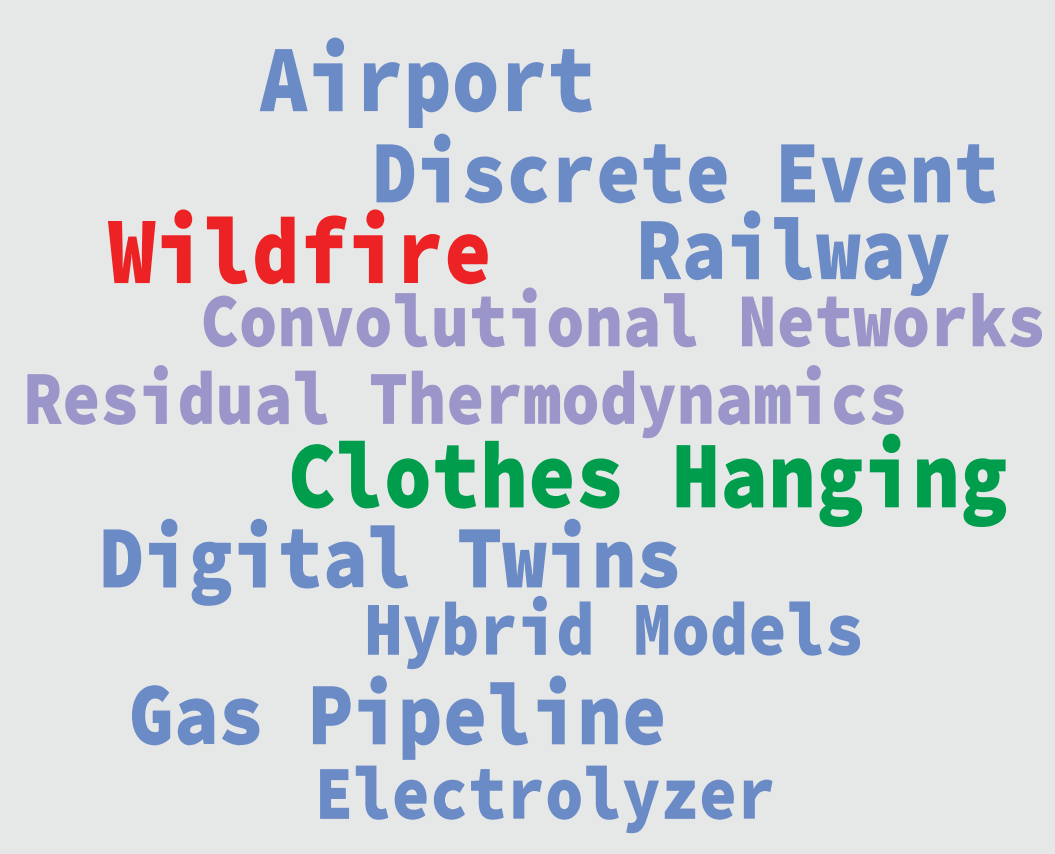

Journal on Developments and Trends in Modelling and Simulation

EUROSIM Scientific Membership Journal

Vol. 31 No.3, Sept. 2021
ISSN Online 2306-0271
ISSN Print 2305-9974
DOI 10.11128/sne.31.3.1057
ISBN Print 978-3-903311-17-6

TU Verlag an der Technischen Universität Wien
ARGESIM

SNE - Aims and Scope

Simulation Notes Europe (SNE) provides an international, high-quality forum for presentation of new ideas and approaches in simulation - from modelling to experiment analysis, from implementation to verification, from validation to identification, from numerics to visualisation - in context of the simulation process.

SNE seeks to serve scientists, researchers, developers and users of the simulation process across a variety of theoretical and applied fields in pursuit of novel ideas in simulation and to enable the exchange of experience and knowledge through descriptions of specific applications. **SNE** follows the recent developments and trends of modelling and simulation in new and/or joining application areas, as complex systems and big data. **SNE** puts special emphasis on the overall view in simulation, and on comparative investigations, as benchmarks and comparisons in methodology and application. For this purpose, **SNE** documents the **ARGESIM Benchmarks** on *Modelling Approaches and Simulation Implementations* with publication of definitions, solutions and discussions. SNE welcomes also contributions in education in/for/with simulation.

A *News Section* in **SNE** provides information for **EUROSIM** Simulation Societies and Simulation Groups.

SNE, primarily an electronic journal, follows an open access strategy, with free download in basic layout. **SNE** is the official membership journal of **EUROSIM**, the *Federation of European Simulation Societies and Simulation Groups* – www.eurosim.info. Members of **EUROSIM** societies are entitled to download **SNE** in an elaborate and extended layout, and to access additional sources of benchmark publications, model sources, etc. **Print SNE** is available for specific groups of **EUROSIM** societies, and starting with Volume 27 (2017) as print-on-demand from TU Verlag, TU Wien. **SNE** is DOI indexed by CrossRef, identified by DOI prefix 10.11128, assigned to the **SNE** publisher **ARGESIM** (*www.argesim.org*).

Author's Info. Individual submissions of scientific papers are welcome, as well as post-conference publications of contributions from conferences of **EUROSIM** societies. **SNE** welcomes special issues, either dedicated to special areas and/or new developments, or on occasion of events as conferences and workshops with special emphasis.

Authors are invited to submit contributions which have not been published and have not being considered for publication elsewhere to the **SNE** Editorial Office.

SNE distinguishes different types of contributions (*Notes*), i.e.

- **TN** Technical Note, 6–10 p.
- **SN** Short Note, max. 5 p.
- **SW** Software Note , 4–6 p.
- **BN** Benchmark Note, 2–10 p.
- **ON** Overview Note – only upon invitation, up to 14 p.
- **EN** Education Note, 6–8 p.
- **PN** Project Note 6–8 p.
- **STN** Student Note, 4-6 p., on supervisor's recommendation
- **EBN** Educational Benchmark Note, 4–10 p.

Further info and templates (doc, tex) at **SNE**'s website.

www.sne-journal.org

SNE Editorial Board

SNE - Simulation Notes Europe is advised and supervised by an international scientific editorial board. This (increasing) board is taking care on peer reviewing of submission to SNE:

Editorial

***Dear Readers**, This SNE Special Issue 'EUROSIM Congress 2019' publishes selected contributions presented at the EUROSIM Congress, July 2019, Logrono, Spain. The EUROSIM Congress is the tri-annual family meeting of the European simulation societies, the next congress to be held in summer 2023 in Amsterdam, the Netherlands. The Special Issue Editorial Board suggested contributions from EUROSIM 2019 with mainly simulation-oriented topics, and with a variety in theory and application. We were surprised by the very positive reactions of many authors, who planned to submit their publication for SNE, and some authors have already sent their contribution – as result this SNE Special Issue with eight contributions, and some more contributions in queue for the next SNE issues. We were also surprised about the really broad area of modelling and simulation, reflecting also the scope of the EUROSIM congresses – and so we have chosen a word cloud for the title page, with subjects from the contributions of this issue: Discrete-event, Digital Twins, Railway, Electrolyzer, Residual Thermodynamics, Gas Pipeline, Wildfire, Clothes Hanging, Convolutional Networks, Hybrid Models – really significant for very broad simulation area.*
We thank the special issue editors for their excellent editorial work (for details, see the special issue editorial). I would like to thank all authors for their contributions to SNE 31(3) showing the broad variety of simulation – and the success of the EUROSIM Congresses. And last but not least thanks to the SNE Editorial Office for layout, typesetting, preparations for printing, electronic publishing, and much more.

Felix Breitenecker, SNE Editor-in-Chief, eic@sne-journal.org; felix.breitenecker@tuwien.ac.at

Contents SNE 31(3)
Special Issue *EUROSIM Congress 2019*

Online SNE 31(3), DOI 10.11128/sne.31.3.1057
ARGESIM Publisher, Vienna, www.argesim.org
Print SNE 31(3) 978-3-903311-17-6
TU Verlag Vienna, Print-on-Demand, www.tuverlag.at

SNE Contact & Info

SNE Online ISSN 2306-0271, SNE Print ISSN 2305-9974

→ ***www.sne-journal.org***

office@sne-journal.org, eic@sne-journal.org

SNE Editorial Office
Johannes Tanzler (Layout, Organisation),
Irmgard Husinsky (Web, Electronic Publishing),
Felix Breitenecker (Organisation, Author Mentoring)
ARGESIM/Math. Modelling & Simulation Group,
Inst. of Analysis and Scientific Computing, TU Wien
Wiedner Hauptstrasse 8-10, 1040 Vienna, Austria

SNE SIMULATION NOTES EUROPE

WEB: → *www.sne-journal.org*, DOI prefix 10.11128/sne

Scope: Developments and trends in modelling and simulation in various areas and in application and theory; comparative studies and benchmarks (documentation of ARGESIM Benchmarks on modelling approaches and simulation implementations); modelling and simulation in and for education, simulation-based e-learning; society information and membership information for EUROSIM members (Federation of European Simulation Societies and Groups).

Editor-in-Chief: Felix Breitenecker, TU Wien, Math. Modelling Group
Felix.Breitenecker@tuwien.ac.at, *eic@sne-journal.org*

Print SNE and Print-on-Demand: TU-Verlag, Wiedner Hauptstrasse 8-10, 1040, Vienna, Austria – *www.tuverlag.at*

Publisher: ARGESIM ARBEITSGEMEINSCHAFT SIMULATION NEWS
c/o Math. Modelling and Simulation Group, TU Wien / 101,
Wiedner Hauptstrasse 8-10, 1040 Vienna, Austria;
www.argesim.org, *info@argesim.org*
on behalf of ASIM *www.asim-gi.org* and
EUROSIM → *www.eurosim.info*

Editorial SNE 31(3) – Special Issue *EUROSIM Congress 2019*

SNE 31(3), the **SNE Special Issue** *EUROSIM Congress 2019,* comprises a selection of outstanding contributions of the **EUROSIM Congress 2019** which took place in July 2019 University of Logrono, La Rioja, Spain. The **EUROSIM Congress** is the tri-annual family meeting of the European simulation societies, among them **CEA-SMSG**, the Spanish, **ASIM** – the German, **DBSS** – The Dutch-Benelux, **SLOSIM** – the Slovenian, and **SIMS** – the Scandinavian simulation society.

For us, the members of the Special Issue Editorial Board, it was not an easy task to select contributions and suggest for post-conference publication in **SNE**: the area of modelling and simulation has become very broad, and so we decided for outstanding publications, which represent very different areas of modelling and simulation. After invitation for postconference publication in **SNE**, many authors have expressed their interest, and some have already sent in their contribution. For this **SNE Special Issue** *EUROSIM Congress 2019* we had to decide for eight contributions, because of space, and we used for the article sequence the red line of application.

This issue stars with aircraft. The contribution *Modelling Landside Logistic Operations of a Mega-hub Airport with Discrete-event Simulation* by R. Romero-Silva, M. Mujica Mota – a plenary talk at the congress. The authors report on a discrete-event model to manage the real logistics operations in Schiphol Airport. To provide practitioners with applicable consolidation and truck-dispatching policies, the contribution proposes some easy-to-implement rules. The authors manage the problem of a consistent event/process description with bravura: a very good readable pseudo-code makes the model function and model complexity clear.

From aircraft to railway: the second and the third contribution deal with simulation of dynamics in railway systems – at very different levels and applications. A. Gálvez and co-authors investigate in the contribution *Hybrid Models and Digital Twins for Condition Monitoring: HVAC System for Railway* the role auf digital twins in monitoring the condition of the HVAC system (Heating, Ventilation and Air Conditioning) where it matters to the comfort and safety of the passengers in the trains. The level 3.0 of digital twin is developed for the diagnosis and prognosis of HVAC by using hybrid modeling. On the other side, J. Malaka examines in his contribution *Application of CAE to Model and Simulate Wheel Ground Contact in Railway Vehicle* the motion-describing equations and the method of solving them in CAE systems on basis of a classical rail vehicle drive system, especially observing the contact of the rail.

From railway to electrolysis – electricity and chemistry. J. J. Caparrós et al. report in their contribution *Optimized Balance of Plant for a Medium-size PEM Electrolyzer. Design, Modelling and Control* on control for safe electrolysis. The authors develop an exhaustive control system to test the working conditions that will allow a PEM (Proton Exchange Membrane) electrolyzer to generate hydrogen in a safe and efficient way.

The aim of this study is to find an equilibrated solution between minimal BoP (Balance of Plant) and a correct performance, always into safety conditions of hydrogen generation.

Now to chemistry and thermodynamics. S. A. Aromada and B. Kvamme present in their first contribution *Modelling of Methane Hydrate Formation and Dissociation using Residual Thermodynamics*. The authors suggest to replace the oversimplifications using the Clausius-Clapeyron by a thermodynamic scheme (residual thermodynamics approach). This thermodynamic scheme is based on residual thermodynamics for all properties like equilibrium (pressure-temperature) curves, free energy change as thermodynamic driving force in kinetic theories and enthalpies of hydrate formation and dissociation.

The authors' second paper *Simulation of Hydrate Plug Prevention in Natural Gas Pipeline from Bohai Bay to Onshore Facilities in China* proposes that the best way to prevent the occasional plugging of the pipeline is to rightly evaluate the upper limit of water that can be permitted in the bulk gas and dehydrate the gas accordingly before transport – based on molecular dynamics simulation and sensitivity analysis.

From 'chemical' thermodynamics to real thermodynamics. J. Carballeira et al. present in their contribution *Wildfire Spreading Simulator using Fast Marching Algorithm present* a prototype wildfire simulation app that uses Fast Marching as its core algorithm. Although a prototype, the developed wildfire basic app is superior to some state-of-the-art simulators regarding certain important features.

And now something completely different: towards cloth hanging. The contribution *Towards Clothes Hanging via Cloth Simulation and Deep Convolutional Networks* by D. Estevez et al. really deals with cloth hanging: cloth hanging by robots with intelligent behaviour. The work presents a step towards automated robot clothes hanging by modeling the dynamics of the hanging task via deep convolutional models. Two models are developed to address two different problems: determining if the garment will hang or not (classification), and estimation of the future garment location in space.

As mentioned, we had to restrict on eight papers in this special issue. Further already submitted contributions – dealing with randomness, neuromorphe information, nutrition and other exciting application – will be published in following **SNE** issues. The editors express their gratitude to all authors for their great effort and cooperation. Last but not least the editors thank the SNE Editorial Office for the support in compiling this special issue.

The editors hope that you will enjoy this **SNE Special Issue**, and that it will encourage you to participate actively in the next congress, which will take place in Amsterdam in summer 2023 – info see www.eurosim2022.eu/

Sincerely, the **SNE 31(3)** Special Issue Editors

Emilio Jiménez, Juan-Ignacio Latorre Biel (**CEA-SMSG**
Miguel Mujica-Mota (**DBSS**), *Borut Zupancic* (**SLOSIM**)
Esko Juuso (**SIMS**)
N. Popper, A. Körner, F. Breitenecker (**ASIM**)

Modelling Landside Logistic Operations of a Mega-hub Airport with Discrete-event Simulation

Rodrigo Romero-Silva[1*], Miguel Mujica Mota[2]

[1]Deapartment of Operations Analytics, Vrije Universiteit Amsterdam, De Boelelaan 1105, 1081 HV, Amsterdam, The Netherlands; *r.romerosilva@vu.nl*

[2]Aviation Academy, Amsterdam University of Applied Sciences, Weesperzijde 190, 1097 DZ Amsterdam, The Netherlands

SNE 31(3), 2021, 111-120, DOI: 10.11128/sne.31.tn.10571
Received: March 10, 2021 (Selected EUROSIM 2019 Postconf. Publ.), Revised: August 31, 2021; Accepted: September 3, 2021
SNE - Simulation Notes Europe, ARGESIM Publisher Vienna, ISSN Print 2305-9974, Online 2306-0271, www.sne-journal.org

Abstract. The need to better understand how to manage the real logistics operations in Schiphol Airport, a strategic hub for the economic development of the Netherlands, created the conditions to develop a project where academia and industry partnered to build a simulation model of the Schiphol Airport Landside operations. This paper presents such a model using discrete-event simulation. A realistic representation of the open road network of the airport as well as the (un)loading dock capacities and locations of the five ground handlers of Schiphol Airport was developed. Furthermore, to provide practitioners with applicable consolidation and truck-dispatching policies, some easy-to-implement rules are proposed and implemented in the model. Preliminary results from this model show that truck-dispatching policies have a higher impact than consolidation policies in terms of both distances travelled by cooperative logistic operators working within the airport and shipments' average flow time. Furthermore, the approach presented in this study can be used for studying similar mega-hubs.

Introduction

Airports are one of the most critical nodes in international trade networks as well as critical hubs for the economic development of a country. Since international airports concentrate a great proportion of cargo value flow into and out of a country (35% of global cargo flows based on value – [1]), the operational performance of an airport is a key factor in the logistic capabilities of a nation and, consequently, in the competitive advantage of a country with respect to other nations [2].

In Europe, the proportion of weight moved by air is 0.8% compared with the 26.7% value of goods of all transport modes [3]; for this reason, airports attain added value with logistics operators with a better flow of goods, i.e. shorter throughput times, instead of exclusively through price competition. Thus, it is increasingly important for international cargo airports to improve their performance in terms of throughput times without a high impact on the costs of moving cargo through their facilities.

Air cargo hub operations (air cargo terminal operations – [4]) can be divided into two main systems: the landside and the airside. Landside operations deal with the interchange of cargo between logistics operators and the airport's ground handlers (GH), which receive cargo from the landside, sort the cargo and then deliver it to the corresponding aircraft (the airside). Landside operations are notoriously difficult to manage as they are comprised of various interconnected and interdependent processes and many agents with possible conflicting goals, as will be explained in the next section. Because of this, many studies have investigated some parts of the problem in a separate manner, e.g., logistics provider freight consolidation [5] or truck scheduling at ground handler terminals [6]; however, to the best of our knowledge, a systems-wide investigation of the landside air cargo terminal operations has not been developed.

This study is concerned with investigating how the Schiphol Airport landside operations (SALO) can be improved with a decision support system that uses a more realistic representation of the system, in contrast with more idealistic models. Owing to the complexities and characteristics of the problem, this system was modelled using discrete-event simulation (DES), as previous studies on complex systems have previously done [7,8].

Furthermore, dynamic policies of shipment consolidation and resource sharing were considered to improve the performance of the system since a static-deterministic

optimization approach was deemed inapplicable to solve such a dynamic and stochastic environment.

The remainder of the paper is organized as follows. In Section 1 a description of the problem at hand is developed. Section 2 presents a short review of the literature related to this study. The methodological approach of the study is explained in Section 3. Section 4 shows the results of the simulation study, while Section 6 presents the discussion and conclusions of the paper.

1 Problem Description

To illustrate the problem at hand, first, we explain the process of an outbound shipment. An outbound shipment could arrive at the air cargo terminal through two main channels. The first one is via a logistics operator with no physical presence within the airport – external logistics operator (ELO). These shipments arrive in a truck directly to the ground handlers' locations where a dock is assigned to the truck and the truck is parked in the dock. Then, the shipment is unloaded and stored in the GH's warehouse until the sorting of shipments for the airside takes place.

The second channel is via a logistics operator with warehousing facilities inside the airport – internal logistics operator (ILO). When a shipment comes through an ILO, it first arrives at the warehouse of the ILO for further consolidation. ILOs need this final step of consolidation because they deliver shipments to different locations (depending on the number of GH) in some airports and, thus, the final route for different shipments can vary, depending on the needed time of delivery (related to flight departure time) and the final delivery point. Therefore, whenever the shipment is ready for delivery, an ILO-managed truck is dispatched to the corresponding GH for delivery, where it must pass the same process as ELO-managed trucks.

In the case of inbound shipments using an ILO, the inverse trip occurs: after the shipment is ready to be picked up from the GH warehouse, it waits for an ILO truck to be picked up. An ILO truck will be dispatched to pick up a shipment, depending on the urgency of the shipment or on an already programmed visit to that specific GH location. Then, the ILO truck will wait to be assigned a loading dock, park in the dock, and load the shipment, after which the shipment will travel to the ILO warehouse to be stored, sorted, and further consolidated for its next destination outside the airport. In the case of an ELO shipment, it will only be picked up by a truck and then leave the airport for a long-haul trip, with the corresponding visit (and possible waiting) to the GH's loading docks.

Following this description, the problem of the landside operations of an air cargo terminal can be described by the dual problem of the planning of the ILO routes for picking-up and delivering shipments while also managing the workload in the GH's docks since very frequent routes between ILO and GH warehouses, i.e. minimal consolidation, could result in a higher workload for the docks and more travelling costs due to repeated, multiple visits; whereas a reduced dock workload and transportation costs could result from more infrequent routes, i.e. more consolidation, but with the trade-off of higher throughput times and possible late deliveries. In addition, an inefficient consolidation would cause an increase in greenhouse emissions which have gained a more important role everywhere as a decision variable to consider when managing transport systems.

To make the previous problem more complex, inbound and outbound arrivals both from ELO and ILO shipments arrive at the system in a dynamic and stochastic manner as some of the shipments arrive unannounced and some others, despite a previous announcement from the logistic operators, arrive at different times and weights than previously announced. Thus, the management of the landside operations of an air cargo terminal is comprised of three interconnected decisions: (i) how shipments are consolidated, (ii) how often consolidated shipments are dispatched, and (iii) which routes should be used to pick up and deliver the cargo.

2 Related Literature

As previously mentioned, landside air cargo terminal operations are a set of interconnected, separate problems. However, since no study has considered these problems jointly, this section will review some of the papers that have tackled each one of the pertaining problems individually in order to better understand the nature and complexity of the problem and summarize previous findings.

The most traditional approach for addressing decisions (i) and (ii) (see section 1) has been to use a decision policy for a non-capacitated vehicle dispatching based on three shipment-consolidation policies: quantity, time, and time-quantity [9]. In a quantity-based shipment consolidation policy, the decision of whether to dispatch a vehicle is taken based on the amount of weight or units, e.g., boxes, that have been accumulated to be transported up until the decision point.

It is highly related to the economic order quantity [10]. On the contrary, a time-based policy depends on the time that has passed since the decision period began, e.g., since the beginning of the day or since the last vehicle dispatch; therefore, a vehicle is only dispatched when a specific period has been reached. Vehicles are dispatched with the available consolidated shipments depending on which of the two thresholds, i.e. quantity or time, is reached first.

Most of the literature that has studied these shipment-consolidation policies [9,11–14] agree that the quantity-based policy is superior in terms of cost minimization to the time-based policy in most instances (even when considering two classes of customers with different priorities – [15]) as this policy finds a good trade-off between inventory holding costs and transportation costs (caused by the number of dispatches). However, some studies have suggested that a time-quantity combined policy could have a better performance in terms of maximum waiting times and average order delay than the quantity-based policy [16], as it has been found to have a subpar performance in terms of customer satisfaction due to late and long delivery times.

Using Battarra et al.'s classification [17], most of the studies concerned with these issues have focused on 1-1 problems, where only one product and commodity needs to be transported from one origin to one destination, although, in general, the actual trip to the destination is not modelled and only the decision in the origin point is taken into account. A notable extension to this simple problem can be found in [18], where they suggest some simple rules-of-thumb for a 1-1 shipment consolidation problem with a capacitated vehicle.

Decision (iii) (see section 1), i.e. which routes to use, on the other hand, has been generally studied with an optimization approach by building routes for delivering and picking up products in a set of nodes using one or many vehicles in order to optimize an objective function, commonly associated with minimizing transportation costs, i.e. distance travelled. While most of the research has focused on a deterministic and static problem [19], stochastic and dynamic VRP are more relevant for the current practice and for this current study as transport requests arrive dynamically to a variety of logistic systems and the actual demand to be transported from point to point and the nodes to be served are random variables.

According to Pillac et al. [20], dynamic problems have been solved with different solution approaches.

Considering a dynamic but deterministic scenario, previous work has used both periodic and continuous re-optimization strategies to cope with the dynamism of the problem. While periodic re-optimization uses a static approach to generate routes at decision intervals, continuous re-optimization generates routes every time the state of the system changes, e.g., a new order arrives. Thus, as continuous re-optimization constantly updates the routes of each vehicle with the latest information, this approach could be difficult to implement in some environments, as the vehicle only knows the next route whenever they have finished their current request.

Overall, it can be concluded that the problem at hand, i.e. the landside operations in an air cargo terminal, has not been studied considering all the interconnected and interdependent processes relevant for a good performance of the cargo terminal. Therefore, in this work, we present a modelling framework that distinguishes from previous research by presenting a holistic approach in which the three main decision problems can be studied together, including all the main elements of the described system. Furthermore, it provides a unique and innovative testbed for investigating the relevance of different operational policies to increase the competitive advantage of air cargo terminals.

3 Conceptual Design for the Implementation of a Discrete-event Simulation Model

A DES simulation model was built by coupling two layers, a GIS layer and, on top of the first layer, the model of Schiphol Airport considering the physical layout of the system, i.e. the roads and warehouse locations. The simulation model was built with Simio software [21] version 10.181 of 64 bits. Thus, a network composed of nodes and edges with functionalities that represented roads was built over the actual roads represented on the GIS map connecting all the relevant logistic points of SALO.

The landside of the cargo terminal of Schiphol Airport has five different ground handlers operating in the facilities of the airport [22]. Table 1 shows the proportional flow that each GH receives both for inbounds (I-GH) and outbounds (O-GH) (based on real Air-Way Bill (AWB) data from 30 days of November 2017) as well as the number of (un)loading docks considered per GH (based on GH's data and visits to GH's facilities). Both ILO and ELO pick up and deliver goods at those five different locations.

Furthermore, more than 100 logistic operators work with airlines departing and arriving at Schiphol while several individual trucking companies service those logistic operators. Because of the difficulty to manage and control all these firms to improve operations, it was decided to divide shipment arrivals into two stream categories depending on the degree of operational control that can be implemented into the firms: ILO shipment arrivals and ELO truck arrivals. ILO shipment arrivals are shipments that arrive at the airport via the most important ILOs operating within the surroundings of the Schiphol airport, based on the total number of inbound and outbound AWB.

ILO shipment arrivals were modeled in this study as individual AWBs arriving at ILO's warehouses to be further consolidated and transported to the corresponding GH destination (and vice-versa). Table 2 describes the process that was used to generate ILO shipment arrivals as well as the average rate of AWB arrivals considered for this model (based on real data).

	Probability of arrival to a specific GH location (ILO + ELO)		Number of docks		Conditional probability of an inbound AWB visiting a specific ILO location given an initial visit to a GH (I-GH-ILO)				
GH Name	Inbound (I-GH)	Outbound (O-GH)	Inbound	Outbound	ILO1	ILO2	ILO3	ILO4	ILO5
GH 1	0.6050	0.5285	12	12	0.7885	0.0840	0.1005	0.0000	0.0269
GH 2	0.1444	0.1494	8	8	0.3512	0.1628	0.2583	0.1612	0.0665
GH 3	0.1104	0.1008	14 (I/O shared)		0.2258	0.4194	0.0000	0.1935	0.1613
GH 4	0.0507	0.0838	11 (I/O shared)		0.0006	0.4572	0.0006	0.3092	0.2323
GH 5	0.0895	0.1375	10	7	0.0003	0.3641	0.0006	0.3220	0.3131

Table 1: Proportion of flows from and to the GHs.

Five ILOs were selected to be modeled in this category as they represented 16% of total cargo flow. Table 2 shows the probability that an outbound AWB arrived at a specific ILO location (O-ILO) as well as the conditional probability that an outbound AWB will visit a GH, given an initial visit to an ILO (O-ILO-GH). The probability of an inbound AWB visiting an ILO location, given an initial visit to a GH (I-GH-ILO) can be found in Table 1.

- → ILO individual shipments identified by an AWB (AirWayBill) number are generated based on the pattern and rate of arrivals of either outbound (9.32 AWB per hour on average) or inbound (25.86 AWB per hour) flow.
- → Random initial node destination is assigned to AWB based on flow proportions.
  - > If inbound, initial GH node is assigned based on data from Table 1 (I-GH).
  - > If outbound, initial ILO node is assigned based on data from Table 2 (O-ILO).
- → Random final node destination is assigned to AWB based on flow proportions.
  - > If inbound, final ILO node is assigned based on initial GH node using data from Table 1 (I-GH-ILO), e.g., if initial node was GH2, then data from the second row will be used to define the probabilities of the AWB's final ILO node.
  - > If outbound, final GH node is assigned based on initial ILO node using data from Table 2 (O-ILO-GH), e.g., if initial node was ILO3, then data from the third row will be used to define the probabilities of the AWB's final GH node.
- → Weight of AWB is randomly assigned based on historic data.
  - > If inbound, exponential distribution with mean 683 kg.
  - > If outbound, exponential distribution with mean 271 kg.
- → Register AWB's arrival time and randomly assign due date (DD).
  - > Weibull distribution with parameters $\lambda = 8$ hours (range) and $k = 5$ (shape).
- → Decide whether AWB is a rush order:
  - > IF DD < 4 hours THEN AWB is a rush order
- → If inbound shipment, AWB is sent to GH node and waits to be consolidated with other AWBs, depending on the AWB consolidation and truck dispatching policies.
- → If outbound shipment, AWB is sent to ILO node and waits to be consolidated with other AWBs, depending on the AWB consolidation and truck dispatching policies

Table 2: Pseudo-code to generate ILO shipment's arrivals.

On the other hand, ELO administered shipments were modelled as consolidated shipments to be picked up (or delivered) by one single truck and, thus, only visited one GH location. It was further assumed that ELO were not collaborating with consolidation efforts inside SALO and thus no specific control over their visits to GH locations could be made. The logic behind the process of generating ELO shipments can be found in Table 4. ELO shipments were represented in the model as truck arrivals following a time-varying Poisson process [23] with a random percentage of the flow.

ILO Name	Probability of outbound arrival to a specific ILO (O-ILO)	Conditional probability of an outbound AWB visiting a specific GH location given an initial visit to an ILO (O-ILO-GH)				
		GH1	GH2	GH3	GH4	GH5
ILO1	0.1660	0.2350	0.3968	0.3524	0.0014	0.0144
ILO2	0.2497	0.0050	0.0269	0.1402	0.4238	0.4040
ILO3	0.2472	0.0072	0.2429	0.1458	0.0104	0.5937
ILO4	0.1546	0.0285	0.1665	0.1430	0.2243	0.4378
ILO5	0.1825	0.0147	0.1419	0.1227	0.1788	0.5419

Table 3: Proportion of flows from and to the ILOs.

Truck arrivals occur with a time-varying Poisson mean arrival rate that depends on both the weekday and the hour of the day [24,25] due to work shifts by both trucking and handling companies as well as flight schedules.

- → Consolidated shipments to be transported by an ELO truck are generated based on pattern and rate of arrivals of either outbound (465 trucks per day on average) or inbound (384 trucks per day) flow.
- → Random GH destination is assigned to ELO-consolidated shipments based on either inbound (I-GH) or outbound (O-GH) proportions shown in Table 1.
- → Weight of ELO-consolidated shipments (WELO) is assigned randomly.
  - > Triangular distribution (min = 0 kg, mode = 5 kg, max = 10 kg), based on a maximum weight of 10 kg per truck, which depends on the typical maximum volume carried by trucks inside Schiphol.
- → Type of containers of ELO-consolidated shipments is assigned randomly.
  - > Discrete distribution (1/3 – ULD, 1/3 – assorted pallets, 1/3 – combined containers).
- → If inbound shipment THEN ELO-consolidated shipment is sent to the respective GH node and a signal is sent for an ELO truck to pick up the consolidated shipments.
- → If outbound shipment THEN ELO-consolidated shipment is generated along with a truck in a node representing an entering road point in the Schiphol Airport landside road network (2 common points for trucks. The truck then carries out the delivery from the entering point to the destination GH node

Table 4: Pseudo-code to generate ELO shipment's arrivals.

3.1 Consolidation and truck-dispatching policies

Due to the dynamism and stochasticity of SALO, it was deemed that a practical way of managing the operations of the system was to implement easy-to-use operating rules instead of inapplicable complex policies and algorithms. Thus, following the shipment consolidation notions from Cetinkaya and Bookbinder [13] and the truck-dispatching concepts from Cook and Lodree [18] a series of policies were considered to be applied separately to inbound and outbound shipments. Table 5 describes the general logic behind the consolidation policies (CP) while Table 6 explains the general logic followed by the truck-dispatching policies (TP). Specific logic for both CPs and TPs can be found in Table 7 via a pseudo-code.

Consolidation policy	Set of shipments considered for consolidation
1-1	Only shipments going from one specific node to another, e.g. GH2 to ILO5
1-N	Shipments to be moved from one single location to multiple destinations, e.g., from ILO3 to GH2, GH4 and GH5 for outbound shipments; or from GH2 to ILO1, ILO2, ILO4 and ILO5 for inbound shipments
N-1	Shipments to be moved from multiple locations to one specific destination, e.g., from GH1, GH2 and GH3 to ILO5 for inbound shipments; or from ILO3 and ILO4 to GH3 for outbound shipments
N-N	Shipments to be moved from multiple locations to multiple destinations, e.g. from ILO2, ILO3, ILO4 and ILO5 to GH1, GH2 and GH4 for outbound shipments, or vice-versa for inbound shipments

Table 5: Shipment consolidation policies.

TPs are inherently associated in this model with CPs as the amount of consolidated weight or number of AWBs to be considered for triggering the TPs will depend on the criteria to consolidate the shipments. For example, if the FT truck-dispatching policy is considered, then a full truck will be calculated based on the accumulated weight of the consolidation policy. Suppose the CP considered is 1-N for inbound shipments, then an FT will be fulfilled only when the total weight accumulated in one GH location to be moved to any set of ILO points is higher than the maximum allowed truckload. This interaction means that the thresholds for dispatching a truck will be reached quicker the more nodes are considered in the consolidation.

Thus, an N-N policy will consolidate enough weight to dispatch a truck quicker than a 1-N or an N-1 policy; whereas a 1-1 policy will take the longest to consolidate enough AWBs to be able to dispatch a truck.

Truck-dispatching policy	Condition that needs to be fulfilled to send a signal to consolidate shipments (see Table 7 for the full logic of the policies)
CD: Continuous Deployment	One truck available for transporting AND at least one AWB ready to be consolidated
ESW (Economic Shipment Weight)	Accumulated consolidated weight is HIGHER than Economic Shipment Weight formula proposed in [9]
ESW+RAWB (ESW+Rush AWBs)	Accumulated *modified* consolidated weight is HIGHER than Economic Shipment Weight formula proposed in [9]. This formula considers rush AWBs (RAWB) having a higher holding cost than normal orders
RAWB (Rush AWBs)	At least one accumulated RAWB waiting to be consolidated. This policy tries to minimize the wait of RAWBs
FT (Full Truckload)	The maximum allowed truckload of accumulated consolidated weight has been reached

Table 6: Truck-dispatching policies.

Since the most common type of truck used to move cargo is the semi-trailer with dimensions 13.6 x 2.48 x 2.80 m., it was considered as the single type of truck to move cargo within the model. Based on experts' feedback regarding the typical density of the goods transported in Schiphol air cargo terminal, it was deemed that the maximum weight load used with combined cargo was 10 tons (the actual maximum load was limited by the volume of the goods, not the weight).

Table 8 shows the rules used to calculate the (un)loading times depending on the type of shipment and container. ELO maximum (un)loading times were modeled following experts' advise while ILO maximum times were taken from [26]. Despite the fact that it has been shown that truck loading takes more time than unloading [26], for this exercise it was assumed that loading and unloading required the same effort.

- → Add the weight of the arriving AWB (W_{AWB}) to the accumulated weights of all consolidation policies 1-1, N-1, 1-N and N-N, e.g., $WI_{gi} = WI_{gi} + W_{AWB,}$ being that *g* is the arriving node and *i* is the departing node for the current AWB.
- → Increase in one the number of AWBs in the counters of all consolidation policies, e.g., $I_{gi} = I_{gi} + 1$.
- → IF the arriving AWB is a rush order, add one rush order to the accumulated number of rush orders of all consolidation policies, e.g., $RI_{gi} = RI_{gi} + 1$.
- → IF $WI_{gi} \geq 10$ tons THEN
  - > Prepare a pallet with I_{gi} - 1 elements (to ensure the weight is never higher than 10 tons.
  - > Reset all accumulated weights and counters accordingly.
  - > Pallet sends request to be picked-up by an ILO truck.
- → IF ConsolidationPolicy = "1-N"
  - > IF $WI\_1N_g \geq 10$ tons (equivalent to TruckDispatchPolicy = "FT") THEN
    - ⇨ Prepare a pallet with I_1N_g - 1 elements.
    - ⇨ Reset all accumulated weights and counters accordingly.
    - ⇨ Pallet sends request to be picked-up by an ILO truck.
  - > ELSE point towards the TruckDispatchPolicy
    - ⇨ IF TruckDispatchPolicy = "ESW" THEN
      - ▫ IF $WI\_IN_g \geq \sqrt{\frac{2D_gS\,(683)}{h}}$, being that D_g is the average of AWB arrivals per hour arriving to node *g*, THEN
        - ○ RUN the next sequence called SEQ_1N
          - ▪ Prepare a pallet with I_1N_g elements.
          - ▪ Reset all accumulated weights and counters accordingly.
          - ▪ Pallet sends request to be picked-up by an ILO truck.
    - ⇨ IF TruckDispatchPolicy = "ESW+DD" THEN
      - ▫ IF $WI\_IN_g \geq \sqrt{\frac{2D_gS\,(683)}{h+5h*RI\_IN_g}}$ (in this case the denominator adds 5 times the normal holding cost for each rush orders waiting to be consolidated), THEN RUN SEQ_1N.
    - ⇨ IF TruckDispatchPolicy = "DD" THEN
      - ▫ IF $RI\_IN_g > 0$ THEN RUN SEQ_1N.
    - ⇨ IF TruckDispatchPolicy = "CD" THEN
      - ▫ IF $I\_IN_g > 0$ AND there are available (not assigned) ILO trucks THEN RUN SEQ_1N.

→ IF ConsolidationPolicy = "N-1"
- > IF *WI_N1*$_i$ ≥ 10 tons (equivalent to TruckDispatchPolicy = "FT") THEN
  - ⇨ As the consolidation is done over multiple GH locations toward one *i* ILO location
    FOR j = 1 to 5
    - ▫ IF I_{ji} > 0 THEN
      - ○ Prepare a pallet with I_{ji} elements unless *j* = *g* in which case prepare a pallet with I_{ji} - 1 elements.
  - ⇨ Reset all accumulated weights and counters accordingly.
  - ⇨ Pallets send a request to be picked-up by the same ILO truck.
- > ELSE point towards the TruckDispatchPolicy.
- > IF TruckDispatchPolicy = "ESW" THEN
  - ⇨ IF $WI\_N1_i \geq \sqrt{\frac{2D_iS\,(683)}{h}}$, being that D_i is the average of AWB arrivals per hour going to node *i*, THEN
    - ▫ RUN the next sequence called SEQ_N1
      - ○ FOR j = 1 to 5
        - ▪ IF I_{ji} > 0 THEN
          - • Prepare a pallet with I_{ji} elements
      - ○ Reset all accumulated weights and counters accordingly
      - ○ Pallets send a request to be picked-up by the same ILO truck
- > IF TruckDispatchPolicy = "ESW+DD" THEN
  - ⇨ IF $WI\_N1_i \geq \sqrt{\frac{2D_iS\,(683)}{h+5h*RI\_N1_i}}$ THEN RUN SEQ_N1
- > IF TruckDispatchPolicy = "DD" THEN
  - ⇨ IF $RI\_N1_i > 0$ THEN RUN SEQ_N1
- > IF TruckDispatchPolicy = "CD" THEN
  - ⇨ IF $I\_N1_i > 0$ AND there are available ILO trucks THEN RUN SEQ_N1

→ IF ConsolidationPolicy = "N-N"
- > IF *WI_NN* ≥ 10 tons (equivalent to TruckDispatchPolicy = "FT") THEN
  - ⇨ As the consolidation is done over multiple *g* locations toward multiple *i* locations
    FOR j = 1 to 5
    FOR k = 1 to 5
    - ▫ IF I_{jk} > 0 THEN
      - ○ Prepare a pallet with I_{jk} elements unless *j* = *g* AND *k* = *i* in which case prepare a pallet with I_{jk} - 1 elements.
  - ⇨ Reset all accumulated weights and counters accordingly.
  - ⇨ Pallets send a request to be picked-up by the same ILO truck.
- > ELSE point towards the TruckDispatchPolicy.
- > IF TruckDispatchPolicy = "ESW" THEN
  - ⇨ IF $WI\_NN \geq \sqrt{\frac{2DS\,(683)}{h}}$, being that *D* is the average of AWB inbound arrivals per hour, THEN
    - ▫ RUN the next sequence called SEQ_NN
      - ○ FOR j = 1 to 5
        FOR k = 1 to 5
        - ▪ IF I_{jk} > 0 THEN
          - • Prepare a pallet with I_{jk} elements
      - ○ Reset all accumulated weights and counters accordingly
      - ○ Pallets send a request to be picked-up by the same ILO truck
- > IF TruckDispatchPolicy = "ESW+DD" THEN
  - ⇨ IF $WI\_NN \geq \sqrt{\frac{2DS\,(683)}{h+5h*RI\_NN}}$ THEN RUN SEQ_NN
- > IF TruckDispatchPolicy = "DD" THEN
  - ⇨ IF $RI\_NN > 0$ THEN RUN SEQ_NN
- > IF TruckDispatchPolicy = "CD" THEN
  - ⇨ IF $I\_NN > 0$ AND there are available ILO trucks THEN RUN SEQ_NN

→ IF ConsolidationPolicy = "1-1"
- > Point towards the TruckDispatchPolicy.
- > IF TruckDispatchPolicy = "ESW" THEN
  - ⇨ IF $WI_{gi} \geq \sqrt{\frac{2D_{gi}S\,(683)}{h}}$, being that D_{gi} is the average of AWB arrivals per hour arriving at *g* and exiting from *i*, THEN
    - ▫ RUN the next sequence called SEQ_11
      - ○ Prepare a pallet with I_{gi} elements
      - ○ Reset all accumulated weights and counters accordingly
      - ○ Pallet sends a request to be picked-up by the same ILO truck
- > IF TruckDispatchPolicy = "ESW+DD" THEN
  - ⇨ IF $WI_{gi} \geq \sqrt{\frac{2D_{gi}S\,(683)}{h+5h*RI_{gi}}}$ THEN RUN SEQ_11
- > IF TruckDispatchPolicy = "DD" THEN
  - ⇨ IF $RI_{gi} > 0$ THEN RUN SEQ_NN
- > IF TruckDispatchPolicy = "CD" THEN

IF $I_{gi} > 0$ AND there are available ILO trucks THEN RUN SEQ_NN

Table 7: Pseudo-code of the consolidation and truck dispatching policies' logic (Refer to Table A1 in the Appendix for the description of the variables in this pseudo-code).

- → Loading and unloading times (LT) for ELO trucks depend on the type of container carrying the ELO consolidated shipment
  - > IF container is ULD THEN LT = WELO/10 tons * 15 mins
  - > IF container is Pallet THEN LT = WELO/10 tons * 60 mins
  - > IF container is Combined THEN LT = WELO/10 tons * 120 mins
- → LT for ILO trucks depend on the amount of weight that is being loaded or unloaded in the node, as some consolidation policies allow for multiple pick-up and/or delivery locations
  - > LT = W_{gi}/10 tons * 30 mins as W_{gi} is what is being (un)loaded in a specific node

Table 8: Pseudo-code to define (un)loading times.

Finally, based on the current fleet of trucks used by the 5 ILOs selected for this study, 6 trucks were considered as the fleet that moves the AWBs between GH and ILO positions and vice-versa, using a collaborative approach [27], i.e. SALO was considered as the owner of the trucks and of this set of AWBs.

Following the previous conceptual design and logic presented, the modelling approach can be adapted to a different airport cargo hub different than the one presented here. Moreover, as it can be appreciated, by implementing the proposed elements, different shipment and truck policies can be evaluated considering for the first time not only the actors present in the system but also the variability which plays a key role in any real system allowing also revealing the emergent dynamics which cannot be revealed by other analytical technique.

4 Results

After a full-factorial experimental design was designed consisting of 4 CP and 5 TP for both inbound and outbound AWBs, resulting in a total of 400 experimental points. For each experimental setting, 10 replications were run with a duration of 40 days with 10 days of warm-up period.

The results revealed the following behaviour: policies that have more consolidation, e.g., FT, have a better performance in terms of total distance travelled by all 6 trucks than policies with lower consolidation efforts, e.g., CD, but a bad performance in terms of AWB flow time and percentage of tardy AWBs.

On the other hand, the N-N policy had the worst performance in terms of distance but the best one in terms of time, whereas the opposite is true for the 1-1 policy. This might be caused by the fact that the N-N policy makes many visits to many locations in a single trip as it considers everything that needs to be moved, while the 1-1 policy only triggers a truck dispatch whenever there's enough material to be moved from one single point to another point.

For outbound shipments, the N-N policy seemed to result in the best compromise between distance travelled and flow time, as its performance in terms of percentage of tardy deliveries and average flow time was outstanding, compared with the relatively low increase in total kilometres travelled (see Table 9).

However, results from Table 9 suggest that the best policy for inbound shipments might be the 1-N policy, which considers all the shipments waiting to be moved from one GH location to the multiple ILO locations in the model.

	Outbound			Inbound		
CP	Distance Travelled (KM)	Flow Time ILO-AWB (hours)	% Tardy shipments	Distance Travelled (KM)	Flow Time ILO-AWB (hours)	% Tardy shipments
1-1	53,987	20.73	54.2%	49,365	4.84	18.3%
1-N	54,968	7.30	33.7%	52,521	2.62	5.3%
N-1	55,971	7.19	27.4%	54,113	2.65	5.3%
N-N	56,466	2.77	5.7%	65,384	2.32	3.9%

Table 9: Average results of applying different consolidation policies either for inbound or outbound AWBs.

Finally, Table 10 suggests that the best compromise between distance and delivery performance for outbound shipments was found with the ESW+RAWB policy. Interestingly, the RAWB policy on its own did not have a good performance in terms of delivery, even though it was designed to reduce the number of late deliveries from rush orders; whereas the best overall performance for inbound shipments was found with the ESW policy.

TP	Outbound			Inbound		
	Distance Travelled (KM)	Flow Time ILO-AWB (hours)	% Tardy shipments	Distance Travelled (KM)	Flow Time ILO-AWB (hours)	% Tardy shipments
CD	75,591	1.89	6.1%	96,600	1.97	3.9%
ESW	50,232	8.69	33.0%	44,480	3.05	7.8%
ESW+ RAWB	51,127	7.39	26.9%	45,892	2.93	6.9%
FT	49,118	16.30	47.2%	42,718	3.89	11.7%
RAWB	50,630	13.22	37.9%	47,144	3.69	10.7%

Table 10: Average results of applying different TP either for inbound or outbound AWBs.

5 Conclusions and Future Research Directions

The paper presents the main elements and conceptual design for developing a discrete-event simulation model of the landside logistic operations of a mega-hub airport considering for the first time elements that enable to evaluate the most common logistics problems of this type of infrastructure in a realistic fashion; we presented the case of Schiphol Airport in the Netherlands to exemplify the potential of this approach. A realistic representation of the road network of the airport as well as the (un)loading capacities of the ground handlers working inside the airport was developed. Several consolidation and truck-dispatching policies were proposed and tested in terms of performance. For the case presented, results suggest that truck-dispatching policies have a higher impact on performance than consolidation policies. Some of the results were counter-intuitive; thus, the platform developed can provide decision-makers excellent support for making decisions about how the best managing policy should be implemented depending on the objective pursued (economic, service, environmental).

A closer examination of the impact of combinations of consolidation and truck-dispatching policies is further needed to better understand their impact on performance. Furthermore, more research is needed regarding the impact of consolidation and truck-dispatching policies in other complex logistics systems as well and incorporating environmental considerations for evaluating which policy can have the best positive effect for reducing greenhouse emissions.

Acknowledgements

The authors would like to thank Dr. Thierry Verduijn and the Aviation Academy of the Amsterdam University of Applied Sciences for supporting this study as well as the Dutch Benelux Simulation Society (www.dutchbss.org) and EUROSIM for the dissemination of the results.

References

[1] IATA. Annual Review 2018. 2018.

[2] The World Bank. Connecting to Compete 2018: Trade Logistics in the Global Economy. Washington, DC, USA: 2018.

[3] European Comission. Statistical Pocketbook. 2018.

[4] Feng B, Li Y, Shen Z-J M. Air cargo operations: Literature review and comparison with practices. Transp Res Part C Emerg Technol 2015;56:263–80. DOI 10.1016/j.trc.2015.03.028

[5] Leung L C, Van Hui Y, Wang Y, Chen G. A 0–1 LP Model for the Integration and Consolidation of Air Cargo Shipments. Oper Res 2009;57:402–12. DOI 10.1287/opre.1080.0583

[6] Ou J, Hsu V N, Li C-L. Scheduling Truck Arrivals at an Air Cargo Terminal. Prod Oper Manag 2010;19:83–97. DOI 10.1111/j.1937-5956.2009.01068.x

[7] Mendoza-Dorantes E E, Alcaraz C Z, Mota M A M, Delahaye D. Simulating Airport Capacity: Mexico City Airport Case. ATOS 2015, 5th Int. Air Transp. Oper. Symp., 2015.

[8] Romero-Silva R, Shaaban S, Marsillac E, Laarraf Z. The impact of unequal processing time variability on reliable and unreliable merging line performance. Int J Prod Econ 2021;235:108108. DOI 10.1016/j.ijpe.2021.108108

[9] Higginson J K, Bookbinder J H. Policy recommendations for a shipment-consolidation program. J Bus Logist 1994;15:87–112.

[10] Goyal S K. Economic Order Quantity under Conditions of Permissible Delay in Payments. J Oper Res Soc 1985;36:335–8. DOI 10.2307/2582421

[11] Bookbinder J H, Higginson J K. Probabilistic modeling of freight consolidation by private carriage. Transp Res Part E Logist Transp Rev 2002;38:305–18. DOI 10.1016/S1366-5545(02)00014-5

[12] Çetinkaya S, Mutlu F, Lee C-Y. A comparison of outbound dispatch policies for integrated inventory and transportation decisions. Eur J Oper Res 2006;171:1094–112. DOI 10.1016/j.ejor.2005.01.019

[13] Çetinkaya S, Bookbinder J H. Stochastic models for the dispatch of consolidated shipments. Transp Res Part B Methodol 2003;37:747–68. DOI 10.1016/S0191-2615(02)00060-7.

[14] Mutlu F, Çetinkaya S, Bookbinder J H. An analytical model for computing the optimal time-and-quantity-based policy for consolidated shipments. IIE Trans 2010;42:367–77. DOI 10.1080/07408170903462368

[15] Satır B, Erenay F S, Bookbinder J H. Shipment consolidation with two demand classes: Rationing the dispatch capacity. Eur J Oper Res 2018;270:171–84. DOI 10.1016/j.ejor.2018.03.016

[16] Çetinkaya S, Mutlu F, Wei B. On the service performance of alternative shipment consolidation policies. Oper Res Lett 2014;42:41–7. DOI 10.1016/j.orl.2013.11.003

[17] Battarra M, Cordeau J-F, Iori M. Pickup-and-Delivery Problems for Goods Transportation. In: Toth P, Vigo D, editors. Veh. Routing Probl. Methods Appl., Philadelphia,PA: SIAM; 2014, p. 161–91. DOI 10.1137/1.9781611973594.ch6

[18] Cook R A, Lodree E J. Dispatching policies for last-mile distribution with stochastic supply and demand. Transp Res Part E Logist Transp Rev 2017;106:353–71. DOI 10.1016/j.tre.2017.08.008

[19] Braekers K, Ramaekers K, Van Nieuwenhuyse I. The vehicle routing problem: State of the art classification and review. Comput Ind Eng 2016;99:300–13. DOI 10.1016/j.cie.2015.12.007

[20] Pillac V, Gendreau M, Guéret C, Medaglia A L. A review of dynamic vehicle routing problems. Eur J Oper Res 2013;225:1–11. DOI /10.1016/j.ejor.2012.08.015

[21] Kelton W D, Smith J S, Sturrock D T. Simio and Simulation: Modeling, Analysis, Applications. 1st ed. Sewickley, PA: Simio LLC; 2014.

[22] Air Cargo Netherlands. Ground Handler members of ACN 2018. http://www.acn.nl/sectoren/afhandelaars/?lang=en (accessed October 23, 2018).

[23] Green L V, Kolesar PJ, Whitt W. Coping with Time-Varying Demand When Setting Staffing Requirements for a Service System. Prod Oper Manag 2007;16:13–39. DOI 10.1111/j.1937-5956.2007.tb00164.x.

[24] Selinka G, Franz A, Stolletz R. Time-dependent performance approximation of truck handling operations at an air cargo terminal. Comput Oper Res 2016;65:164–73. DOI 10.1016/j.cor.2014.06.005

[25] Yan S, Chen C-H, Chen C-K. Short-term shift setting and manpower supplying under stochastic demands for air cargo terminals. Transportation (Amst) 2008;35:425–44. DOI 10.1007/s11116-007-9151-7

[26] Burdzik R, Cieśla M, Sładkowski A. Cargo Loading and Unloading Efficiency Analysis in Multimodal Transport. PROMET -Traffic&Transportation 2014;26:323–31. DOI 10.7307/ptt.v26i4.1356

[27] Gansterer M, Hartl R F. Collaborative vehicle routing: A survey. Eur J Oper Res 2018;268:1–12. DOI 10.1016/j.ejor.2017.10.023

Appendix

- Weight accumulated for inbound AWBs going from GH *g* to ILO *i* (1-1 policy): WI_{gi}
- Weight accumulated for inbound AWBs whose initial node is *g* (1-N): WI_1N_g
- Weight accumulated for inbound AWBs whose final node is *i* (N-1): WI_N1_i
- Weight accumulated for inbound AWBs in all GH nodes going to all ILO nodes (N-N): *WI_NN*
- Number of inbound AWBs going from GH *g* to ILO *I* (1-1 policy): I_{gi}
- Number of inbound AWBs whose initial node is *g* (1-N): I_1N_g
- Number of inbound AWBs whose final node is *i* (N-1): I_N1_i
- Number of inbound AWBs in all GH nodes going to all ILO nodes (N-N): *I_NN*
- Number of inbound *rush* AWBs going from GH *g* to ILO *I* (1-1 policy): RI_{gi}
- Number of inbound *rush* AWBs whose initial node is *g* (1-N): RI_1N_g
- Number of inbound *rush* AWBs whose final node is *i* (N-1): RI_N1_i
- Number of inbound *rush* AWBs in all GH nodes going to all ILO nodes (N-N): *RI_NN*
- Weight accumulated for outbound AWBs going from ILO *i* to GH *g* (1-1 policy): WO_{ig}
- Weight accumulated for outbound AWBs whose initial node is *i* (1-N): WO_1N_i
- Weight accumulated for outbound AWBs whose final node is *g* (N-1): WO_N1_g
- Weight accumulated for outbound AWBs in all ILO nodes going to all GH nodes (N-N): *WO_NN*
- Number of outbound AWBs going from ILO *i* to GH *g* (1-1 policy): O_{ig}
- Number of outbound AWBs whose initial node is *i* (1-N): O_1N_i
- Number of outbound AWBs whose final node is *g* (N-1): O_N1_g
- Number of outbound AWBs in all ILO nodes going to all GH nodes (N-N): *O_NN*
- Number of outbound rush AWBs going from ILO *i* to GH *g* (1-1 policy): RO_{ig}
- Number of outbound rush AWBs whose initial node is *i* (1-N): RO_1N_i
- Number of outbound rush AWBs whose final node is *g* (N-1): RO_N1_g
- Number of outbound rush AWBs in all ILO nodes going to all GH nodes (N-N): *RO_NN*

Table A1: Set of variables for consolidation and truck dispatching policies' logic.

Hybrid Models and Digital Twins for Condition Monitoring: HVAC System for Railway

Antonio Gálvez[1,2*], Jokin Rubio[1], Dammika Seneviratne[1], Asier Gonzalez[1], Alberto Jimenez[1], Unai Martinez-de-Estarrona[1], Diego Galar[1,2], Esko Juuso[3]

[1]TECNALIA, Basque Research and Technology Alliance (BRTA), 48170 Derio, Spain; *antonio.galvez@tecnalia.com, Dammika.seneviratne@tecnalia.com, diego.galar@tecnalia.com

[2]Division of Operation and Maintenance Engineering, Department of Civil, Environmental and Natural Resources Engineering, Luleå University of Technology, 971 87 Luleå, Sweden; *antonio.galvez@ltu.se, diego.galar@ltu.se

[3]Control Engineering Group, Faculty of Technology, University of Oulu, 90014 Oulu, Finland; esko.juuso@oulu.fi

SNE 31(3), 2021, 121-126, DOI: 10.11128/sne.31.tn.10572
Received: March 10, 2021 (Selected EUROSIM 2019 Postconf. Publ.), Revised: August 30, 2021; Accepted: September 2, 2021
SNE - Simulation Notes Europe, ARGESIM Publisher Vienna, ISSN Print 2305-9974, Online 2306-0271, www.sne-journal.org

Abstract. Safety passenger transportation is more important than efficiency or reliability. Therefore, it is vital to maintain the proper condition of the equipment related to the passengers' comfort and safety. This manuscript presents the methodology of complete development and implementation of both hybrid model and digital twin 3.0 for an HVAC in railways. The objective of this is to monitor the condition of the HVAC where it matters to the comfort and safety of the passengers in the trains. The level 3.0 of digital twin will be developed for the diagnosis and prognosis of HVAC by using hybrid modeling. The description illustrated in this paper is focused on the methodology used to implement a hybrid model-based approach, and both the need and advantages of using hybrid model approaches instead of data-based approaches. The development considers the importance of safety and environmental risks, which are included in the risk quantification of failure modes. Railway's maintainers replace critical components in early stages of degradation; thus, the use of a data-driven model loses essential information related to advanced stages of degradation which might decrease the accuracy of the maintenance instructions provided. Physics-based model can be used to generate synthetic data to overcome the lack of data in advanced stages of degradation, and then, the synthetic data can be combined with the real data, which is collected by sensor located in the real system, to build the data-driven model. The combination leads to form hybrid-model based approach with a large number of failure modes that were unpredictable. Finally, the outcome is beneficial for the proper functioning of systems; hence, safety of the passengers.

Introduction

The diagnostics and prognostics are the main processes in condition-based maintenance (CBM). These processes are broadly used in industrial assets, mainly, at levels of part, components, sub-systems, and systems. Fault detection and diagnostics (FDD) is the identification of a faulty component through the detection and isolation of a fault. Once a fault appears in a system, diagnostics process might detect that fault and identify the faulty part. Prognostics process is performed for estimating the remaining useful life (RUL) of a system. It is estimated using the behavior data while the system works, allowing maintainers to avoid the corrective maintenance [1]. Thus, appropriate implementation of CBM leads to reduce costs and increase the reliability and safety of systems.

As it is shown in Figure 1, there are highlighted four techniques for estimating the RUL and, on a consequence, for implementing FDD and prognostics processes [1]: experience-based approaches, model-based approaches, data-driven approaches, and hybrid model-based approaches (HyMAs).

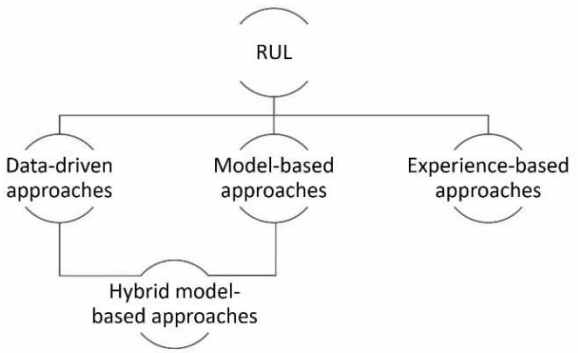

Figure 1: Remaining useful life (RUL) estimation models.

The model-based approach are mathematical models of the physical system [2]. These models incorporate such characteristics as material properties, thermodynamic, and mechanical responses. Furthermore, different operational conditions, components defect, and degradation must be modelled for fault detection. Thus, these models accurately describe the behaviour of systems [3] [4].

Data-driven approaches use operational data collected by sensors embedded in the system for obtaining information related to the degradation state of components. Thus, these approaches can trace the relationship between the data acquired from the system with its degradation [5] [6].

As Figure 1 shows, HyMAs is the combination of data-driven and model-based approaches. The main advantage of this combination is the reduction in both the historical information required to train a data-driven model and the information needed for a robust physics-based model. This data fusion aims to improve FDD and prognostics processes. The model-based approaches generates synthetic data to overcome the lack of historical data, thus improving the ability of a data-driven apprach to detect failure modes (FMs) and reducing the appearance of hidden FMs, metaphorically known as "black swan losses" [7].

1 Problem Discussion

The case study used in this research work is a heating, ventilation and air conditioning (HVAC) system which is installed in a high-speed passenger train.

Currently, many types of research are based on data-driven approaches but missing important information and failures. This occurs because maintainers replace critical elements in early stages of degradation for safety, reliability, economic, and environmental reasons. Therefore, it is challenging to acquire data in faulty stages of the system and advanced stages of degradation [3].

The solution proposed in this manuscript is to transfer the methodology to railway subsystems to scale, develop, and validate an HyMAs for railway equipment through the combination of modeling based on physical laws and modeling based on data. As a primary purpose, it will be developed to improve the diagnostics and prognostics processes of components of railway systems.

The outcome will be to provide railway companies with the necessary tools to reach a level 3 of digital twin based on HyMA. The Digital twin levels are listed in Table 1 and shown in Figure 2, Figure 3, and Figure 4.

Digital Twin	Data	Layer	Level
1.0	SCADA Data Online Data	OT (SCADA)	**Operational** Alarms based on anomalies
2.0	Adding: Offline data, GMAO, ERP, taxonomy, ontology management data	OT (SCADA) and IT (ERP, management data...)	**Tactical** Planning of corrective maintenance instructions.
2.1	Context data	Operative context	
3.0	Physics model Hybrid digital twin	OT + IT + Engineering technology	**Strategic** Renew of assets, performance improvements

Table 1: Digital twins levels description.

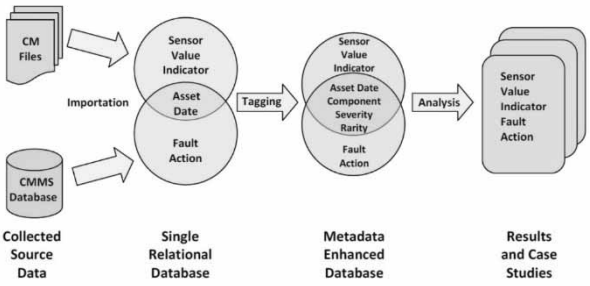

Figure 2: Digital twin 2.0, extracted from [8].

Figure 3 shows the Digital Twin 2.1, who combines the Digital Twin 2.0 (see Figure 2) and context data. Context-awareness is considered as an application's ability to adapt to changing circumstances and respond according to the context of use.

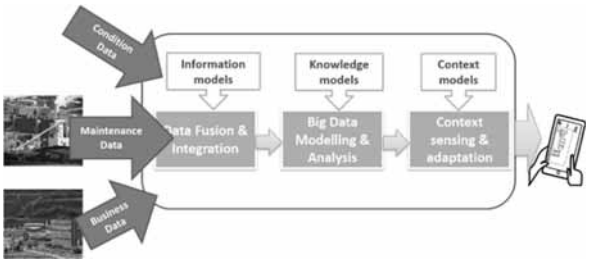

Figure 3: Digital twin 2.1, extracted from [8]).

Figure 4 shows the Digital Twin 3.0, who combines the Digital Twin 2.0 with a HyMA. It could be used from component to system level.

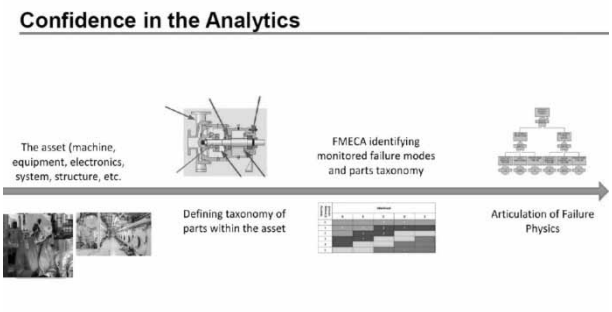

Figure 4: Digital twin 3.0, extracted from [8].

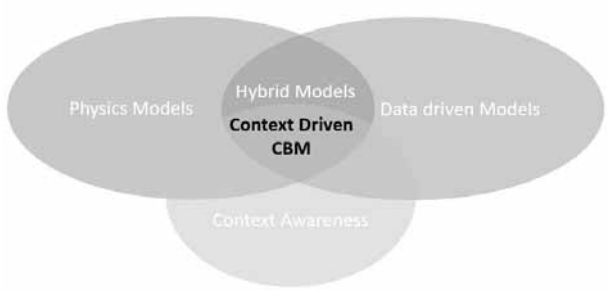

Figure 5: Context-Driven CBM Digital twin 3.0, modified from [8].

2 Objectives

The aim of this research work is to provide maintainer of the HVAC system with the necessary tools to reach a level 3 of Digital Twin based on HyMA – see Table 1. The objectives of this development are listed below.

1. Study the different approaches to achieve a robust hybrid model of the HVAC system. Model must consider the number of variables monitored in the real system, the information contained in it, and the information available in other sources, such as expert knowledge, other papers, the history of failures and alarms, and work orders. The selection of information is crucial for developing a robust HyMA because it helps to identify the balance between the resources needed for modeling versus the accuracy of FDD and prognostics processes. Then, this leads to propose a methodology for combining data-driven and model-based approaches; thus, for implementing the HyMA. This approach will be firstly applied to HVAC use case.
2. Study the available models of the under-study asset, and then, develop models based on the physics of the monitored system that represent the response of the HVAC system. This includes electrical modeling of motors such as electric circuits, modeling of moving parts such as rotation of rigid solids, or modeling of heat exchangers through the energy balance, among others.
3. Definition the methodology for synchronizing the model with the real system. This step fixes the values of key unknown parameters of the physics-based models. The synchronization of the model is carried out using the data collected by the available sensors. The data used will be considered under normal operating behavior.
4. Validation of the HyMA will be carried out by comparing the response of the the physics-based model with the response of the real system. The validation will focus on fault detection, fault location, and fault identification.

3 Advantages of the Hybrid Approach

Industries where safety is more important than efficiency or reliability, as it is the case of the railway sector, components are replaced in the initial stages of degradation, sometimes far from their maintenance limit, due to regulations and regulations, such as the standard EN 13848-5:2017 which stablishes strong replacement criteria for the railway sector.

This early substitution of components implies a lack of data of the complete degradation of replaced elements. This lack of data limits the visibility of FMs and the appearance of the aforementioned black swan losses, which are events associated with failures not foreseen or contemplated [8]. This can be avoided by using synthetic data generated by physics-based models, which is built for reproducing the behavior of the asset in degraded or unusual conditions and complete database on failures and degradation of systems. It should be noted that the assets are usually complex systems composed of several subsystems and their components, which makes it difficult to perform an accurate maintenance model. Consequently, the interaction between components and subsystems makes it challenging to obtain a global failure scenario due to sub-systems work together and they can fail individually or together. Thus, complex systems have many possible combinations of faults.

It is, therefore, necessary to develop a strategy to overcome the lack of data which might provide information on the evolution of system degradation. This strategy must be hybrid, considering both model-based approaches, that is, models based on physical laws; and models based on data, in such a way that their combination can supply the shortcomings of each method. The primary objective of the project is the transfer of a methodology to build a HyMA for obtaining more information of faults and how these faults change over time.

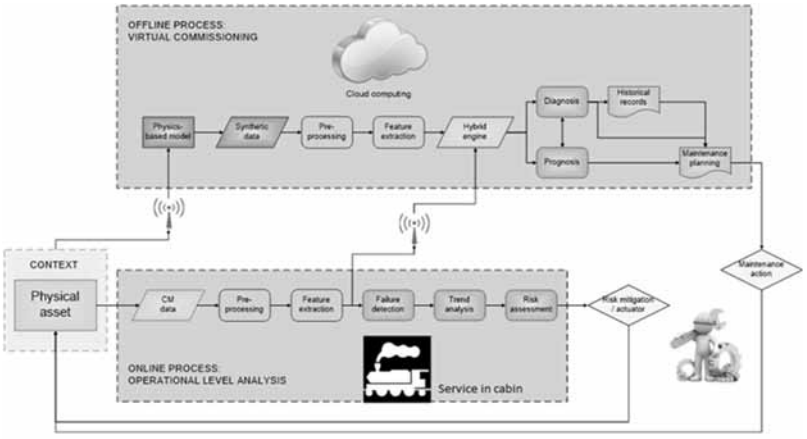

Figure 6: Proposed architecture scheme (modif. from [9]).

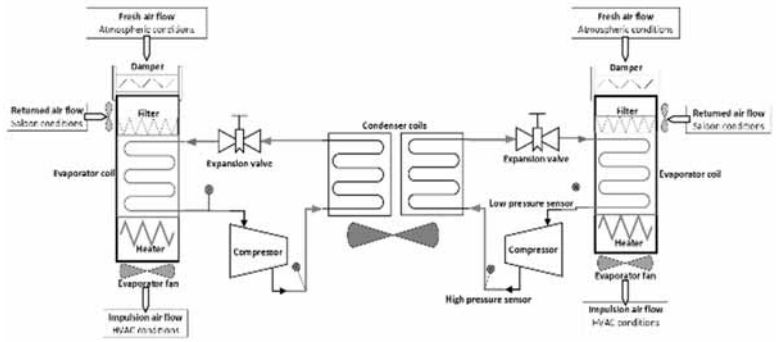

Figure 7: HAC saloon scheme.

As it is shown in Figure 6, a dataset with operational data is generated; then, this data is used for performing diagnostics and prognostics processes. These processes generate the necessary information that constitutes the knowledge base for maintenance planning will be generated.

4 Case study on HVAC

The HVAC system is installed in a passenger train carriage. These systems are composed by many vital components. The main parts can be identified as compressor, condenser coil, evaporator coil, bypass valve, dehydrator filter, and airflow units (Figure 7).

Compressor. Move the refrigerant liquid from the low-pressure chamber to a high-pressure chamber by scroll mechanism without excessive noise and vibrations. The monitoring of compressor status can be performed indirectly through the parameters/variables, for example, inlet pressure, outlet pressure, engine current, vibration, the temperature of the compressor parts, etc.

Condenser coil and Evaporator coil. Heat exchanger between airflow and refrigerant liquid. These components do not usually have movable elements; their performance is mostly controlled by inlet and outlet temperatures.

Bypass valve. Regulates the refrigerant flow.

Dehydrator filter. Retains the moisture and solid particles existing in the refrigerant circuit.

Air diffusion unit. Composed mainly of fans connected to electric motors. This component can be monitored through the vibrations of the fans, the airflow and electrical consumption.

5 Methodology

The methodology shown in this section is a general approach used in many research studies where CBM is deployed in an industrial environment.

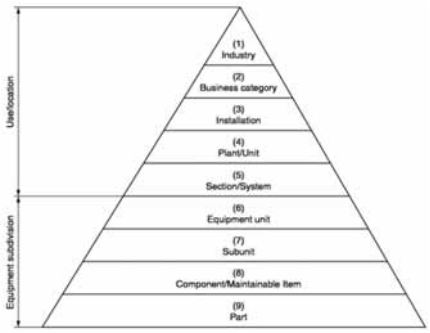

Figure 8: Taxonomy classification with taxonomic levels (from standard ISO 14224-2016).

The methodology followed is composed of the items below:

1. Analysis of the information related to the HVAC system, such as design, operational conditions, maintenance tasks, etc., and analysis of the data acquired by the sensors embedded in the system.
2. Evaluation of the current capabilities; the maintainers of the HVAC system understudy use a data-driven model to perform diagnostics and prognostics. Therefore, it is necessary to evaluate the limitations of the current data-driven model and the maturity of the deployed diagnostics and prognostics processes. Level 2.1 of the Digital Twin confirmed but improvable.

3. Taxonomy of the system considering the standard ISO 14224-2016. Before developing the taxonomy of the system, the taxonomic level of interest must be identified – see Figure 8 [7]. Identification of the subsystems, equipment, subunits, and components for building the hybrid model. This step reaches until level 8 of the taxonomy classification shown in Figure 8.
4. Analysis of the current list of FMs, their effects and causes. Moreover, study the possibility to add new FMs.
5. FMs classification by their criticality. Then, quantification of safety and environmental risks.
6. Selection of variables and parameters to perform the physics-based model, definition of appropriate models for each component based on the sensors installed in the system.
7. Identification of critical items and significant variables.
8. Analysis of models developed by the railway company. Adaptation of models, if possible, or development of new physics-based models and data-driven models; these models will be developed separately. Digital Twin 2.1 enhanced.
9. Integration of physics-based models and data-driven models to build the hybrid model considering subsystems. Level 3.0 of Digital Twin reached.
10. Validation of the final HyMA. Level 3.0 of Digital Twin reached and tested.

6 Planning

The research work will be addressed in two phases: the first phase will provide an early evaluation of the scope of the HyMA; and the second phase leads to develop the diagnostics and prognostics processes from model defined in the first phase. The scope of this research work includes both phases for the HVAC system.

6.1 Phase 1: Viable minimum product for evaluation of the scope of the hybrid approach on HVAC

The first phase involves the firsts contact between the technical team and the customer. This allows the technical team to study all the documentation, data, information related to the components and system understudy.

1. Visit and study the real system, analysis available data, and mapping of FMs and variables.
2. Estimation of diagnostics and prognostics performance.
3. Analysis of the models developed by the railway company; then, proposal of models for deploying both the diagnostics and prognostics performance.

6.2 Phase 2: Development of diagnostics and prognostics processes using a hybrid approach to HVAC (HyMA-HVAC)

After the study and proposal submitted in the first phase. The project should be narrowed down and ready to start this phase.

1. Modeling of the system and subsystems chosen. Determination of the most appropriate modeling in each case: compressors, heat exchangers, air diffusion, blowers....
2. Parametrization and fine-tune of models with available operational information.
3. Selection of FMs based on the performed analyses and modeling capabilities.
4. Giving an understanding of the physics of the selected FMs for integrating them in the model.
5. Generation of synthetic data under unique fault conditions, if possible, varying severities.
6. Study of the most suitable hybridization strategy in each case for the export of results to intermediate files; so that, the railway company provides data of failure to its system: limit values, rules, data export for data-based modeling... expanding the database of knowledge of FMs and operation parameters.
7. Implementation of diagnostics and prognostics processes based on the hybridization of data sources.
8. Transversely, transfer and integration of developed models, services, and work methodology; thus, the railway company may integrate the new strategy and tool in their current system.

7 Discussion

Once the digital twin 3.0 is tested and ready for the use, it can analyze the behavior of the system. The data will be taken from the sensors every thirty minutes; the system will record the operational data, parameters, and variables in a dataset as a fingerprint. It will be compared with the fingerprints previously saved. There are two possible situations: first, an alarm is not detected. Second, an alarm is detected. In the second case, the algorithm chooses the data with the biggest changes in the value in comparison with the previous value.

If it is a false alarm is detected, the fingerprint and the operational data will be deleted; if it is not a false alarm, the algorithm will estimate the RUL considering the operational data. The RUL will also be estimated when the algorithm does not detect any alarm.

The RUL is estimated using the fingerprint, operational data, and context data [10]. It is important to highlight the importance of FMs related to critical components in train transportation. One of the peculiarities of this implementation is the effort made to evaluate the safety and environmental risk, this means that in this field, the implementation cannot consider just the operational and reliability risks. This is because a failure in this field can affect people or the environments; thus, safety and environmental risks become more important than reliability of systems.

The development allows us to know the behavior of the system and its progression. Thus, it shows and analyses how the degradation of the system varies in real-time, which reduces the time between maintenance instructions, and gives supports to maintenance area for managing the maintenance tasks.

8 Conclusions and Future Work

This research work starts with a rigorous study and evaluation of the maturity level of the current diagnostics and prognostics methodology developed for HVAC system. It is crucial for both knowing the utility of the available information and for having an overview of the personnel abilities related to CBM, which is important for the posterior staff training.

The data-driven approaches have a good result, but in train transportation, maintainers replace the critical components in early stages of degradation; thus, information is missing, and most of them are part of the advanced stages of degradation, this means that the approaches cannot identify several FMs in these stages. The HyMA proposed will use physics-based model, which uses real data, to generate synthetic data to overcome the aforementioned lack of data. Thus, many FMs in advanced stages of degradation will be identified by the proposed model.

The knowledge of more FMs and the possibility to predict accurately the RUL of a system reduce maintenance cost; a robust CBM supports decision making process; therefore, this allows maintainers to give components longer service life under required operational conditions.

Longer times between maintenance tasks implies the reduction of the spare parts inventory, and then, the reduction of maintenance cost.

The data-driven model is trained using data acquired from the real system and synthetic data, which is generated by the physics-based model. The synthetic data contains FMs that are already defined in the literature, experience, or other sources; thus providing a HyMA fully useful. Nevertheless, giving critical components a longer service life could results with the appearance of new FMs which have never been detected before, the aforementioned “black swan losses”.

The future of this work is focusing on detecting and identify black swan losses for researching methods to identify the behaviour of every unknown failure.

References

[1] Galar D, Kumar U. eMaintenance: Essential Electronic Tools for Efficiency. Academic Press, 2017.

[2] An D, Kim N H, Choi J.*Practical options for selecting data-driven or physics-based prognostics algorithms with reviews.* Reliability Engineering and System Safety, vol. 133, pp. 223-236, 2015.

[3] Leturiondo U, Mishra M, Galar D, Salgado O. *Synthetic data generation in hybrid modelling of rolling element bearings.* Insight - Non-Destructive Testing and Condition Monitoring, vol. 57, nº 7, pp. 395-400, 2015.

[4] Heng A, Zhang S, Mathew J. *Rotating machinery prognostics: State of the art, challenges and opportunities.* Mechanical Systems and Signal Processing, vol. 23, nº 3, pp. 724-739, 2009.

[5] Turner W, Staino A, Basu B. *Residential HVAC fault detection using a system identification approach.* Energy and Buildings, vol. 151, pp. 1-17, 2017.

[6] Iyengar S, Lee S, Irwin D, Shenoy P, Weil B. *WattHome: A Data-driven Approach for Energy Efficiency Analytics at City-scale.* 2018.

[7] Aven T. *On the meaning of a black swan in a risk context.* Safety Science, vol. 57, pp. 44-51, 2013.

[8] Galar D. *Hybrid Models & Digital twins as prognosis enablers*. In 3rd Maintenance Congress, Bilbao, 2019.

[9] Leturiondo U, Salgado O, Ciani L, Galar D, Catelani M. *Architecture for hybrid modelling and its application to diagnosis and prognosis with missing data.* Measurement, vol. 108, pp. 152-162, 2017.

[10] Galar D, Thaduri A, Catelani M, Ciani L. *Context awareness for maintenance decision making: A diagnosis and prognosis approach*. Measurement, vol. 67, pp. 137-150, 2015.

Application of CAE to Model and Simulate Wheel-ground Contact in Railway Vehicle

Julian Malaka

Faculty of Mechanical Engineering, Silesian University of Technology, Konarskiego 18A, 44-100 Gliwice, Poland
julian.malaka@polsl.pl

SNE 31(3), 2021, 127-132, DOI: 10.11128/sne.31.tn.10573
Received: March 10, 2021 (Selected EUROSIM 2019 Postconf. Publ.); Revised: August 24, 2021; Accepted: August 30, 2021
SNE - Simulation Notes Europe, ARGESIM Publisher Vienna, ISSN Print 2305-9974, Online 2306-0271, www.sne-journal.org

Abstract. Drive is one of the most vital elements of technological machines, transport equipment and vehicles. Its selection process is to ensure appropriate motion parameters, that it why mechanical analysis is crucial. Modern CAE (Computer Aided Engineering) tools facilitate and accelerate designers' work, but they can also be misleading if obtained results are misinterpreted. Scepticism with regard to computer simulations is indispensable so as not to hastily recognise something as an ultimate solution to a given problem hastily. In the software based on the visualisations of designed systems, a user is usually not able to influence the motion-describing equations and the method of solving them directly. Most results can yet be evaluated on the basis of the mathematical descriptions of systems under consideration.
This is the procedure which I used to conduct the verification and validation of a model created with the application of a CAE tool. In the article I described the object of the research, the process of its preparation and analysis as well as the results which eventually determine the usefulness of the selected technique in the modelling of vehicle drive mechanics. I named the problems related to the creating of simulations and I suggested solutions to them. The activities carried out provide information helpful in the correct use of the tools that facilitate calculations as well as in the interpretation of the results.

Introduction

The multitude of phenomena which may accompany the contact of rigid bodies results in the complexity of the contact modelling and simulation.

In order to perform the calculations it is necessary to know the parameters determined experimentally in a given combination of materials and geometry. One should also perform the preliminary assessment of the factors which influence the behaviour of modelled objects, and know the approximate course of the simulation. The computer analysis of the deformation of bodies and the dynamics of their contact requires high computing power, which is why only the phenomena of the actual significance are taken into consideration.

I suggest the use of the dynamic simulation method, which is available in CAD program and which can be easily and swiftly apply in the design process. The objective of the research described in the publication was to verify and analytically validate the model of the wheel and suspension system of a railway vehicle, created in the CAE environment. By the verification I mean the determination whether the implementation of a model is in accordance with the assumptions and allows to show specific features of an object. The validation is to determine whether a model in a given field of application accurately reflects the reality [1, 2, 3, 4]. The considerations to the issue in question lead to the development of knowledge in respect of the techniques of the drive system simulation. It is particularly vital in the process of the virtual prototyping of vehicles, transport equipment or technological machines. The fast and adequately accurate numerical analysis of the behaviour of objects enables the streamlining of the design process and the reduction of the adverse event risks in the reality.

In the simulation of the system under consideration it is important to present the events resulting from the wheel-ground contact. It is known that if a wheel is driven at too high acceleration, the slip occurs. The limit value of the acceleration can be easily determined analytically. The phenomenon was observed in an actual, physical model of a vehicle.

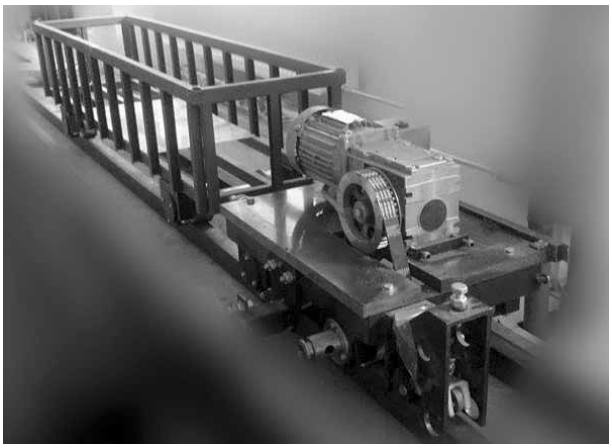

Figure 1: View of physical model of system under consideration.

The research is to demonstrate whether the CAE model enables its representation with a high degree of accuracy. The solution can be assessed on the basis of the mathematical description of the simple case under consideration. The use of the suggested technique in the analysis of complex mechanisms is conditioned by obtaining the satisfactory results of the simulation in question. I adopted the hypothesis that the limit value of the acceleration conditioning the traction of the driving wheels which results from the simulation corresponds to the value calculated analytically. The appropriate preparation of the object and the station in the nature of the model created in the CAE software and the tools for the analysis of the simulation data enables the verification of the assumptions. This way, one can assess the usefulness of given solutions in the modelling of the phenomenon described, as well as identify problems and the key aspects in the process of creating its computer simulation.

1 Methods

The system under consideration was represented in the CAE environment in order to enable the verification of the chosen modelling method. I conducted the validation research through the comparison of the results of the computer simulation with those of the analytical calculations. For this purpose it was necessary to formulate mathematical formula and substitute relevant number values into it.

1.1 Mechanical analysis

Certain assumptions pertaining to the conditions of the operation of the physical system under consideration were adopted.

No additional slip-increasing elements (such as water, lubrication, contamination) occur during the drive, and the forces acting on individual bodies result from the distribution of the mass of the object and the front axle drive.

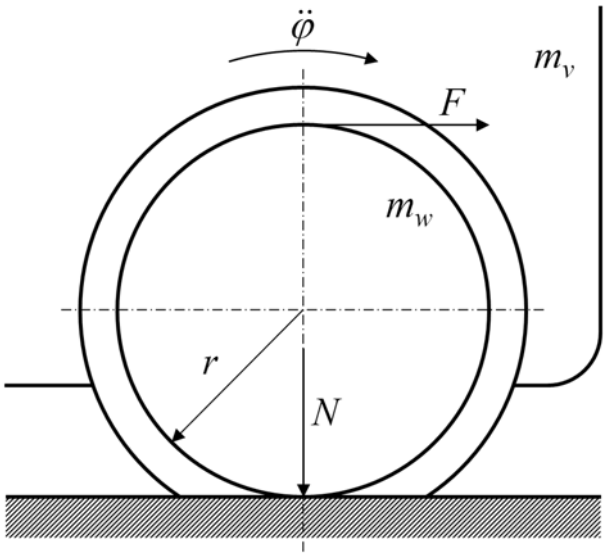

Figure 2: Mechanical diagram of vehicle drive system.

The object under consideration is presented in Figure 2, where:

$\ddot{\phi}$ – angular acceleration of vehicle wheels $\left[\frac{\text{rad}}{s^2}\right]$,
F – resultant force on the circumference of wheels $[N]$,
m_w – mass of one set of wheels [kg];
m_v – mass of vehicle, sitting on wheels [kg].
N – pressure force in the point of wheel-ground contact $[N]$,
r – vehicle wheel radius $[m]$.

The mechanical analysis enables to formulate the mathematical description of the system under consideration and determine the anticipated values of individual parameters. In the case under consideration it is the limit value of the angular acceleration of the wheels $\ddot{\phi}$ with respect of their traction to the ground. It was assumed in the calculations that the $\ddot{\phi}$ value was constant. This way the electric drive accelerates the vehicle in the physical model of the system.

The results of the calculations served as a model of the actual behaviour of the examined object. They constitute the reference during the validation of the model and the simulation being the subject matter of the research.

1.2 Modelling and CAE simulation

The examined model was created in the Siemens NX program. This environment enables the definition of the geometry and the physical features of the individual elements constituting the vehicle and the ground, their kinematic relations, parameters of the contact of the bodies and drive sources.

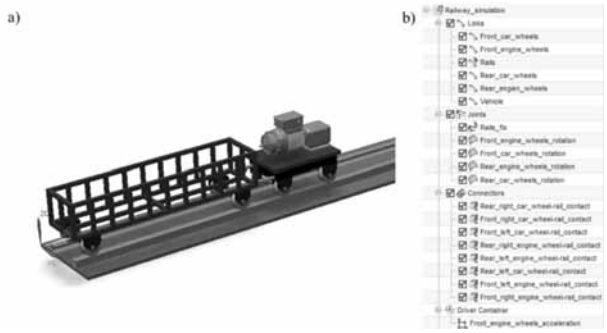

Figure 3: Siemens NX program windows with the definition of the parameters of the model: a) system geometry, b) links, kinematic joints, body contact and drive.

In order to perform the dynamic analysis in the chosen software, Multi-Body Dynamics (MDB) RecurDyn-type CAE tool was used; it is based on the ordinary differential equations and relative coordinates [6].

Conducting the simulation allows to generate the charts of the physical quantity course in the system under consideration as well as to visualise its operation in the form of a 3D animation. This allows to first verify the model, determining whether the data resulting therefrom are as expected and useful in the analysis of the contact of the drive wheels with the ground. The virtual object should behave in a way that is close to the actual one and show its specific features. In the created simulation the instantaneous value of the rotational velocity of a chosen wheel as well as other parameters can be read.

In the drive defining window the constant angular acceleration of a given rotational joint is entered – in the case under consideration it pertains to the rotation of the drive wheels in the bearing support. After the defined value is exceeded, the drive wheel slip should occur, causing the wheels turning with the velocity higher than the one of the wheels actuated by pulling the vehicle. The comparison of the course of the velocity of two elements – the drive wheel and the driven wheel – constitutes the basis for the identification of a slip in the examined system.

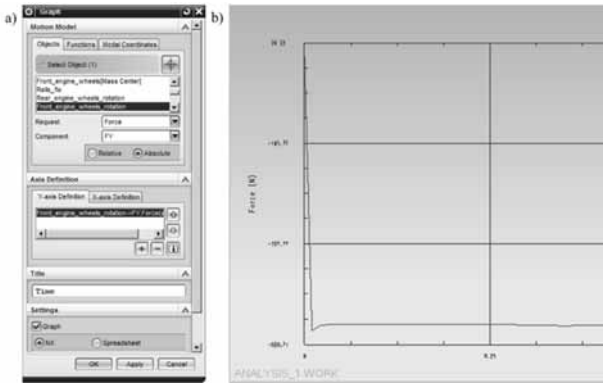

Figure 2: Chart definition window in the simulation in Siemens NX program (a) and an excerpt from the chart presenting the value of the pressure force of driving wheels on the ground (b).

The model accurately presents the reality providing the difference of the velocity occurs after there was defined the angular acceleration exceeding its limit value determined in the analytical calculations. By checking this condition one could evaluate the validity of the assumed hypothesis.

2 Results

The obtained results pertained to the mathematical description of the mechanical case under consideration and the simulation of the system in the chosen CAE environment. They made it possible to conduct the verification and validation of the analysed model of the railway vehicle in respect of the representation of the wheel-ground contact.

2.1 Results of mechanical analysis

The dynamic equation of the motion of the drive wheels had the following form (1).

$$J_{red} \cdot \ddot{\phi} = r \cdot F \tag{1}$$

In terms of retaining the traction, the cylindrical surface of wheels and the ground surface did not move with respect to each other.

The angular velocity of the driving wheels $\dot{\phi}$ is then is then fully translated into the linear velocity of the vehicle $\dot{x}$, expressed in equation (2).

$$\dot{x} = r \cdot \dot{\phi} \tag{2}$$

On the basis of (2) and the relation between the kinetic energy and the mass moment of inertia, I calculated the mass moment of the inertia of the vehicle reduced to the vehicle wheels.

$$J_{red} = 4 \cdot J_w + (4 \cdot m_w + m_v) \cdot r^2, \tag{3}$$

where J_w was a mass moment of inertia of one set of wheels [$\mathrm{kg} \cdot m^2$].

The resultant force acting at the circumference of the drive wheels could be calculated by conversion (4).

$$F = \frac{J_{red} \cdot \ddot{\phi}}{r}, \tag{4}$$

The slip of drive wheels did not occur as long as the force F did not exceed the stiction threshold T. Its value depended on the pressure N in the point of contact of the bodies and on the stiction coefficient μ between the wheel and ground materials. This was expressed in equation (5).

$$T = \mu \cdot N, \tag{5}$$

The traction limit is the situation of balancing the driving force F and the stiction threshold T. The conversions (6) resulted in a formula for the maximum angular acceleration of the drive wheels taking into account the adopted conditions.

Quantity	Symbol	Unit	Value
Mass moment of inertia of one set of wheels	J_w	$\mathrm{kg} \cdot m^2$	0.0035
Mass of one set of wheels	m_w	kg	4.4100
Mass of vehicle, sitting on wheels	m_v	kg	141.7200
Pressure in the point of the contact of drive wheels with the ground	N	N	511.6000
Vehicle wheel radius	r	m	0.0420
Coefficient of wheels-ground stiction (steel on steel)	μ	–	0.3000
Permissible angular acceleration of drive wheels	$\ddot{\phi}_{max}$	$\frac{\mathrm{rad}}{s^2}$	21.8100

Table 1: Data and results of mechanical analysis.

$$\begin{gathered} F_{max} = T \Rightarrow \\ \Rightarrow \frac{J_{red} \cdot \ddot{\phi}_{max}}{r} = \mu \cdot N \Rightarrow \\ \Rightarrow \ddot{\phi}_{max} = \frac{\mu \cdot N \cdot r}{J_{red}} \end{gathered} \tag{6}$$

Using the formulas presented, I determined the permissible angular acceleration of the drive wheels, the exceeding of which resulted in the occurrence of slip.

Data and results are collated in Table 1. The obtained value $\ddot{\phi}_{max}$ constituted the reference in the model validation process.

2.2 Simulation results

After the model had been adjusted, I conducted the simulation of the drive and generated the charts of the velocity of the drive wheel and the driven wheel at a defined acceleration.

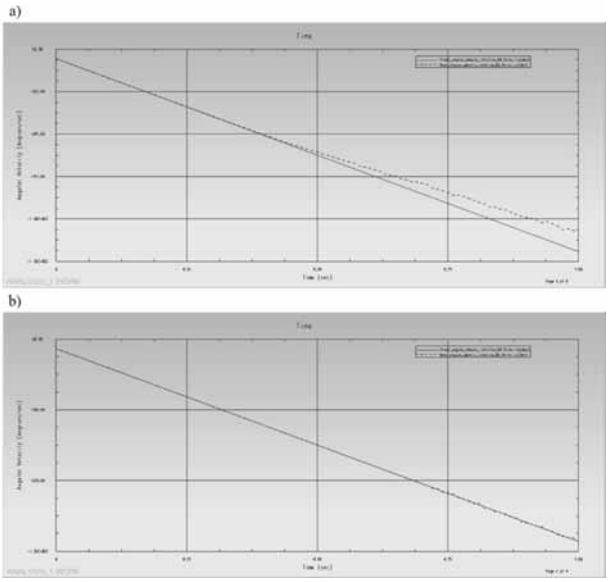

Figure 5: Charts of velocity of analysed wheels:
a) at the defined acceleration equalling 23 $\frac{\mathrm{rad}}{s^2}$ – visible velocity divergence,
b) at the defined acceleration equalling 22 $\frac{\mathrm{rad}}{s^2}$ – convergent velocities.

I observed what happened to the system when the value of the acceleration defined in the simulation was lower than the calculated one, when it equalled to it and exceeded it. I conducted a set of trials at various acceleration values. It allowed to indicate the highest of the examined values of this parameter, at which the divergence between the analysed velocities did not occur yet.

No. of trial	Defined acceleration $\left[\frac{\text{rad}}{s^2}\right]$	Discrepancy of velocity
1	22.00	No
2	23.00	Yes
3	22.34	No
4	22.50	No
5	22.70	Yes
6	22.60	Yes
7	22.55	No

Table 2: Simulation results.

Table 2 presents the results of the simulations during the trials at various values of the defined angular acceleration of the vehicle drive wheels.

3 Discussion and Conclusions

What stems from the conducted simulation trials is that the divergence of the rotational velocity of the drive wheel and the driven wheel in the modelled vehicle occurs when the threshold of the angular acceleration, equal to 22.55 $\frac{\text{rad}}{s^2}$, is exceeded.

According to the adopted assumptions and the method of the analysis of the simulation data, this is the limit value at which the slip does not occur. The value resulting from the analytical calculations was equal to 21.81 $\frac{\text{rad}}{s^2}$. It means that the inconsistency between the numerical model, created in the chosen CAE environment, and the mathematical model is approx. 3%.

On the basis of such a low level of error, it can be ascertained that the validation of the suggested solution gives a positive result. Minor discrepancies may result from rounding the values in calculations and averaging the values read from the charts throughout the simulation. The results of the research demonstrate that the modelled object behaves in a way consistent with the mathematical description, which confirms the adopted hypothesis.

3.1 Problems during verification of the model

In order to present the dynamic features of the examined system, in the model there was defined the spatial contact of rigid bodies between each of the vehicle wheels and the rails on which the wheels roll.

The software documentation [5] contains the guidelines concerning the parameters of the contact taking into consideration the materials of which the objects are made. After the application thereof, it turned out that the model did not show what had been expected. In the simulation the vehicle did not follow the expected motion path after the angular acceleration of the drive wheels had been defined. Strong bounces of the contacting surfaces occurred and the object was "thrown" out of the stage.

The major problem was the geometric form of the objects coming into contact with each other. When the convex object is located inside the concave object, their angles should not be closely adjacent to each other. This can be remedied by rounding off sharp convex edges in the geometric model [5]. In the case under consideration this situation occurred in the point of the contact of a wheel edge and the rail. The correction of the model, as shown in Figure 6, was made.

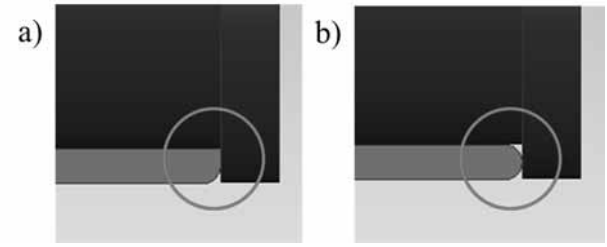

Figure 6: Point of contact of rail and wheel angle in vehicle model: a) before geometry correction, b) after geometry correction.

On the basis of the observation of the visualisation of the vehicle motion it was stated that once the correction had been made the modelled object behaved as expected.

In order to perform analytical calculations, the value of the pressure force in the point of the contact of the drive wheels and the ground was necessary. Once the simulation begins, the force should stabilise at a constant level when the vehicle is at rest (only gravity acts on it). When the default accuracy of the simulation and the contact parameters proposed in the documentation were used, the generated course of the pressure force value was strongly turbulent. It resulted from the unevenness of the objects, causing their motion with respect to each other, which was visible in the simulation at a large zoom.

The unevenness occurred even though the contact surfaces had been defined as smooth, so they should be perfectly adjacent to each other. The model was fine-tuned by adjusting the individual parameters according to the guidelines in the software documentation.

Table 3 presents the parameters which were changed from the default values.

Parameter	Default value / Value suggested in software documentation	Correct value determined experimentally
Stiffness	100000.0	10000.0
Maximum Facet Size Factor	2.0	0.5
Plane Tolerance Factor	3.0	1.0

Table 1: Wheel-ground contact parameters of model fine-tuning.

Once the experimentally defined parameters had been applied, the model met expectations and the simulation returned the values needed for the research.

3.2 CAE modelling in view of other methods of mechanical analysis

The CAE tools are an integral part of numerous design-assisting computer programs. They enable to create with ease a dynamic simulation on the basis of the geometrical model of a designed system.

In this way, neither is it necessary to build or transform equations of motion not to write a code to solve them. The methods of numerical calculations are implemented in the CAE environment. Its operation mostly boils down to defining the physical parameters of the elements of the analysed mechanism. In the chosen software ordinary differential equation and relative coordinates are applied instead of differential algebraic equations with global coordinates. This reduces the number of equations and the time needed to solve them [6].

The validation and verification of the model allowed me to select appropriate simulation settings based on the mathematical analysis. The model correctly reflecting a given phenomenon in one case with a high probability will also work in others - more complicated but similar in respect of conditions. In addition to the numerical results, the visualization of the operation of the examined system is also helpful in the analysis of solutions created.

The techniques of the preparation as well as the verification and validation of the numerical model suggested in the article improve the device prototyping process and make it more accurate. It is particularly essential for the development of modern means of transport. Modern environmental and market requirements lead to their optimisation with regard to energy consumption and motion parameters [7, 8]. The simulation calculations in the CAE environment may facilitate the choice and configuration of drives as well as predicting their operation, helping to avoid unwanted situations in reality.

References

[1] Balci O. *Verification, validation, and certification of modeling and simulation applications*. In: Proceedings of the 2003 Winter Simulation Conference, pp. 150-158. New Orleans, USA, December 2003.

[2] Karkula M. *Weryfikacja i walidacja dynamicznych modeli symulacyjnych procesów logistycznych*. Logistyka 2, pp. 717-726 (2012).

[3] Sargent R G. *Verification and validation of simulation models*. In: Proceedings of the 2011 Winter Simulation Conference, pp. 183-198. Phoenix, USA, December 2011.

[4] Schlesinger S, Crosbie R E, Gagné R E, Innis G S, Lalwani C S, Loch J, Sylvester R J, Wright R D, Kheir N, Bartos D. *Terminology for model credibility*. Simulation 3(32), pp. 103-104 (1979).

[5] Siemens Documentation: NX 12 Help. https://docs.plm.automation.siemens.com/tdoc/nx/12/nx_help, last accessed 2019/06/09.

[6] Using RecurDyn. http://www2.me.rochester.edu/courses/ME204/nx_help/en_US/graphics/fileLibrary/nx/tdoc_motion/using_recurdyn.pdf, 2019/06/09.

[7] Walker P D, Abdul Rahman S, Zhu B, Zhang N. *Modelling, Simulations, and Optimisation of Electric Vehicles for Analysis of Transmission Ratio Selection*. Advances in Mechanical Engineering 2015 (340435), pp. 1-13 (2015).

[8] Yifan D, Yugong L, Wenbo C, Keqiang L. *Optimum tyre force distribution for four-wheel-independent drive electric vehicle with active front steering.* Int. J. of Vehicle Design 65(4), pp. 336-359 (2014).

Optimized Balance of Plant for a Medium-size PEM electrolyzer. Design, Modelling and Control

Julio José Caparrós[1*], Francisco José Vivas[1], Francisca Segura[1], José Manuel Andújar[1]

[1]Centro de Investigación en Tecnología, Energía y Sostenibilidad - CITES (Research Center for Technology, Energy, and Sustainability), University of Huelva, Campus El Carmen, 21071 Huelva, Spain
julio.caparros@diesia.uhu.es

SNE 31(3), 2021, 133-141, DOI: 10.11128/sne.31.tn.10574
Received: March 10, 2021 (Selected EUROSIM 2019 Postconf. Publ.); Revised: August 31, 2021; Accepted: September 3, 2021
SNE - Simulation Notes Europe, ARGESIM Publisher Vienna
ISSN Print 2305-9974, Online 2306-0271, www.sne-journal.org

Abstract. This paper presents the design, modelling and control simulation of the Balance of Plant (BoP) for a medium-size PEM (Proton Exchange Membrane) electrolyzer. Taking into consideration the main chemical process that occurs in the electrolysis of a PEM electrolyzer, the BoP must be clearly divided into two main parts: water management and hydrogen production. An exhaustive control system is developed to test the working conditions that will allow the PEM electrolyzer to generate hydrogen in a safe and efficient way. The aim of this study is to find an equilibrated solution between minimal BoP and a correct performance, always into safety conditions of hydrogen generation. Automation software is used to model the system and perform a control logic, according to the desirable operation of the PEM electrolyzer. The BoP developed, along with the electrolyzer model and the control logic proposed contribute the PEM electrolysis technology to be expanded in the industrial market and the hydrogen to be widely used as energy carrier, as part of the renewable energy systems.

Introduction

More and more governments, companies and general society are committed to a change in energy policies, always oriented towards more energy efficient actions and more renewable energy use. But renewable energy technologies present a high dependence on climatic factors and they have not yet achieve enough reduced cost to compete with conventional supply energy systems [1]. Additionally, most of renewable sources-based systems implement their energy storage capacity in battery-based solutions.

But the use of battery presents some limitations as the relation size-energy density and the useful lifetime due to charging-discharging cycles. Then, the use of hybrid power systems based on hydrogen as backup is presented as an ideal solution to fill the gaps in the energy supply that the different renewable energy sources may provoke [2]. Studies have proven their key influence in improving the operation of hybrid energy systems and their application in smart grids [3].

Regarding the hydrogen production technology, nowadays electrolysis as a sustainable method to produce hydrogen from water, as long as the electricity required comes from a renewable energy source is the option most used in real systems [4]. Therefore, an electrolyser can convert electrical energy into chemical energy, with the use of hydrogen as an energy vector [3]. Within the types of DC electrolysis, according to the nature of the electrolyte, it is possible differentiate between Alkaline electrolysis and PEM (Proton Exchange Membrane) electrolysis.

Alkaline technology uses liquid electrolyte, with high concentrations of potassium hydroxide to provide ionic conductivity and to participate in the electrochemical reactions. By cons, PEM technology replaces the liquid electrolyte by a solid polymer electrolyte, which selectively conducts positive ions such as protons. The protons participate in the water-splitting reaction instead of hydroxide, creating a locally acidic environment in the cell [5].In alkaline electrolysis, Figure 1, the two electrodes are immersed in an electrolyte, which is usually a KOH or NaOH solution [6]. In this way, an alkaline environment is achieved, where the electrical resistivity of the water will be reduced, making the process easier. The DC voltage to be applied must be greater than that required for the water splitting and thus cause the faradaic current [7]. The electrodes are separated by a diaphragm, which allows to keep the gases separated, while being permeable to water and the passage of hydroxide ions.

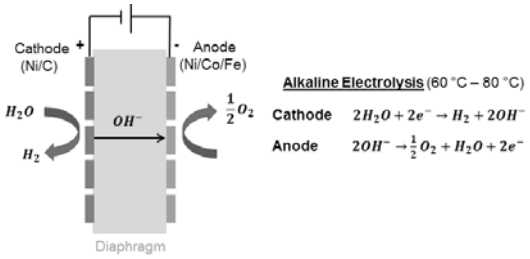

Figure 1: Alkaline electrolytic cell.

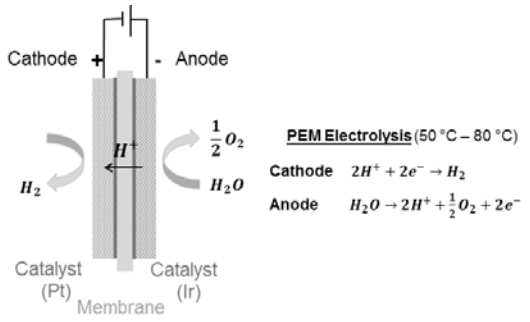

Figure 2: PEM electrolytic cell.

On the other hand, in PEM electrolysis, Figure 2, the two electrodes are in contact with the electrolyte which is a solid polymer, usually Nafion. Bipolar plates are also typically added between the solid electrolyte and the electrodes, made of platinum for the cathode and iridium for the anode, with the aim of adding resistance to corrosion [8], produced during the uncontrolled polarity of the cells and fluctuating charges.

Comparing both technologies, the main disadvantages of alkaline technology are the limited current density (0.4 Acm-2), low partial power range, limited by the inertia of the liquid electrolyte (higher than 20%-40%) [9], crossover of gases and low operating pressure (< 10-15 bar) [10]. By contrast, PEM electrolyzers can reach a current density of up to 2 Acm-2, the polymer electrolyte membrane guarantees a low gas crossover, allowing the PEM electrolyzers to work under a lower partial load range (0-10%), and it can have a compact design. This allows obtaining high enough operating pressures (30-40 bar) [11] to directly fill hydrogen tanks [5].

Additionally, regarding alkaline technology, the KOH electrolyte is highly corrosive in comparison with the PEM technology. However, poisoning by foreign ions appears and thus it has to be highly considered. The water can be easily contaminated by the impurities it contains, as well as by the corrosion produced in the metallic components of the system, such as the water pipes or even the stack components themselves.

This poisoning will result in an increase in the cell cathodic overvoltage and a reduction in operating performance [12], in addition to affecting the membrane in a reduction of its proton conductivity. Then, these are the reasons why an exhaustive design and control of the BoP (involving water management, conductivity, and purity) is important to make PEM electrolysis technology will become a competitive hydrogen production option [10].

This paper contributes to hydrogen technology implantation into the energy industrial sector. Additionally, although previous studies have been conducted in the simulation of PEM electrolyzers as power-hardware-in-loop (PHIL) simulator [13], dSPACE Hardware-in-the-Loop simulators [14], multiphysics simulators [15], dynamic simulators based on MATLAB [16] and mathematical dynamic Simulink simulators [17], it is hard to find papers that use software tools based on totally integrated automation logic.

This work combines the modelling of the control design, necessary for the safe and effective performance of the system, with the simulation of its parameters, providing compatibility and a simulation environment and quality testing. This paper describes the design, modelling and control simulation of the BoP for a medium-size PEM electrolyzer. In Section 1 the BoP is described, differentiating the hydrogen subsystem from the water subsystem. Next, Section 2 shows the control logic developed to control the electrolysis plant. Modelling and control simulation results obtained by automation software are presented in Section 3 and Conclusions from Section 4.

1 Balance of Plant of a PEM Electrolyzer

In this section it is provided a solution for the implementation of the BoP, within the specifications of safety and performance. With hydrogen technologies, it is important to carry out a study of the equipment in subsystems that capture in the BoP, which has been shown to be essential to achieve a reliable design with optimal production [18]. As it has been have seen previously, in PEM technology it is very important to ensure specific water conditions at time that safe hydrogen production conditions, in order to guarantee the correct functioning of the electrolyzer. Therefore, a specific water treatment and control system is proposed, Figure 3. This system starts acquiring water from a distilled water tank, which is convenient to have low conductivity, to ensure a longer life of the electrolytic stack.

Once the water has been introduced into the system, an injection pump is used to ensure an adequate input flow into the system. After passing through the injector pump, the water is passed through a two-phase filtering system to give it a low conductivity. Otherwise, the PEM stack could be critically impaired. In the first phase, it is obtained a Type II conductivity (ASTM Standards for Laboratory Reagent Water (ASTM D1193-91), (<1 μScm^{-1}), and in the second phase, the conductivity level achieves Type I conductivity (<0.056 μScm^{-1}).

Next the filtering stage, the water is introduced into a tank that has a double function: 1) to be a buffer with the aim to adjust the water flow inside the circuit, and 2) to act as a sink that collects the water obtained in the different drying stages of the hydrogen produced by the PEM stack. From the water level control tank, the water continues its flow to the water-control and recirculation phase. The recirculation pump regulates the water flow after the water level control tank, and the sensors' block is used by the controller to have information of all critical water parameters, such as temperature, pressure, flow, conductivity and purity, before being injected into the PEM stack. The recirculation line is proposed as a means to correct the conductivity of the water, in case it is not within the allowed range.

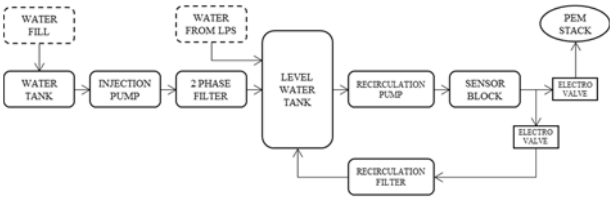

Figure 3: Balance of plant (BOP) of a PEM electrolytic stack: Water subsystem.

Additionally to the water subsystem, the hydrogen subsystem must be thoroughly designed to guarantee the safety parameters, as well as the correct drying, in order to eliminate the humidity that may be contained, sending it back to the water level tank.

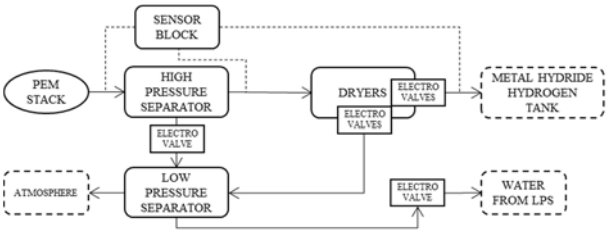

Figure 4: Balance of plant (BOP) of a PEM electrolytic stack: Hydrogen subsystem.

The hydrogen subsystem, Figure 4, is made up the PEM stack, followed by a high pressure separator. The separator takes advantage of the pressure difference in water contained in the form of moisture to dry the hydrogen. Once a high humidity gradient is reached in the high pressure separator, it allows the wet hydrogen flow (*dirty hydrogen*) to enter into the low pressure separator. Here, the hydrogen that can be mixed into the atmosphere is released, and the water is sent to the level water tank (water subsystem, Figure 3). By contrast, the dry hydrogen (*clean hydrogen*) from the high pressure separator, continues to the dryers' stage. Here, a pressure swing adsorption drying stage (PSA) is proposed, which stores and expels the water in three drying cycles. The released water is sent to the low pressure separator, following the same process previously described. After the drying phase, he hydrogen produced will be stored in metal hydride tanks. Throughout the process of hydrogen production, there is a sensors' block, which serves to control the pressure and temperature parameters of hydrogen flow in its different production and drying stages, prior to final storage.

2 Design of the Control System

The control system to be implemented into the PEM electrolyzer should be able to have information and act accordingly into the two main parts of the BoP: water management subsystem and hydrogen production subsystem. Additionally, the control logic must include the sequence of the operating states, the cooling stage, the nitrogen inertization stage, the power supply control and the management of the warnings and alarms generated during the electrolyzer operation.

2.1 Water management subsystem

Regarding the water management subsystem, Figure 5, the control logic includes three main parts: water level control block, conductivity control block and physical variables measurement and control block. Then, regarding the first control block, the activation of the level sensor in the water level tank, it activates the injection pump when the system requires more water, having a mid level. When the level is high enough, the pump is deactivated. In case of lowering the level too much, at a low level, the PEM electrolyzer stops.

In relation to the conductivity control block, the water conductivity is regulated by acting over an electrovalve to put in work the recirculation line.

Then, when the conductivity is low, the water is supplied directly to the stack without the need to subject the water to more purification treatment. In case the conductivity is medium (Type I < conductivity < Type II), before production, the recirculation circuit will be open to recirculate the water back to the purification filter. If this occurs during production, a warning is activated. And finally, if the conductivity rises above type II, the electrolyzer will be kept stopped, an alarm will be triggered, and through a process of disconnection and inertization, and an alarm will be triggered.

The physical parameters as temperature, pressure and water flow are watched with the aim to guarantee the system performance inside its operating specifications, useful life and safe conditions Otherwise, the system stops.

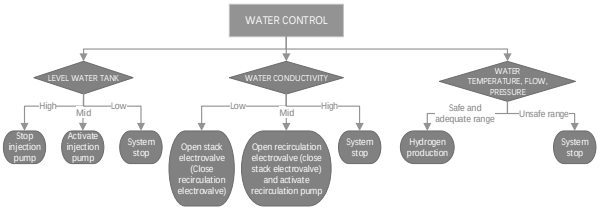

Figure 5: PEM stack control flow diagram; control diagram of the water management subsystem.

2.2 Hydrogen production subsystem

For the hydrogen subsystem control, Figure 6, it is necessary to detect the water level both in the high pressure separator (HPS) and the low pressure separator (LPS). When a mid level is detected in HPS, the valve will be open to let the accumulated water passing towards the LPS. When this happens, and the level drops, the valve closes again. In case of a high level is detected, the electrolyzer stops. Level control in LPS works in a similar way, allowing the water to pass to the water level tank when it has enough water accumulated into the LPS, as long as the valve to LPS, from HPS, is closed. In an electrolysis process, it is crucial to avoid direct contact between the water and hydrogen lines. If the level in LPS is low, the valve closes since there is not enough water to transport.

After de HPS and LPS, the dryers of the PSA stage follow a three-phase cyclic process during production. This is defined temporarily with the opening and closing of electrovalves that allow the hydrogen flow to the final storage, the accumulation of water and the purge of the water accumulated through the LPS. During all the process, temperature and pressure are controlled, entering the system in stop if they are outside the established range.

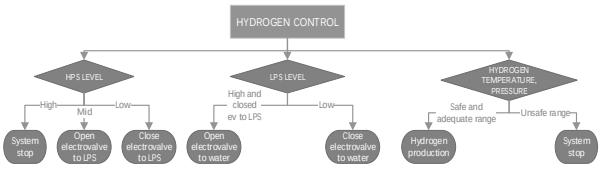

Figure 6: PEM stack control flow diagram; Hydrogen control diagram.

3 Testing of the Control Logic. Simulation Results

In this section, there will be presented the results that show the proper operation of the system following the sequence established by the developed control logic. The hardware-software tool used to implement the control logic is based on Siemens® SIMATIC STEP 7 Basic V15 platform, with TIA Portal tools for modelling, in addition to PLCSIM and WinCC RT for simulation.

Then, all the processes involved into the electrolysis plant are visualized trough the main screen, PEM electrolyzer management monitor, Figure 7a. This monitor shows the operating state of the system, allows to activate, stop or pause the production as well as to start a nitrogen inerting process. Additionally, this monitor shows operating conditions of the water and hydrogen subsystems, and it allows the cooling subsystem operation and the alarm management.

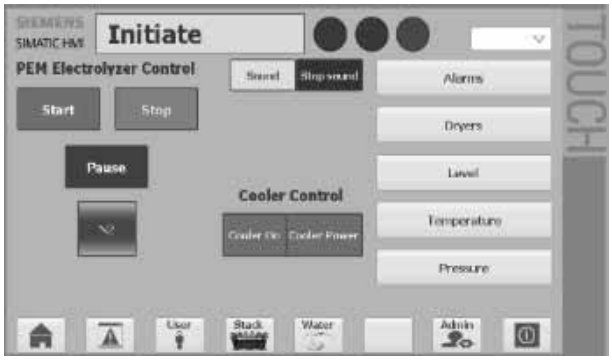

Figure 7a: Screen 1: PEM Electrolyzer management monitor.

The control system also has an interface for the stack parameters, Figure 7b, through which the simulation of the current and voltage values can be monitored, in addition to the power graph in real time.

The simulation of the hydrogen drying process, Figure 7c, shows in real time the status of each of the dryers, process status and remaining time.

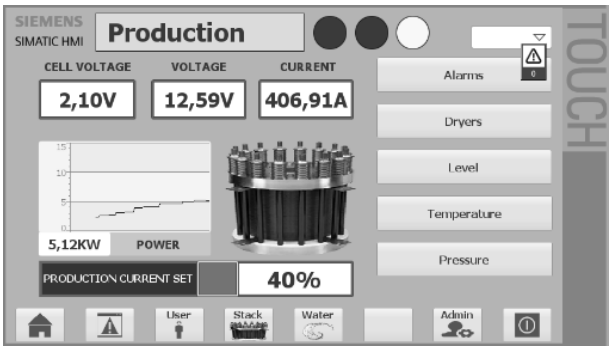

Figure 7b: Stack interface.

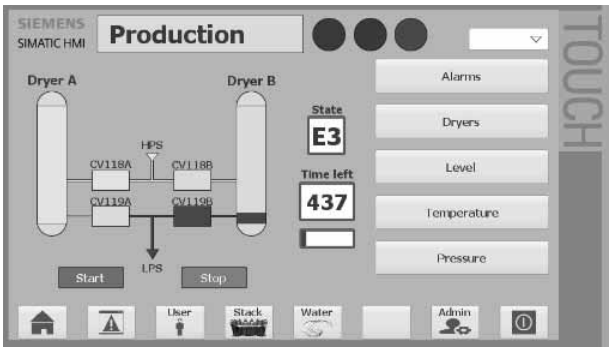

Figure 7c: Dryers stage interface.

3.1 Simulation test of water subsystem control

In this case, regarding the scheme of the balance of plant presented in Figure 3 and the control diagram developed in Figure 5, the test will be used to check the proper operation of the water management subsystem. Then, the system starts from a low level of water, Figure 8a. This involves the activation of the injection pump until the water level rises the higher level allowed, Figure 8b -Fi gure 8c. After this, the water pump will be disconnected and the water level decreases; no water is injected into the line while the stack is consuming it for the hydrogen production, Figure 8d.

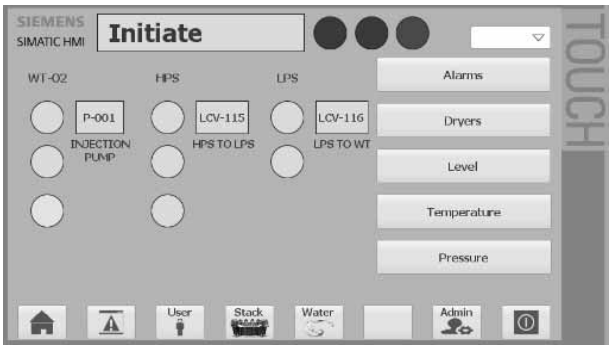

Figure 8a: Water subsystem. Low level of water; increasing.

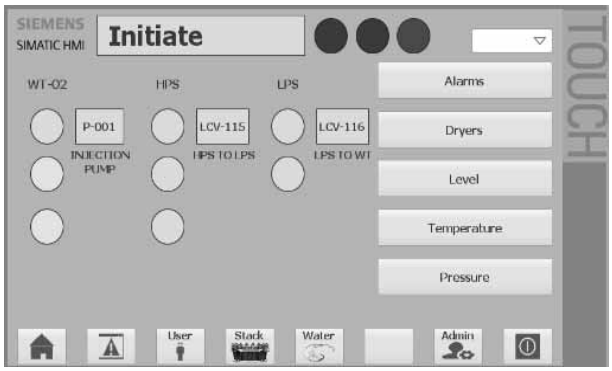

Figure 8b: Water subsystem. Mid level of water; increasing.

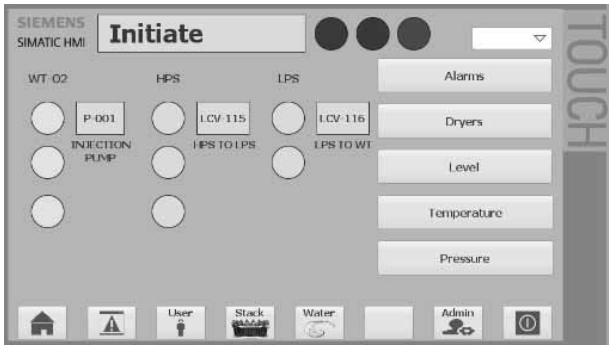

Figure 8c: Water subsystem. High level of water.

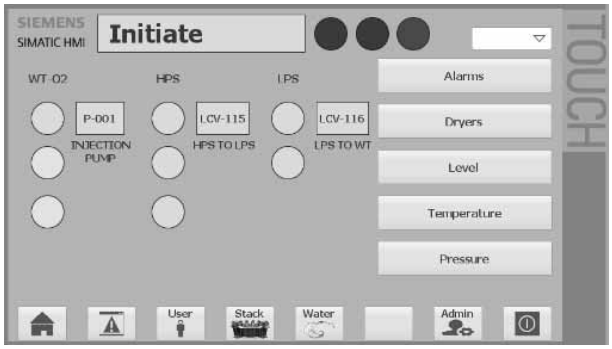

Figure 8d: Water subsystem. Mid level of water; decreasing.

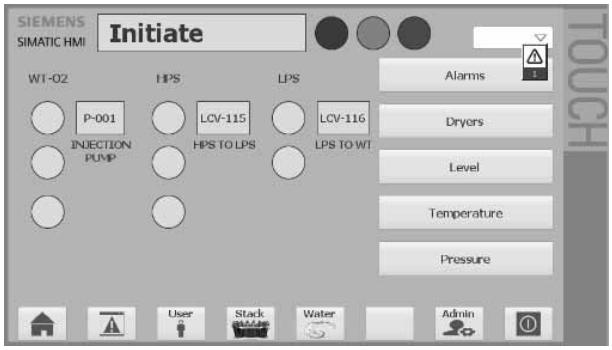

Figure 8e: Water subsystem Alarm: low level of water.

As the injection pump is deactivated, the water level begins to decrease until returning to the low level when it will be reactivated. A red colour led warms that the level has drop completely, Figure 8e.

Additionally, in case an error measurement due to a sensor malfunctioning, a yellow-colour warning light advise about this, Figure 8f.

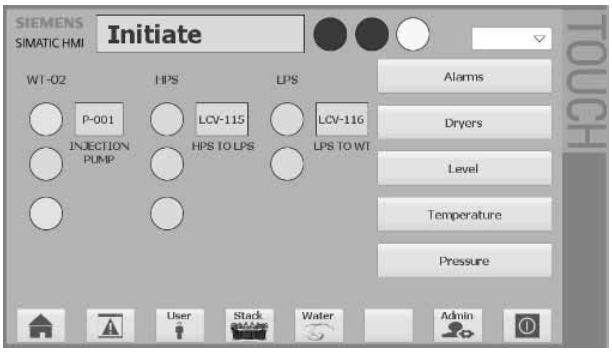

Figure 8f: Water subsystem Warning: failure of level sensor measurement.

On the other hand, from the main monitor interface it is possible to show if the water flow meets with the water conductivity and temperature requirements, Figure 9a. Then, in case Type I < conductivity < Type II, a warming led is activated, Figure 9b, and it will turn into an alarm and the system stop (inertization stage) when the water conductivity rises Type II, Figure 9c.

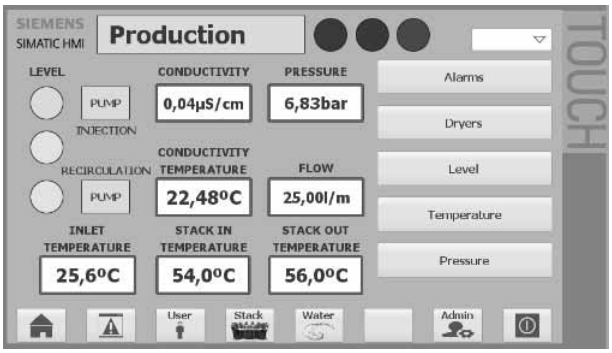

Figure 9a: Water management monitor.

In the same way, the control logic is responsible for controlling the water temperature, Figure 10a. Then, when the water temperature increases above the higher allowed value (68 ºC), the warning led is activated and the cooler is put into operation, Figure 10b.

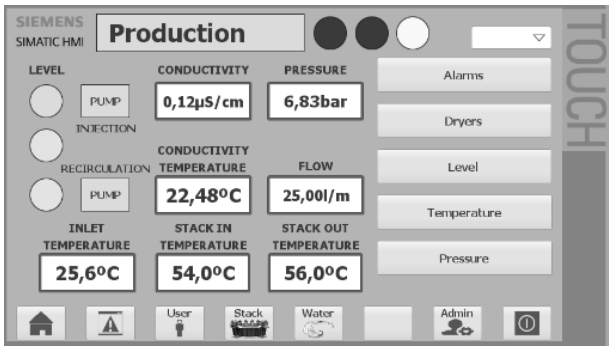

Figure 9b: Water subsystem. Warning: middle conductivity value.

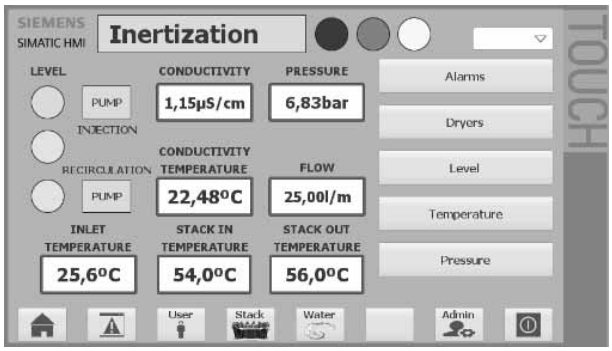

Figure 9c: Water subsystem. Alarm and inertization: high conductivity value.

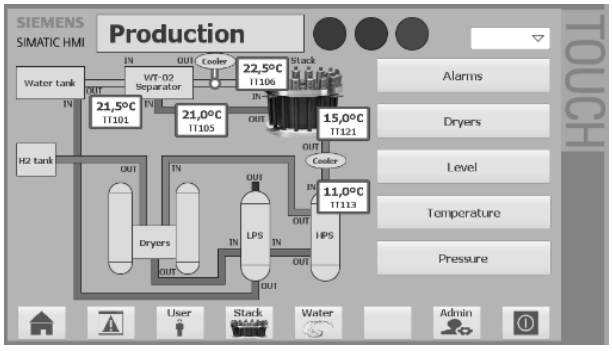

Figure 10a: Water subsystem. Temperature interface.

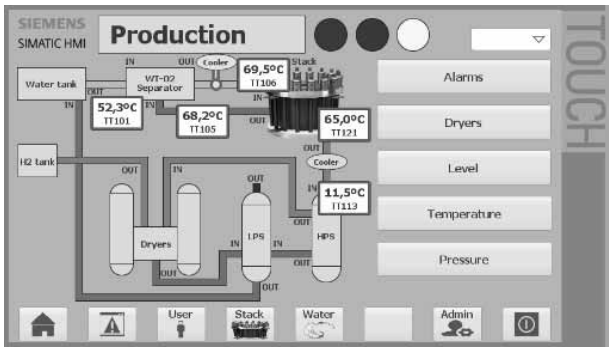

Figure 10b: Water subsystem. Warning: high water temperature.

3.2 Simulation test of hydrogen subsystem control

This second test will show the behaviour of the hydrogen production subsystem according to the balance of plant shown in Figure 4 and the logic control designed in Figure 6. Then, the test start considering a low level of condensates in HPS, Fig Figure 11a, and it will rise. When it reaches the medium level, the valve is opened, Figure 11b.

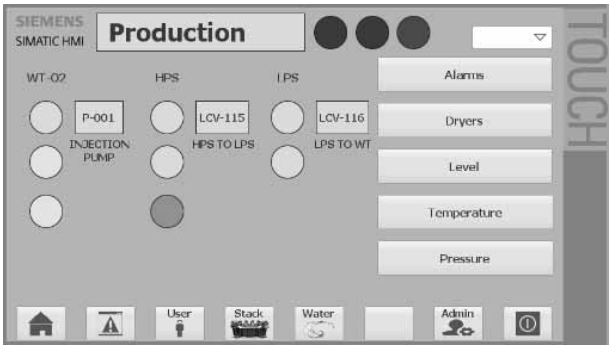

Figure 11a: Hydrogen subsystem. Low level in HPS; increasing.

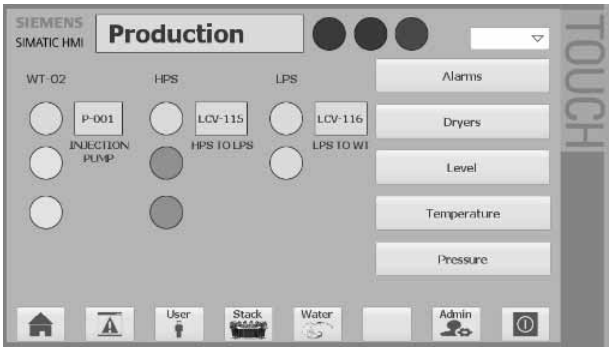

Figure 11b: Hydrogen subsystem. Mid level in HPS; valve opening.

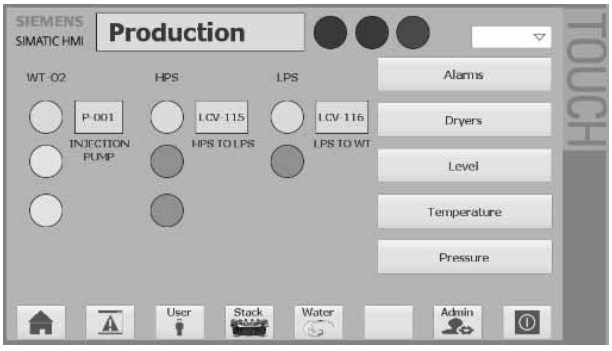

Figure 11c: Hydrogen subsystem. Low level in LPS; increasing.

Then, the condensates start their passage towards LPS, Figure 11c, until reaching the high level of LPS, Figure 11d. At this moment, it is necessary to wait for the level to drop in HPS, and with this the valve of the step to LPS, so that the opening of the LPS outlet valve is allowed, Figure 11e.

In case the HPS achieves its highest level, an alarm is activated and the production is stopped, Figure 11f.

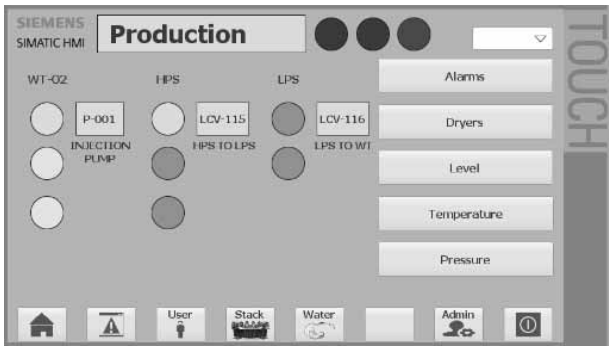

Figure 11d: Hydrogen subsystem. High level in LPS; closed valve.

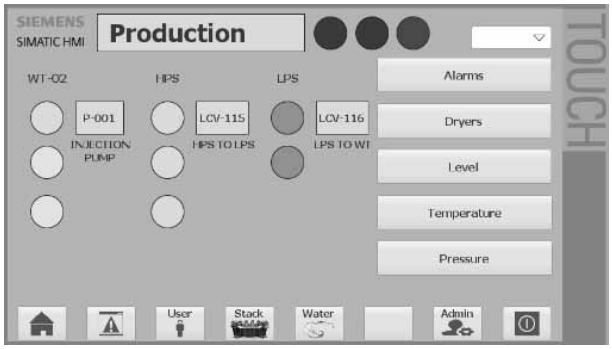

Figure 11e: Hydrogen subsystem. High level in LPS; open valve.

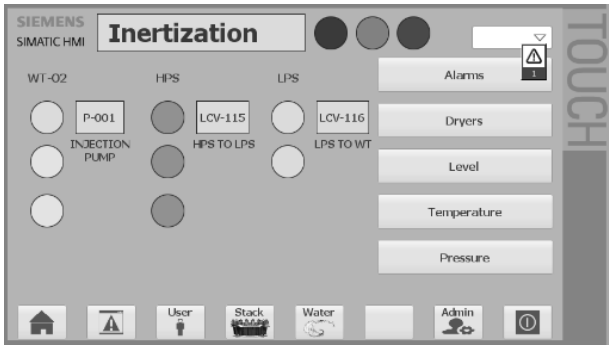

Figure 11f: Hydrogen subsystem. Alarm: high level in HPS.

Similar to water management test, it is possible to check the temperature of the hydrogen flow. In case the hydrogen temperature is above the highest allowed value (72 ºC), a warning will advise us, Figure 12a and if it continues increasing (75 ºC), an alarm is activated and the system stops; it pass from production to inertization state, Figure 12b.

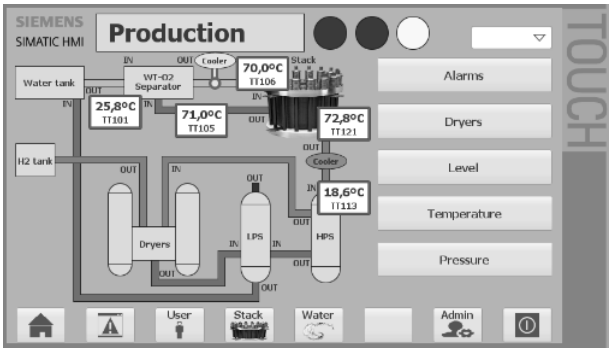

Figure 12a: Hydrogen subsystem. Warning in the temperature interface.

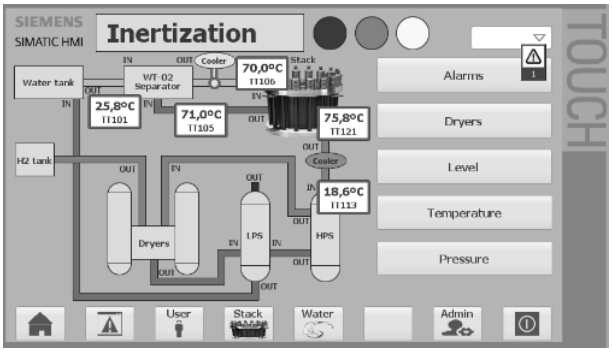

Figure 12b: Hydrogen subsystem. Alarm in the temperature interface.

4 Conclusions

Beside hydrogen is a well-known fuel to be used as energy carrier, its production by means green processes based on renewable sources hasn't yet achieved sufficient relevance into the industrial sector. Nevertheless, it is expected that the hydrogen demand increases in the next years especially in distributed generation applications; micro grids based on renewable energy with hydrogen as backup.

Then, it is necessary to focus the efforts towards the development of hydrogen production systems: improving the technology, optimizing the balance of plant and giving control proposals that contribute in the reach of a greater impact of the PEM technology in renewable energies and hydrogen as an energy carrier in power systems.

In this paper, it has been designed the balance of plant of a medium-size PEM electrolyzer and it has been implemented the control system, taking into account operating variables, automation parameters and energy and power efficiency, always under safe conditions.

The PEM electrolyzer requires two main parts that are the water management subsystem and the hydrogen subsystem. In the first part, the control system is responsible for ensuring the water level inside the allowed range, the water flow along the water pipeline, the water temperature and pressure during the production process and the water conductivity to guarantee both the efficiency of the process and the lifetime of the stack.

The hydrogen subsystem need than the controller tracks the levels in the pressure separators (HPS and LPS), acting over the valves that communicates both separators. Additionally, the control system includes the thermal management of the hydrogen flow, the pressure control along the hydrogen flow line and the control the PSA sequence in the final drying stage.

To validate the developed control logic, both subsystems, water and hydrogen, have been simulated. The results show that water and hydrogen subsystems works inside proper operating conditions and in case of warning or sensor malfunctioning, the electrolyzer is stopped through an inertization phase.

Acknowledgment

This work is a contribution of the Projects DPI2017-85540-R and UNHU15-CE-3264 supported by the Spanish Ministry of Economy and Competitiveness and by the European Union Regional Development Fund. Additionally, this work is part of the collaborations between the Research Group TEP-192of the University of Huelva, supported by the European Social Fund (ESF) and Junta de Andalucía and Ariema Energía y Mediambiente S.L.

References

[1] Daher S de F D. A multicriteria model for selecting renewable energy systems in a distributed generation context. In *2014 IEEE International Conference on Systems, Man, and Cybernetics (SMC)*, 2014, pp. 625–629. doi: 10.1109/SMC.2014.6973978

[2] Goel S, Sharma R. Performance evaluation of stand alone, grid connected and hybrid renewable energy systems for rural application: A comparative review. *Renew. Sustain. Energy Rev.*, vol. 78, pp. 1378–1389, Oct. 2017. doi: 10.1016/j.rser.2017.05.200

[3] Andujar J M, Segura F, Dominguez T. Study of a renewable energy sources-based smart grid. requirements, targets and solutions. In *2016 3rd Conference on Power Engineering and Renewable Energy (ICPERE)*, 2016, pp. 45–50. doi: 10.1109/ICPERE.2016.7904849

[4] Gandia L M, Arzamendi G, Diéguez PM. *Renewable hydrogen technologies: production, purification, storage, applications and safety*. Elsevier Science, 2013.

[5] Ayers K E, *et al.*Research Advances towards Low Cost, High Efficiency PEM Electrolysis. In *ECS Transactions*, 2010, vol. 33, no. 1, pp. 3–15. doi: 10.1149/1.3484496

[6] Manabe A, *et al.* Basic study of alkaline water electrolysis. *Electrochim. Acta*, vol. 100, pp. 249–256, 2013. doi: 10.1016/j.electacta.2012.12.105

[7] Zou H, Chen J, Fang Y, Ding J, Peng W, Liu R. A dual-electrolyte based air-breathing regenerative microfluidic fuel cell with 1.76 V open-circuit-voltage and 0.74 V water-splitting voltage. *Nano Energy*, vol. 27, pp. 619–626, Sep. 2016. doi: 10.1016/J.NANOEN.2016.07.036

[8] Bordons C, García-Torres F, Valverde L. Gestión Óptima de la Energía en Microrredes con Generación Renovable. *Rev. Iberoam. Automática e Informática Ind. RIAI*, vol. 12, no. 2, pp. 117–132, Apr. 2015. doi: 10.1016/J.RIAI.2015.03.001

[9] Carmo M, Fritz D L, Mergel J, Stolten D. A comprehensive review on PEM water electrolysis. *International Journal of Hydrogen Energy*, vol. 38, no. 12. pp. 4901–4934, 2013. doi: 10.1016/j.ijhydene.2013.01.151

[10] Vivas F J, De las Heras A, Segura F, Andújar J M. A review of energy management strategies for renewable hybrid energy systems with hydrogen backup. *Renew. Sustain. Energy Rev.*, vol. 82, 2018. doi: 10.1016/j.rser.2017.09.014

[11] Medina P, Santarelli M. Analysis of water transport in a high pressure PEM electrolyzer. *Int. J. Hydrogen Energy*, vol. 35, no. 11, pp. 5173–5186, Jun. 2010. doi: 10.1016/J.IJHYDENE.2010.02.130

[12] Andolfatto F, Durand F, Michas A, Millet P, Stevens P. Solid polymer electrolyte water electrolysis: electrocatalysis and long-term stability. *Int. J. Hydrogen Energy*, vol. 19, no. 5, pp. 421–427, May 1994. doi: 10.1016/0360-3199(94)90018-3

[13] Ruuskanen V, *et al.* Design and implementation of a power-hardware-in-loop simulator for water electrolysis emulation. *Renew. Energy*, vol. 119, pp. 106–115, Apr. 2018. doi: 10.1016/J.RENENE.2017.11.088

[14] Sanchez V M, Barbosa R, Arriaga LG, Ramirez J M. Real time control of air feed system in a PEM fuel cell by means of an adaptive neural-network. *Int. J. Hydrogen Energy*, vol. 39, no. 29, pp. 16750–16762, Oct. 2014. doi: 10.1016/J.IJHYDENE.2014.05.153.

[15] Agbli K S, Péra MC, Hissel D, Rallières O, Turpin C, Doumbia I. Multiphysics simulation of a PEM electrolyser: Energetic Macroscopic Representation approach. *Int. J. Hydrogen Energy*, vol. 36, no. 2, pp. 1382–1398, Jan. 2011- doi: 10.1016/J.IJHYDENE.2010.10.069

[16] Awasthi A, Scott K, Basu S. Dynamic modeling and simulation of a proton exchange membrane electrolyzer for hydrogen production. *Int. J. Hydrogen Energy*, vol. 36, no. 22, pp. 14779–14786, Nov. 2011. doi: 10.1016/J.IJHYDENE.2011.03.045

[17] Yigit T, Selamet O F. Mathematical modeling and dynamic Simulink simulation of high-pressure PEM electrolyzer system. *Int. J. Hydrogen Energy*, vol. 41, no. 32, pp. 13901–13914, Aug. 2016. doi: 10.1016/J.IJHYDENE.2016.06.022

[18] de las Heras A, Vivas F J, Segura F, Andújar J M. How the BoP configuration affects the performance in an air-cooled polymer electrolyte fuel cell. Keys to design the best configuration. *Int. J. Hydrogen Energy*, vol. 42, no. 17, pp. 12841–12855, Apr. 2017. doi: 10.1016/J.IJHYDENE.2016.11.051

Modelling of Methane Hydrate Formation and Dissociation using Residual Thermodynamics

Solomon Aforkoghene Aromada[1*], Bjørn Kvamme[2]

[1]Department of Physics and Technology, University of Bergen, Allegaten 55, 5007 Bergen, Norway;
Solomon.Aromada@student.uib.no, saromada@gmail.com

[2]Strategic Carbon LLC, Vestre Holbergsallmenningen 17, 5011 Bergen, Norway; *kvamme@strategic-carbonllc.com*

SNE 31(3), 2021, 143-150, DOI: 10.11128/sne.31.tn.10575
Received: March 10, 2021 (Selected EUROSIM 2019 Postconf. Publ.); Revised: August 30, 2021; Accepted: September 2, 2021
SNE - Simulation Notes Europe, ARGESIM Publisher Vienna
ISSN Print 2305-9974, Online 2306-0271, www.sne-journal.org

Abstract. The available experimental data in literature for enthalpies of hydrate formation and dissociation are limited and often lacks relevant information required for interpretation. Commonly missing information include hydrate composition, hydration number, temperature and/or pressure data, and degree of super heating during dissociation of hydrate.

Clausius-Clapeyron equations used with measured or calculated hydrate formation pressure-temperature equilibrium data is the simplest indirect methods used for evaluating enthalpy change involved in phase transition during hydrate formation or dissociation. This approach involves over-simplifications. These oversimplifications make all the data based on Clausius-Clapeyron to be unreliable. And old data using Clapeyron do not have appropriate volume corrections. We therefore propose a thermodynamic scheme (residual thermodynamics approach) which does not have these limitations. This method is based on residual thermodynamics for all properties like equilibrium (pressure-temperature) curves, free energy change as thermodynamic driving force in kinetic theories and enthalpies of hydrate formation and dissociation. The pressure-temperature equilibrium curve obtained in this work agrees well with literature.

Introduction

Natural gas hydrates are non-stoichiometric crystalline inclusion compounds (ice-like substances) formed when hydrogen-bonded water molecules form three-dimensional solid cage-like structures with cavities which entrap suitably small sized molecules of certain gases and volatile liquids known as guest molecules, under the condition of high pressure and low temperature. Unlike ice, they exist above 273.15 K (0 ˚C). Lighter hydrocarbon components [1,2] and some inorganic gases [3,4] are guest molecules that can form hydrate in their pure form.

A vast amount of natural occurring methane hydrates is distributed all over the world in the permafrost and in the oceans [5]. This huge amount of methane gas trapped in the naturally existing hydrate could be a potential source of unconventional energy. In a time when decarbonazation and the use of low-carbon energy resources have become exigent, successfully exploiting this huge amount of natural gas stored in form of hydrate will be important.

To produce this methane, any method that could be used will require supply of heat [6] to dissociate the methane hydrate. Therefore, a study of the heat of dissociation and formation of methane hydrate is important. Thus, it is essential to examine how best these heat (exothermic for formation and endothermic for dissociation) can be better evaluated. The amount of heat required for dissociation of the hydrate is the same amount that is released when the hydrate is form. The difference in representation is in the sign, negative for formation and positive for dissociation.

Hydrate formation is a complex exothermic process that involves competing phase transition mechanisms and routes where kinetics and thermodynamics play important role. The exothermic heat released (enthalpy of formation) during the phase transition is one of the most significant thermodynamic properties that we need for proper understanding of the phase transition process. This heat is either measured directly [7] by experiment or indirectly using Clausius-Clapeyron [8] or Clapeyron [9] modelling approaches. These approaches have some limitations and the results obtainable in literature often lack important information.

For example, the available experimental data in literature for enthalpies of hydrate phase transition are limited and often lacks relevant information required for interpretation. Frequently missing information are composition of the hydrates, hydration number, temperature and/or pressure data, and degree of super heating required during dissociation of hydrate. Clausius-Clapeyron equations used with measured or calculated hydrate formation pressure-temperature equilibrium data is the simplest indirect methods used for evaluating enthalpy change during hydrate phase transition. This approach involves over-simplifications. These oversimplifications make all the data based on Clausius-Clapeyron to be unreliable. And old data from Clapeyron do not have appropriate volume corrections.

Therefore, a consistent thermodynamic scheme, residual thermodynamics approach is proposed in this work and implemented based on the the trivial thermodynamic relationship between enthalpy change and free energy change. This method is based on using residual thermodynamics for all properties like equilibrium (pressure-temperature) curves, free energy change as thermodynamic driving force in kinetic theories and enthalpies of hydrate formation and dissociation. The approach eliminates the limitations.

The relevant modelling equations are presented, and simulations were performed. The results are discussed are compared with literature.

1 Modelling of Hydrate Dissociation with Residual Thermodynamics

Our modelling approach is summarized in this section. The free energy change for a specific hydrate phase transition can expressed as:

$$\Delta G^{(H_1)} = x^H_{H_2O}\left(\mu^H_{H_2O}\left(T,P,\overrightarrow{x^H}\right) - \mu^{water}_{H_2O}(T,P,\vec{x})\right) + \sum_j x^H_j\left(\mu^H_j\left(T,P,\overrightarrow{x^H}\right) - \mu^{gas}_j\left(T,P,\overrightarrow{y^{gas}}\right)\right) \quad (1)$$

The superscript H_1 distinguishes the specific heterogeneous phase transition from other hydrate formation phase transitions. T is temperature, P is pressure. x is mole-fraction in either liquid or hydrate (denoted with a subscript H) while y is mole-fraction in gas (or liquid) hydrate former phase. j is an index for hydrate formers.

Superscript *water* denotes water phase that is converted into hydrate. Generally, this is ice or liquid but, in this work, we only consider liquid water. μ is chemical potential. These chemical potentials are convenient in discussing other routes to hydrate formation and associated hydrate former chemical potentials since any variation in chemical potential of hydrate formers will lead to changes in hydrate compositions and hydrate free energies. This is fundamentally important since any assembly of molecules with unique density and composition is a unique phase. Liquid water chemical potential is calculated from the symmetric excess conventions as:

$$\mu_{H_2O}(T,P,\vec{x}) = \mu^{pure,H_2O}_{H_2O}(T,P) + R.Tln\left(x_{H_2O}.\gamma_{H_2O}(T,P,\vec{x})\right) \approx \mu^{pure,H_2O}_{H_2O}(T,P) + R.Tln\left(x_{H_2O}\right) \quad (2)$$

$$\lim(\gamma_{H_2O}) = 1.0 \text{ when } x_{H_2O} \text{ tends to unity}$$

The focus here is to illustrate the complexity of multiple hydrate formation in systems of water and CH_4. We used a simpler kinetic model which is more visible in terms of the various contributions to the hydrate phase transition dynamics. As such the approximation on the right-hand side of equation (2) is accurate enough for the purpose. The solubility of CH_4 in water is small and the right-hand side will be close to pure water chemical potential. Chemical potential for water in the hydrate structure is given by [10]:

$$\mu^H_{H_2O} = \mu^{O,H}_{H_2O} - \sum_{k=1,2} RTv_k \ln\left(1+\sum_i h_{ij}\right) \quad (3)$$

in which H denote hydrate and 0 in the superscript on first term on right hand side means empty clathrate. These chemical potentials are readily available from model water (TIP4P) simulations [11]. The number of cavities per water, v_k is 1/23 for small cavities of structure I and 3/23 for large cavities. With CH_4 as only the guest, i is 1 in the sum over the canonical partition functions for small and large cavities.

$$h_{ki} = e^{\beta[\mu_{ki} - \Delta g_{ki}]} \quad (4)$$

The enthalpy change is trivially related to the corresponding free energy change by the thermodynamic relationship:

$$\frac{\partial\left[\frac{\Delta G^{Total}}{RT}\right]_{P,\vec{N}}}{\partial T}=-\left[\frac{\Delta H^{Total}}{RT^2}\right] \quad (5)$$

The superscript total is introduced to also include the penalty of pushing aside the old phases.

Practically the total free energy change will be equation (2) plus the interface free energy times contact area between water and hydrate forming phase during the nucleation stage divided by number of molecules in the specific core size. Since critical nuclei sizes are small the whole particle can be considered as covered with water due to capillary forces. Above critical core size the penalty diminishes rapidly relative to the free energy benefits from (2).

$$\frac{\partial\left[\frac{\mu^{H}_{H_2O}}{RT}\right]_{P,\vec{N}}}{\partial T}=\frac{\partial\left[\frac{\mu^{0,H}_{H_2O}}{RT}\right]_{P,\vec{N}}}{\partial T}-\left[\frac{\partial}{\partial T}\right]_{P,\vec{N}}\left[\sum_{k=1,2}v_k\ln\left(1+\sum_i h_{ki}\right)\right] \quad (6)$$

For the liquid water phase in (2), as wcell as for the empty hydrate chemical potential on right hand side of equation (6) results are trivially obtained from [12] while the second term on right hand side is reorganized as:

$$\left[\frac{\partial}{\partial T}\right]_{P,\vec{N}}\left[\sum_{k=1,2}v_k\ln\left(1+\sum_i h_{ki}\right)\right]=\left[\sum_{k=1,2}v_k\frac{\sum_i\left[\frac{\partial h_{ki}}{\partial T}\right]_{P\vec{N}}}{\left(1+\sum_i h_{ki}\right)}\right] \quad (7)$$

And the derivatives of the cavity partition functions can be written as:

$$\left[\frac{\partial h_{ki}}{\partial T}\right]_{P\vec{N}}=h_{ki}\left[-\frac{1}{RT^2}(\mu_{ki}-\Delta g_{ki})+\frac{1}{RT}\left(\frac{\partial\mu_{ki}}{\partial T}-\frac{\partial\Delta g_{ki}}{\partial T}\right)\right] \quad (8)$$

The partial derivatives in the last term on right hand side is numerically differentiated from the polynomial fits of [11].

$$\frac{\partial\left[\frac{\mu^{H}_{H_2O}}{RT}\right]_{P\vec{N}}}{\partial T}=\frac{\partial\left[\frac{\mu^{0,H}_{H_2O}}{RT}\right]_{P\vec{N}}}{\partial T}+\left[\sum_{k=1,2}v_k\frac{\sum_i h_{ki}\left[\frac{1}{RT^2}(\mu_{ki}-\Delta g_{ki})-\frac{1}{RT}\left(\frac{\partial\mu_{ki}}{\partial T}-\frac{\partial\Delta g_{ki}}{\partial T}\right)\right]}{[1+\sum_i h_{ki}]}\right] \quad (9)$$

$$H^{0,H}_{H_2O}=-RT^2\frac{\partial\left[\frac{\mu^{H,0}_{H_2O}}{RT}\right]_{P\vec{N}}}{\partial T}+\left[\sum_{k=1,2}v_k\frac{\sum_i h_{ki}\left[\frac{1}{RT^2}(\mu_{ki}-\Delta g_{ki})-\frac{1}{RT}\left(\frac{\partial\mu_{ki}}{\partial T}-\frac{\partial\Delta g_{ki}}{\partial T}\right)\right]}{[1+\sum_i h_{ki}]}\right] \quad (10)$$

For liquid water, the enthalpy is even more trivially obtained by numerical differentiation of the polynomial fit of chemical potential as function of T given by [10].

In an equilibrium situation, chemical potential of the same guest in the two cavity types must be the same and these have to be equal to the chemical potential of the same molecule in the phase that it came from. For the heterogeneous case this means chemical potential of the molecule in gas (or liquid) hydrate former phase. But outside of equilibrium the gradients in chemical potentials as function of *T, P* and mole-fractions have to reflect how the molecule behaves in the cavity.

Enthalpies for various guest molecules in the two types of cavities can be evaluated by Monte Carlo simulations along the lines described by [10-12] by sampling guest water interaction energies and efficient volumes from the movements of the guest molecules. That is:

$$H^R_{ki}=U^R_{ki}+(z_{ki}-1)RT \quad (11)$$

where U is energy and superscript R denote residual (interaction) contribution. z_{ki} is compressibility factor for the guest molecule i in cavity k. Consistent ideal gas values for the same interaction models that were applied in calculation of the residual values is trivial.

$$z_{ki}=\frac{PV_{ki}}{k_BT} \quad (12)$$

In which k_B is Boltzmann's constant and is the excluded volume of a molecule of type *i* in cavity of type *k*. This latter volume is calculated from the sampled volume of centre of mass movements plus the excluded volume due to water/guest occupation. Slightly more complex sampling and calculation for molecules which are not monoatomic (or approximated as monoatomic as methane) but still fairly standard (6, 7) and explicit discussion on this is not needed here. The derivative of the chemical potential of a guest molecule *i* in cavity type *k* with respect to temperature as needed in equation (9) is the negative of partial molar entropy for the same guest molecule and can be calculated according to:

$$\left[\frac{\partial \mu_{ki}}{\partial T}\right]_{P\vec{N}} = \frac{\mu_{ki} - H_{ki}}{T} \tag{13}$$

Equation (10) can then be rearranged into:

$$H_{H_2O}^{0,H} = -RT^2 \frac{\partial\left[\frac{\mu_{H_2O}^{H,0}}{RT}\right]_{P\vec{N}}}{\partial T} + \left[\sum_{k=1,2} v_k \frac{\sum_i h_{ki}\left[H_{ki} - \Delta g_{ki} + T\frac{\partial \Delta g_{ki}}{\partial T}\right]}{[1+\sum_i h_{ki}]}\right] \tag{14}$$

Residual enthalpies for hydrate former in a separate hydrate former phase are trivially given by:

$$H_{ki}^{R} = -RT^2 \sum_i y_i \left[\frac{\partial \ln \phi_i^{gas}}{\partial T}\right]_{P, y_{j\neq i}} \tag{15}$$

In which the same equation of state (SRK) is utilized as the one used for calculating fugacity coefficients for the chemical potentials.

2 Methane Hydrate Equilibrium Pressure - Temperature

Hydrate equilibrium pressures for methane hydrate formation were estimated for a temperature range of 273K to 290 K as can be seen in Fig. 1. The estimates are compared with literature [9, 13] and there is a very good agreement even though we did not fit interaction parameters, which is not the priority here.

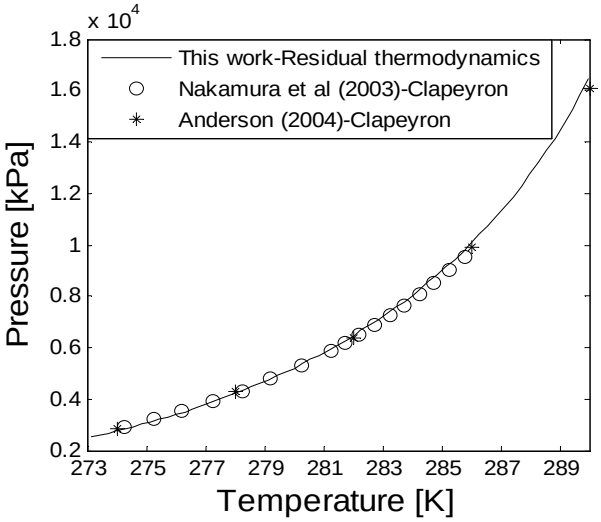

Figure 1: Estimated methane hydrate equilibrium pressures using residual thermodynamics (this work) compared with literature [9,15].

The priority is to keep the statistical mechanical model free of adjustable parameters in all terms, together also with empty hydrate chemical potentials and chemical potentials for ice and liquid water.

3 Enthalpies of Methane Hydrate Formation along Equilibrium Curve

The experimental data available in literature for enthalpies of hydrate formation and dissociation are limited and often lacks significant information required for interpretation. Commonly missing information include hydrate composition, hydration number, temperature and/or pressure data, and degree of super heating in the course of dissociation of hydrate. Hydrate dissociation enthalpy are measured directly or evaluated indirectly. Calorimetry, NMR, Raman, pressure drop X-ray diffraction are some of the methods used for direct measurement. And for the indirect method,

Clapeyron and Clausius-Clapeyron equations are the approaches that are usually employed. The simplest indirect method is the Clausius-Clapeyron equation [8] and it is used with measured or calculated hydrate formation pressure-temperature equilibrium data. The simplifications in this approach limit the accuracy of results for higher pressures. Therefore, more recent studies use the original Clapeyron equation with various models for the volume changes associated with the phase transitions [9].

These oversimplifications make data based on Claussius-Clapeyron to be unreliable. In addition, the old data using Clapeyron do not have appropriate volume corrections. The data from Anderson involves very high filling fractions of the hydrate. Some of the calculated filling fractions reported by Anderson [9] seem very high, even up to 282 K. And most calorimetry data do not have any measured filling fraction and often use a con

Therefore, there is a need for consistent and reliable enthalpies of hydrate formation or dissociation data, and that is why we propose the use of residual thermodynamics. This method is based on residual thermodynamics for all properties like equilibrium (pressure-temperature) curves, free energy change as thermodynamic driving force in kinetic theories, and enthalpies of hydrate formation and dissociation. This scheme is also not limited to heterogeneous hydrate formation from water, and a separate hydrate former phase. It can be used to evaluate associated enthalpy change in homogeneous hydrate formation from dissolved hydrate forming guest molecules in water. Even though we have applied the theory to one component (methane) because of the acceptable limit of work to be presented, there is no limitation in its application to other guest molecules and mixtures of hydrate formers (as we shall demonstrate in subsequent work), the formalism is written for mixtures. Another important advantage of this approach, unlike the Clapeyron method is that it can easily be extended to conditions outside of equilibrium as well as to other hydrate phase transitions. Applicable examples are enthalpy changes associated with hydrate forming from dissolved hydrate guest molecules in water, and the reverse process of hydrate dissociation to water under-saturated with guest molecules. Additional applicable hydrate phase transitions are nucleation of hydrate towards mineral surfaces. Our filling fractions seem realistic and reproduce equilibrium pressures as shown in Figure 1. Anderson [9] used a specific code. This code is based on fitting of also the difference between chemical potential of empty hydrate and water as well as associated fitting of several related differences needed to calculate chemical potential differences up to actual temperatures and pressures. Fitting fundamental properties like chemical potentials is by itself questionable.

Our estimates of enthalpy change for methane hydrate formation from pure methane and liquid water along the hydrate equilibrium (P, T) curve, that is three-phase co-existence conditions (liquid water, hydrate and gas simply represented as L-H-V) are presented in Figure 2 and have been calculated using residual thermodynamics.

In this figure, our intention is not to validate our scheme using these literature values. Based on all the limitations we have pointed out above, we do not expect our result to agree perfectly with literature. However, Nakamura et al. [12] results are closer to the results of our work compared to the other literature. The results estimated from Clapeyron approaches by Nakamura et al. [13] and Anderson [9] disagree significantly both in values and trend. There is a very wide difference or deviation in their results. The work of Nakamura et al. [13] even though it shows a very weak dependence on temperature till around 280 K, follows similar trend with our work, therefore, we have Table 1 for easy comparison. Table 2 gives the results from using our scheme and some literature [9, 14, 15]. Kang et al. [15] estimated enthalpy change of phase transition at 274.15 K from isothermal micro-calorimeter experiment is only also close to result of this scheme at 274.10 K. it is only 0.4 % higher than the estimated values from the residual thermodynamic approach. The pressure at this temperature is missing in the paper of Kang et al. [15]. It is also important to keep in mind that also experiments have various limitations. Some of these are discussed by Kvamme et.al. [16]. Anderson's [9] results are the lowest and the trend is opposite to those of Nakamura et al. [13] and this work. Application of this scheme for CO_2 guest molecule and the implication of enthalpy changes of hydrate phase transitions for simultaneous methane production from in-situ methane hydrates and storage of CO_2 (zero-emission concept) as CO_2 hydrate can be found in [17, 18].

Claussius approach, or simplified Claussius-Clapeyron approach, is generally not applicable for mixtures. At least not in the simple form used by Anderson [9] and others. For a pure component there is no composition dependency on either side of the co-existence curve. This changes the formal derivation of Claussius when changing to mixtures and might make it difficult to use. Hydrate is a mixed component and even the use of Clapeyron for hydrate is not straightforward. There are publications that formaluate a fugacity for hydrate, which at best is empirical. Fugacity is uniquely related to chemical potential on individual component basis.

To the best of our knowledge, there are no other models for enthalpy that can be utilized for gas mixtures [19, 20], and for different hydrate phase transitions like for instance hydrate formation from dissolved hydrate formers in water [21]. In principle there is no limit in the various hydrate formation possibilities.

As long as chemical potential for water and hydrate formers can be calculated then the model cam be utilized. See for instance Kvamme et. al [22] for example of work in progress on hydrate formation from adsorbed methane in structured water towards mineral surfaces. And since the model is derived from Gibbs free energy model it is also consistent [19] and incorporates impact of component in water that affects chemical potentials for water, also on enthalpies.

In this work, hydration number was also estimated as given in Table 2 where the results from this work are compared with literature. The enthalpies are negative because hydrate formation is exothermic. The hydrate formation enthalpy is the heat of hydrate crystallization that must be transported out of the system, the system must lose this heat if the hydrate must form when every other condition favourable for hydrate to form is met. The heat transport is about 2-3 times [23] the magnitude of mass transport, that is more rapid. Heat transport limitation could lead to hydrate dissociation. These enthalpy values are the same for methane hydrate dissociation. But for hydrate dissociation, the values will be positive since heat is added to the system, or heat is required by the system for hydrate dissociation to proceed.

4 Conclusion

We used a consistent thermodynamic approach to evaluate the enthalpies of hydrate formation and dissociation and hydration number of methane hydrate. The methane hydrate equilibrium pressure-temperature curve estimated with this scheme agrees well with literature.

The results estimated from Clapeyron approaches by Nakamura et al. [12] and Anderson [8] disagree significantly both in values and trend. Nakamura et al. [12] are closer to the results of this work compared to the other literature. The residual thermodynamic method does not have the limitations of Clausius-Clapeyron and Clapeyron approaches. The scheme has more capabilities like the ability for easy calculation of enthalpies of hydrate phase transitions for other phase transitions like for instance, in case of hydrate forming from aqueous solution, and it can straightforwardly be extended to conditions outside of equilibrium as well as to other hydrate phase transitions

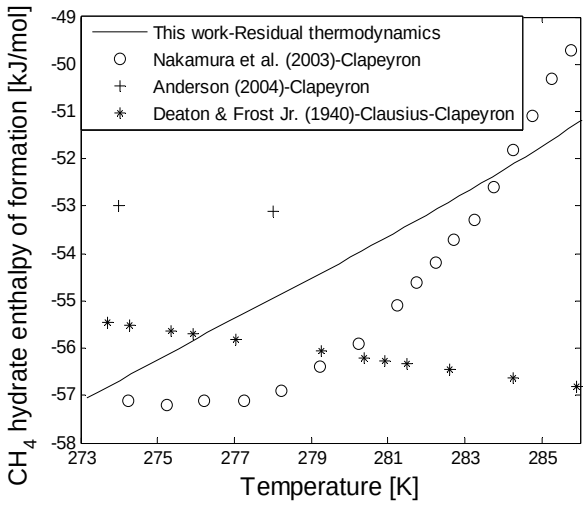

Figure 2: Estimated enthalpies of methane hydrate formation using residual thermodynamics (this work), Clapeyron equation [9, 15], and Clausius-Clapeyron equation [8].

Clapeyron equation (Nakamura et al. (2003))			Residual thermodynamics (This work)		
Temperature [K]	Pressure [bar]	Enthalpies of dissociation [kJ/mol]	Temperature [K]	Pressure [bar]	Enthalpies of formation [kJ/mol]
274.25	29.2	57.1	274.24	28.2	56.6
275.25	32.2	57.2	275.24	31.4	56.1
276.22	35.5	57.1	276.19	34.7	55.7
277.24	39.2	57.1	277.26	38.9	55.3
278.24	43.3	56.9	278.24	43.1	54.9
279.23	47.9	56.4	279.21	47.8	54.4

Table 1: Enthalpies of methane hydrate formation or dissociation [7].

	Method	Temperature [K]	Pressure [bar]	Enthalpy of formation/ dissociation [kJ/mol]	Hydration number (n)
This work	Residual Thermo-dynamics	273.15	25.19	-57.07	6.46
		274.10	27.82	-56.64	6.43
		278.02	42.15	-54.94	6.35
Anderson, G. K. (2004)	Clapeyron equa-tion	274.00	28.50	53.00	5.89
		278.00	42.80	53.10	5.79
Deaton & Frost (1946)	Clausius-Clapeyron equa-tion	273.15	n/a	55.12	n/a
Kang et al. (2001)	Experiment-Iso-thermal microcalo-rimeter	274.15	n/a	56.84	n/a

Table 2: Enthalpies of hydrate formation and dissociation and hydration number [8, 13, 14].

References

[1] Aromada S A, Kvamme B. New approach for evaluating the risk of hydrate formation during transport of hydrocarbon hydrate formers of sI and sII. *AIChE Journal* 65(3), 1097-1110, (2019). DOI: 10.1002/aic.16493

[2] Kvamme B, Aromada S A. Risk of hydrate formation during the processing and transport of Troll gas from the North Sea. *Journal of Chemical & Engineering Data* 62(7), 2163-2177 (2017). DOI: 10.1021/acs.jced.7b00256

[3] Aromad S A, Kvamme B. Impacts of CO_2 and H_2S on the risk of hydrate formation during pipeline transport of natural gas. *Frontiers of Chemical Science and Engineering*, 1-12 (2019). DOI: 10.1007/s11705-019-1795-2

[4] Kvamme B, Aromada S A, Saeidi N. Heterogeneous and homogeneous hydrate nucleation in CO_2/water systems. *Journal of Crystal Growth*, 522, 160-174 (2019).

[5] Anderson R, Llamedo M, Tohidi B, Burgass R W. Experimental measurement of methane and carbon dioxide clathrate hydrate equilibria in mesoporous silica. *The Journal of Physical Chemistry* B, 107(15), 3507-3514 (2003). DOI: 10.1021/jp0263370

[6] Kvamme B. Environmentally Friendly Production of Methane from Natural Gas Hydrate Using Carbon Dioxide. *Sustainability* 11(7), 1-23 (2019). DOI: 10.3390/su11071964

[7] Gupta A, Lachance J, Sloan E D, Koh C A. Measure-ments of methane hydrate heat of dissociation using high pressure differential scanning calorimetry. *Chemical Engineering Science,* 63, 5848-5853 (2008). DOI: 10.1016/j.ces.2008.09.002

[8] Deaton W M, Frost Jr E M. In: Proceeding of American Gas Association, 1940, 122, Houston, Texas, May 6 (1940). Cross referenced from [6]

[9] Anderson G K. Enthalpy of dissociation and hydration number of methane hydrate from the Clapeyron equation. *The Journal of Chemical Thermodynamics*, 36(12), 1119-1127, (2004). DOI: 10.1016/j.jct.2004.07.005

[10] Kvamme B, Tanaka H. Thermodynamic stability of hydrates for ethane, ethylene, and carbon dioxide. *The Journal of Physical Chemistry*, 99(18), 7114-7119, (1995).

[11] Kvamme B, Kuznetsova T, Stensholt S, Sjöblom S. Investigations of the Chemical Potentials of Dissolved Water and H_2S in CO_2 Streams Using Molecular Dynamics Simulations and the Gibbs–Duhem Relation. *Journal of Chemical & Engineering Data*, 60(10), 2906-2914 (2015). DOI: 10.1021/acs.jced.5b00267

[12] Kvamme B, Førrisdahl O K. Polar guest-molecules in natural gas hydrates. *Fluid Phase Equilibria*, 83, 427–435, (1993). DOI: 10.1016/0378-3812(93)87047-5.

[13] Nakamura T, Makino T, Sugahara T, Ohgaki K. Stability boundaries of gas hydrates helped by methane-structure-H hydrates or methylcyclohexane and cis-1,2-dimethyl-cyclohexane. *Chemical Engineering Science*, 58(2), 269-273. (2003). DOI: 10.1016/S0009-2509(02)00518-3

[14] Deaton W M, Frost Jr E M. Gas hydrate composition and equilibrium data. *Oil Gas Journal*, 45, 170-178 (1946). Cross referenced from [6]

[15] Kang S P, Lee H, Ryu B J. Enthalpies of dissociation of clathrate hydrates of carbon dioxide, nitrogen, (carbon dioxide + nitrogen), and (carbon dioxide + nitrogen + tetrahydrofuran). *The Journal of Chemical Thermodynamics*, 33(5), 513-521 (2001). DOI: 10.1006/jcht.2000.0765.

[16] Kvamme B, Aromada S A, Gjerstad P B. Consistent enthalpies of the hydrate formation and dissociation using residual thermodynamics. *Journal of Chemical & Engineering Data*, 64(8), 3493-3504 (2019).

[17] Aromada S A, Kvamme B, Wei N, Saeidi N. Enthalpies of hydrate formation and dissociation from residual thermodynamics. *Energies*, 12(24), 4726 (2019).

[18] Aromada S A, Kvamme B. Production of Methane from Hydrate and CO_2 Zero-Emission Concept. Presented at the 10th EUROSIM2019 Congress, Logroño (La Rioja), Spain, Preprint: 1-5 (2019, July).

[19] Kvamme B. Kinetics of hydrate formation, dissociation and reformation. *Chemical Thermodynamics and Thermal Analysis*, 1–2, 100004, March (2021).

[20] Kvamme B, Clarke M. Hydrate Phase Transition Kinetic Modeling for Nature and Industry–Where Are We and Where Do We Go? *Energies*, 14(14), 4149 (2021).

[21] Kvamme B. Enthalpies of hydrate formation from hydrate formers dissolved in water. *Energies,* 12(6), 1039 (2019).

[22] Kvamme B, Zhao J, Wei N, Sun W, Saeid N, Pei J, Kuznetsova T. Hydrate production philosophy and thermodynamic calculations. *Energies*, 13(3), 672 (2020).

[23] Svandal A. Modeling Hydrate Phase Transitions Using Mean-Field Approaches [PhD dissertation], Bergen, Norway: University of Bergen, (2006).

Simulation of Hydrate Plug Prevention in Natural Gas Pipeline from Bohai Bay to Onshore Facilities in China

Solomon Aforkoghene Aromada[1*], Bjørn Kvamme[1]

[1]Department of Physics and Technology, University of Bergen, Allegaten 55, 5007 Bergen, Norway; **Solomon.Aromada@student.uib.no, saromada@gmail.com*

[2]Strategic Carbon LLC, Vestre Holbergsallmenningen 17, 5011 Bergen, Norway; *kvamme@strategic-carbonllc.com*

SNE 31(3), 2021, 151-157, DOI: 10.11128/sne.31.tn.10576
Received: March 10, 2021 (Selected EUROSIM 2019 Postconf. Publ.); Revised: Sept. 1, 2021; Accepted: September 3, 2021
SNE - Simulation Notes Europe, ARGESIM Publisher Vienna
ISSN Print 2305-9974, Online 2306-0271, www.sne-journal.org

Abstract. Natural gas hydrates occasionally plug the 58 km subsea pipeline that transports natural gas from Platform QK18-1 in southwest of Bohai Bay to the processing facility onshore in Northeast China. This is because it is a wet gas subsea pipeline that operates at high pressures and low temperatures, which are the conditions that are appropriate for hydrate formation to occur. In this study, we proposed that the best way to prevent the occasional plugging of the pipeline is to rightly evaluate the upper limit of water that can be permitted in the bulk gas and dehydrate the gas accordingly before transport. Current industrial techniques are mainly based on water dewpoint evaluations. In our recent work we have proposed another approach that considers the impact of the rust (Hematite) on the internal walls of pipelines. These two methods have been used for this study. The results of the method of adsorption of water onto rusty (Hematite) surfaces suggest that the current approach (dewpoint method) overestimates the safe-limit of water about 18 to 19 times higher. Thus, the risk of hydrate formation may still exist if the dewpoint method is used as basis for drying the gas. Sensitivity analysis shows the influence of pressure on the upper limit of water- the higher the pressure the lower the maximum concentration of water that is safe to accompany the gas. Our calculations were done using a FORTRAN code that utilize thermodynamic data from molecular dynamics simulation.

Introduction

Hydrate discovery is dated back to 1810 and credited to Sir Humphrey Davy [1-3]. But natural gas hydrate (NGH) formation in pipeline transporting natural gas became a major research focus in the 1930's through the work of Hammerschmidt [4]. NGH are non-stoichiometric crystalline inclusion compounds formed when hydrogen-bonded water molecules form three-dimensional solid cage-like structures with cavities which entrap suitably small sized molecules of certain gases and volatile liquids known as guest molecules. Methane, ethane, propane, isobutane, carbon dioxide (CO_2) and hydrogen sulphide (H_2S) [5, 6] are guest molecules that can form hydrate in their pure form. Hydrates are ice-like solid substances that form at high pressures and low temperatures conditions when free water (liquid) is available in a gas containing guest molecules. Hydrate formation is a crucial flow assurance challenge to the oil and gas industry since water is always produced together with hydrocarbons. This water can drop out of the bulk gas. With the appropriate thermodynamic conditions of high pressure and low temperature [6-8], and favourable mass and heat transport, this could lead to hydrate formation. Subsequently, accumulation and agglomeration of the formed hydrate can occur and eventually lead to plugging [4] of pipelines. This results in stopping of operations which means economic losses [9]. Sometimes there could be destruction [9, 10] of pipelines and equipment, and even loss of live [5].

There are many pipeline networks all over the world transporting hydrocarbons [11]. In this work we have focused on the 58 km subsea pipeline [12] from Platform QK18-1 in southwest of Bohai Bay (part of the Bohai Gulf), transporting natural gas to the processing facility

onshore in Northeast China. It is a wet gas subsea pipeline and it is exposed to elevated pressure and low temperature [12]. Plugging of the pipeline by hydrate occurs once in a while [12]. Li et al. [12] performed an experimental study on the pipeline and suggested the following solutions: pressure reduction or raising the temperature (heating the pipeline), dehydration of gas before subsea pipeline transport, and thirdly, addition of chemical additives such as kinetic hydrate inhibitors (KHI), to ensure safe operations.

In this work, our focus is on the second recommendation. This is also in accordance with what Li et al. [12] proposed as the best choice out of their three recommendations. However, their work did not go into details of how to estimate the upper limit of water content in the gas for prevention of hydrate formation in the subsea pipeline. In a recent work [13], we hproposed an alternative approach for evaluating the upper limit of water in natural gas during pipeline transport to avoid the risk of hydrate formation. The study focused on hydrocarbon components of methane, ethane, propane and isobutane which are the primary hydrocarbon hydrate guest molecules. Therefore, there is a need to carry out this study with a real and specific gas field data. This also involves some content of inorganic gases like CO_2 which is a very strong hydrate former. Nitrogen cannot form hydrate in its pure form [14] but can still enter hydrate which is mainly stabilized by other components. In the other end of the guest molecule size scale is normal butane [15-17], which does not make hydrate as pure component, but gauche conformation can fit into large cavity of structure I when methane fills small cavities. Both trans and gauche conformations fit large cavities of structure II although the trans configuration gives low stabilization and will only form hydrate with methane or other good hydrate former in small cavities.

1 Thermodynamics of Hydrate: Description and Validation of Model

We used residual thermodynamics with Soave–Redlich–Kwong (SRK) equation of state [18] for all components in each phase (hydrate, ice and liquid water). We did that by making use of molecular dynamics (MD) simulations results for water in empty hydrates, liquid water, and ice phases [19]. We used equation (1) to estimate the chemical potential of component *j* in the gas phase.

To ensure the same reference value for free energy of all the estimates of chemical potentials, regardless of the phase, ideal gas is used as the reference state:

$$\mu_j(T,P,\vec{y}) = \mu_j^{ideal\ gas}(T,P,\vec{y}) + RTln\emptyset_j(T,P,\vec{y}) \quad (1)$$

$$\lim(\emptyset_i) \rightarrow 1.0 \text{ ...for ideal gas}$$

Where $\emptyset_i$ is the fugacity coefficient for component *j* in the given phase, *R* is universal gas constant, $\vec{y}$ is the mole fraction vector of the gas, *P* and *T* are pressure and temperature respectively. The chemical potential of component *j* in water is estimated as:

$$\mu_j(T,P,\vec{x}) = \mu_j^{ideal\ liquid}(T,P,\vec{x}) + RTln\gamma_j(T,P,\vec{x}) \quad (2)$$

$$\lim(\gamma_j) \rightarrow 1.0 \text{ when } x_j \rightarrow 1.0$$

Where γ_j stands for the activity coefficient of component *j* in the liquid phase and $\vec{x}$ is the mole fraction vector of the liquid. It is also proper to use a reference state of infinite dilution since the solubility of methane and higher hydrocarbons in water is low:

$$\mu_j^{H_2O}(T,P,\vec{x}) = \mu_j^{H_2O,\infty}(T,P,\vec{x}) + RTln\left[x_j^{H_2O}.\gamma_j^{H_2O,\infty}(T,P,\vec{x})\right] \quad (3)$$

$$\lim(\gamma_j^{H_2O,\infty}) \quad \text{when } x_j \rightarrow 0$$

Where $\mu_j^{H_2O,\infty}$ represents the chemical potential of component *j* in water, ∞ denotes infinite dilution, $\gamma_j^{H_2O,\infty}$ stands for activity coefficient of component *j* in aqueous phase based on the same reference state. The solubility of methane and higher hydrocarbons are each very low. Thus, equation (4) could be applied together with equation (3):

$$\mu_j^i(T,P,\vec{x}) \approx \mu_j^{i,\infty}(T,P,\vec{x}) + RTln\left[x_j^i.\gamma_j^{i,\infty}(T,P,\vec{x})\right] \quad (4)$$

Superscript *i* stands for different phases with low solubility, while subscript *j* represents different components. We evaluated the chemical potential of water in hydrate using the statistical mechanical model for water in hydrate (equation 5). This is a typical Langmuir type of adsorption model. The version we used is different from that of van der Waal and Platteuw [20] which assumes rigid lattice.

It is the one proposed by Kvamme and Tanaka [19]. This one takes into account the movements of the lattice and the corresponding impacts of different guest molecules. That is, the collisions between guest molecules and water which are adequately strong enough to affect the water motion.

$$\mu_{H_2O}^{(H)} = \mu_{H_2O}^{(0,H)} - \sum_{i=1}^{2} R.T.v_i.ln\left(1 + \sum_{j=1}^{n_{guest}} h_{ij}\right) \quad (5)$$

Where H stands for hydrate phase, $\mu_{H_2O}^{(H)}$ refers to the chemical potential of water in hydrate, $\mu_{H_2O}^{(0,H)}$ signifies the chemical potential of water in empty hydrate structure, and v_i is the fraction of cavity type *i* per water molecule. The h_{ij} in equation (11) is the canonical cavity partition function of component *j* in cavity type *i,* and n_{guest} is the number of guest molecules in the system. We evaluated the canonical partition function using the relation:

$$h_{ij} = e^{-\beta\left(\mu_i^H - \Delta g_{ij}^{inc}\right)} \quad (12)$$

Where β is inverse of gas constant times temperature ($\frac{1}{R.T}$), and Δg_{ij}^{inc} is the effects of inclusion of the guest molecules *j* in the cavity *i* on hydrate water. The free energy change related to hydrate phase transition (Δg^H) is evaluated using equation (14):

$$\Delta g^H = \delta \sum_{j=1}^{n^H} x_j^H\left(\mu_j^H - \mu_j^P\right) \quad (14)$$

Where *H* refers to hydrate phase of molecule *j, P* here is parent phase of molecule *j.* And equation (15) gives the relation between the filling fraction, the mole fractions and cavity partition function as shown below:

$$\theta_{ij} = \frac{x_{ij}^H}{v_j(1-x_T)} = \frac{h_{ij}}{1+\sum_j h_{ij}} \quad (15)$$

Where x_T signifies total mole fractions of all hydrate formers in the hydrate, θ_{ij} refers to the filling fraction of component *j* in cavity type *i*, and x_{ij}^H stands for mole fraction of component *j* in cavity type *i*.

2 Composition of the Natural Gas from Bohai Bay

The composition of the wet natural gas from the southwestern Bohai Bay and the dry gas (City gas) used by Reference [12] are given in the Table 1. All other hydrocarbon components after iC_4, that is nC_4 and C_{5+} and CO are not considered in this study as they are not relevant. Therefore, the molar compositions are normalised.

Components	Composition [Mole fractions]	
	Wet gas from subsea pipeline	Dry gas
C_1	0.8868	0.9259
C_2	0.0612	0.0319
C_3	0.0332	0.0136
iC_4	0.0066	0.0034
CO_2	0.0072	0.0093
N_2	0.0050	0.0159

Table 1. Composition of the Natural gas from Bohai Bay [12]

3 Model Validation

The estimates of hydrate equilibrium pressures from our theoretical model used for the simulations in FORTRAN are compared with experimental data relevant for the compositions of the gas in this study. Experimental data of Reference [21] (Figure 1) and Reference [22] (Figure 2) are the best we could find for this comparison based on closeness to the composition of the gas.

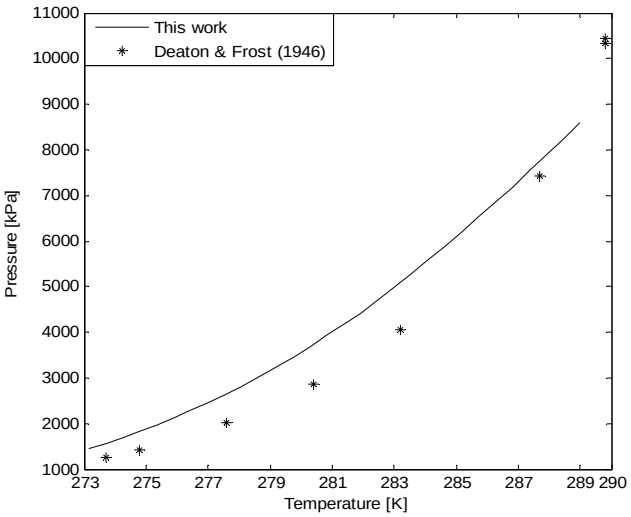

Figure 1. Estimated equilibrium pressures for hydrate formed from a gas mixture containing 96.50 mole % CH_4, 0.90 mole % C_2H_6, 1.80 mole % C_3H_8, 0.20 mole % CO_2, and 0.60 mole % N_2 [21].

It is important to state that the free energy of inclusions has been evaluated by MD simulations. And that we did not tune the model (no empirical data fitting was done) because our priority is to keep the statistical mechanical model [19] free of adjustable parameters in all terms.

These comprises the chemical potentials of empty hydrate, ice, and liquid water. Therefore, a fair qualitative

agreement is adequately acceptable for this study. So, the expectation is not perfect match with experimental data. The deviations are satisfactorily acceptable for further illustration of the maximum concentration of water content that should be allowed without the risk of hydrate formation.

It is also imperative to point out that more than one hydrate, that is having different densities, composition, and free energies do result from multicomponent gas mixtures [8, 13]. We know that the most stable hydrate will first form [13] based on the combined first and second laws of thermodynamics, then formation of a variety of hydrate compositions will occur. Therefore, the hydrate that would probably form in case of Figure 1 ought to be a mixture both structure I and II. But based on the very low concentration of propane, Reference [21] assumed only structure I hydrate is formed. In Figure 2, we took the presence of propane into consideration (the solid line) and disregarded it (dash-dot line) in a second run. That revealed that Wilcox et al. [22] also assumed only structure I hydrate is formed. The solid line in Figure 2 shows that there is a phase split by the propane (liquid and gas) at 278.5 K [7]. Most literature are wrong for straightening the curve as it is not the real situation. CO_2 also undergo a phase split [24] as pressure increases. Therefore, the final hydrate that would form as in these figures could likely be a mixture of several hydrates (sI and sII) with varying compositions of the initial hydrate formers from gas or liquid will result [13].

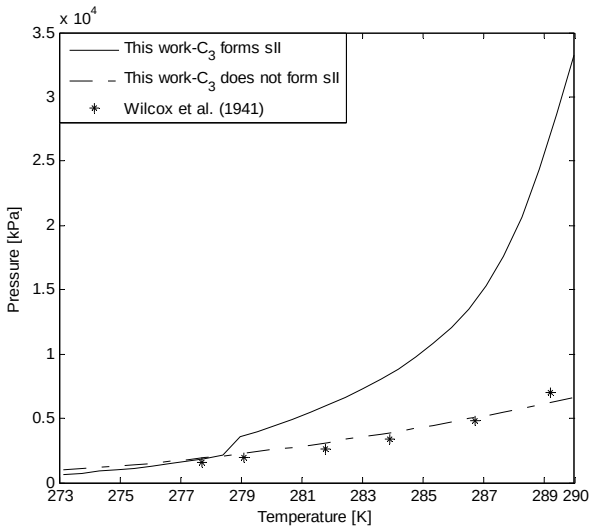

Fig.2. Estimated equilibrium pressures for hydrate formed from a gas mixture containing 93.20 mole % CH_4, 4.25 mole % C_2H_6, 1.61 mole % C_3H_8, 0.51 mole % CO_2, and 0.43 mole % N_2 [22].

4 Safe-limits of Water in Natural Gas from Bohai Bay through Subsea Pipeline to Onshore Facilities in China and the City Gas

4.1 Alternative evaluation approaches: Impact of rust

The typical industrial practice for evaluating the risk of hydrate formation during pipeline transport of natural gas assumes that liquid water will condense out from the bulk gas stream to form a separate liquid water phase that can subsequently cause hydrate nucleation. This is done by estimating the dew-point pressure of water in the gas stream, then, check whether the computed dew-point pressure at the local temperature is within the temperature and pressure projection of the hydrate stability zone. If it is, it means water will drop out as liquid droplets. Afterwards, the theoretical amount of water that would condense out can be estimated and steps are taken to dry the gas. Or else, the necessary amount of a hydrate inhibitor that can adequately shift the hydrate stability curve's pressure and temperature projections beyond the risk zone is calculated and applied in the system to avoid hydrate formation. This we refer to as the dew point method.

In our recent work [13], we proposed an alternative approach for evaluation of the risk of hydrate formation in pipelines for gas mixtures containing methane, ethane, propane, and iso-butane which we call the Hematite approach. By Hematite we mean the most dominant and most thermodynamically stable form of rust. In this study, we have applied both methods (dew point method and hematite approach) to study a real gas mixture [12], a wet gas transported from offshore China to onshore processing facility using a 58 km subsea pipeline that is exposed to high pressures and low temperatures. However, in this situation, the gas mixture contains some inorganic gases, CO_2 that is a strong hydrate former compared to the hydrocarbons, and nitrogen that can also fill the small cages of sI hydrate in the presence of a helping molecule (methane). Nitrogen in its pure form cannot form hydrate [6], rather it has a dilution effect, that is why it has been proposed for use to reduce the reactivity of CO_2 during a simultaneous CO_2 storage in form of CO_2 hydrate and production of CH_4 [23].

The results of our investigation using the two approaches are presented in Figure 3 for the wet gas and Figure 4 in the case of the dry gas. Pressure range of 5000-25000 kPa and temperature range of 273 -280 K are used because these are the relevant ranges in such operations, for instance in the North Sea of Norway [6]. The maximum concentration of water that can be permitted in both the wet gas and dry gas are plotted in logarithm to base 10 (log10) to enable us plot results with both methods on the same figure. The only essence of including the dry gas in this analysis is merely for sensitivity analysis: to show how a slight change in composition of the same components in the gas mixture can cause slight change in water tolerance as can be observed in Figure 5 and Figure 6.

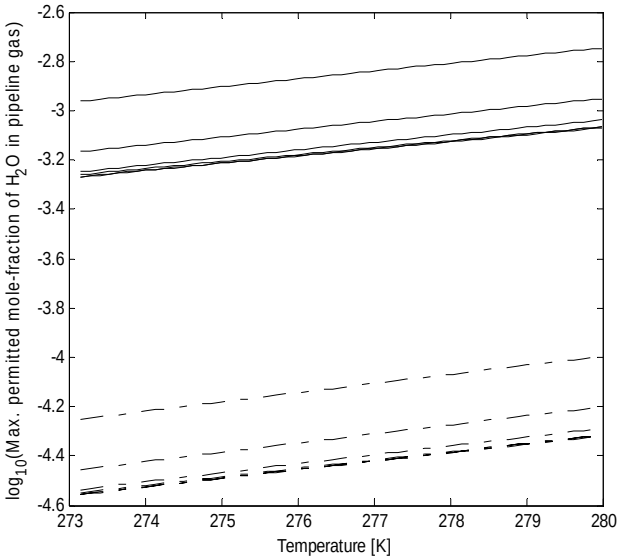

Figure 3. Estimated maximum concentration of water that should be permitted in the pipeline gas (wet gas) in logarithm to the base 10 ($\log_{10}$) vs temperature. Upper solid lines (-) represent estimates with the conventional dew point calculation, lines from top to bottom are for 5000 kPa, 9000 kPa, 13000 kPa, 17000 kPa, 21000 kPa, and 25000 kPa respectively. Lower dash-dot lines (-.) represent estimates with the approach of adsorption of water onto hematite, lines from top to bottom are also for 5000 kPa, 9000 kPa, 13000 kPa, 17000 kPa, 21000 kPa, and 25000 kPa respectively.

After processing the gas, the dry gas (city gas) is slightly richer in the lightest hydrocarbon component (methane) and that also caused the permitted water concentration to also move up slightly, which indicate that presence of the heavier hydrocarbon components like ethane, propane, and isobutane means a lower allowable water content [6,7,13] to avoid the risk of hydrate formation in a subsea pipeline operating at a high pressure and low temperature.

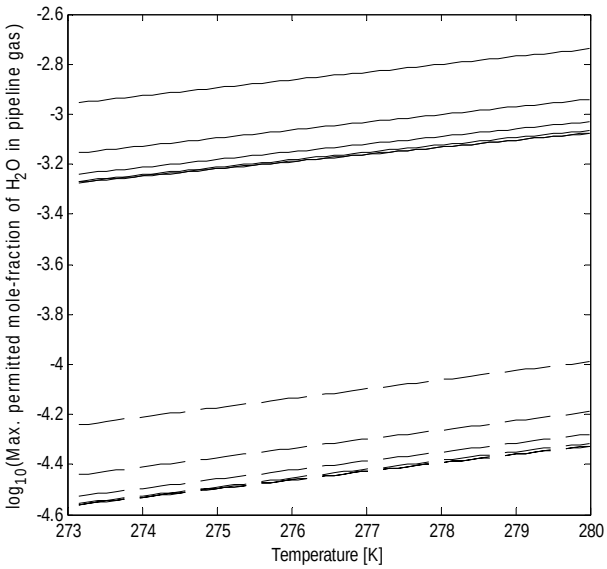

Figure 4. Estimated maximum concentration of water that should be permitted in the pipeline gas (dry gas) in logarithm to the base 10 ($\log_{10}$) vs temperature. Upper solid lines (-) represent estimates with the conventional dew point calculation, lines from top to bottom are for 5000 kPa, 9000 kPa, 13000 kPa, 17000 kPa, 21000 kPa, and 25000 kPa respectively. Lower dash lines (--) represent estimates with the approach of adsorption of water onto hematite, lines from top to bottom are also for 5000 kPa, 9000 kPa, 13000 kPa, 17000 kPa, 21000 kPa, and 25000 kPa respectively.

How much lower depends on the amount of the higher hydrocarbons present in mixture with methane.

In this analysis, estimation of maximum allowable water content using the dew point method instead of the new approach may not ensure safe operation in respect of hydrate formation, since rust (Hematite) which is usually present in surfaces of inner walls of pipelines would still make water available through the mechanism of adsorption even at much lower mole-fractions than what is estimated by the dew point method. Hematite acts as a catalyst that helps to pull out the water from the bulk gas stream through adsorption, then hydrate can subsequently form slightly outside of the first two or three water layers of about 1 nm. Using the dew point approach overestimates the safe-limit of water about 18 to 19 times more than what is calculated by the method of water adsorption on Hematite. Additionally, the chemical potential of adsorbed water is about -3.4 kJ/mol lower [6, 7] than that of ordinary liquid water.

This mean absorbed water on rusty surfaces will more readily lead to hydrate formation than ordinary liquid water based on the combined first and second laws of thermodynamics (thermodynamic systems strive towards the least free energy). Therefore, the approach of adsorption of water on rusty surfaces dominates, and possibly will have an impact on designing natural gas dehydration systems.

4.2 Impacts of temperature and pressure

The work of Reference [12] focused on the impacts of pressure on temperature, density, and flowrate. But in this work our focus is on the recommended best measure to prevent [12] hydrate formation, that is reducing the water concentration to allowable limits.

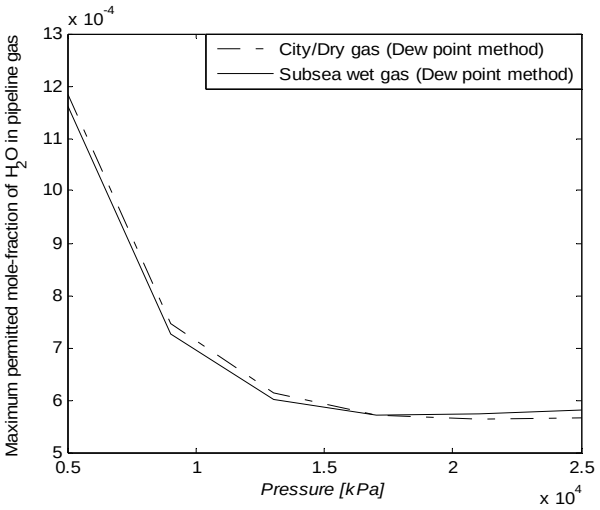

Figure 5. Impact of pressure on the maximum amount of water that should be permitted in the pipeline gases, conventional dew point estimates

The higher the temperature, the higher the upper limit of water in the gas stream to prevent hydrate formation during transport through the subsea pipeline as can be seen in Figure 3 and Figure 4. While Figure 5 and Figure 6 show that the higher the pressure, the lower the safe-limit of water in the gas. The results are the same with evaluations by both approaches. The only difference is the absolute values of mole-fractions of water. The last three lines for pressures of 17000 kPa, 21000 kPa and 25000 kPa as can be observed in Figure 3 and Figure 4., almost overlap. Figure 5 and Figure 6 make that clearer. This is a result of the high density of the non-polar hydrocarbons at these very high pressures.

The maximum water content becomes almost insensitive to increase in pressure due to the resistance of the tightly packed molecules of the non-polar hydrocarbon gases present in the system. It can also be seen on Figure 5 and Figure 6 that the slightly heavier wet gas curve crosses that of the slightly lighter city (dry) gas. This only shows that the heavier wet gas responds slightly faster in resistance to pressure than the slightly lighter city gas.

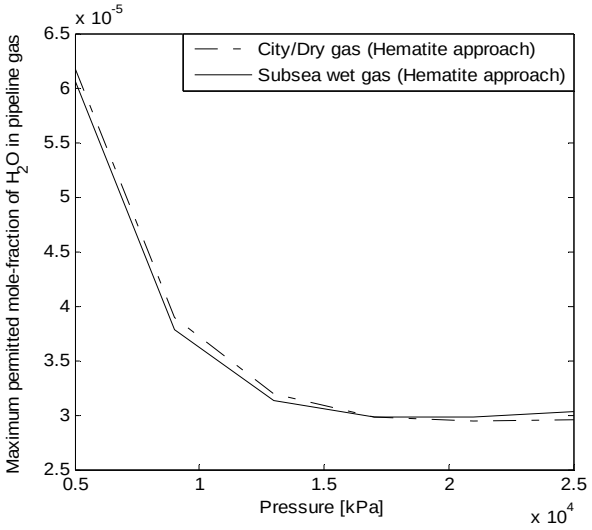

Figure 6. Impact of pressure on the maximum amount of water that should be permitted in the pipeline gases, hematite approach.

5 Conclusion

We conducted a study on how to prevent the occasional plugging of the wet gas subsea pipeline that transports natural gas from Platform QK18-1 in southwest of Bohai Bay to the processing facility onshore in Northeast China. This pipeline is operated at temperature and pressure conditions that are suitable for hydrate to form: high pressures and low temperatures. The thermodynamic scheme we used was simulated using a FORTRAN code based on the results of Kvamme and Tanaka molecular dynamics simulations. We used residual thermodynamics by means of Soave–Redlich–Kwong (SRK) equation of state for each component in every phase: hydrate, ice, and liquid water phases. The typical schemes currently employed by the petroleum industry for hydrate risk analysis are normally based on evaluation of water dewpoint, with the assumption that water will drop out of the bulk gas at the temperature and pressure conditions of dewpoint if the amount of water is up to or above the dewpoint concentration.

This water can subsequently lead to hydrate formation and eventually to plugging of the pipeline. In our recent work, we have proposed an alternative route for water to drop out of the bulk gas, that is through the process of adsorption of water onto rusty (Hematite) surfaces of the internal walls of pipelines. Pipelines are usually rusty before they are mounted in place for natural gas transport. The results of the method of adsorption of water onto rusty (Hematite) surfaces suggest that the current method based on water dewpoint calculation overestimates the allowable upper limit of water about 18 to 19 times higher. This means the risk of hydrate forming in the subsea pipeline may still exist if the dewpoint method is used. A pressure sensitivity analysis was also performed, and it shows that the higher the pressure the lower the maximum content of water that is safe to follow the gas.

References

[1] Campbel J M. Gas Conditioning and Processing. Vol. 1. Basic Principles. 157-200, (2003).

[2] Schroeder W: In Ahren's Sammlung Chemischer und Chemisch-Technik Vortrage, 21- 71, (1926-28). Cross referenced from [4].

[3] Vafaei M T. Reactive transport modelling of hydrate phase transition dynamics in porous media. PhD Dissertation, University of Bergen, Norway, 2015.

[4] Hammerschmidt E G. Formation of gas hydrates in natural gas transmission lines. Industrial & Engineering Chemistry 26(8), 851-855 (1934).

[5] Sloan Jr E D, Koh C. Clathrate hydrates of natural gases. 3rd edn. Boca Raton, Florida CRC press, (2007).

[6] Kvamme B, Aromada S A. Risk of hydrate formation during the processing and transport of Troll gas from the North Sea. Journal of Chemical & Engineering Data 62(7), 2163-2177 (2017). DOI: 10.1021/acs.jced.7b00256

[7] Kvamme B, Aromada S A. Alternative routes to hydrate formation during processing and transport of natural gas with a significant amount of CO_2: Sleipner Gas as a Case Study. Journal of Chemical & Engineering Data 63(3), 832-844 (2018). DOI: 10.1021/acs.jced.7b00983

[8] Aromada, S A, Kvamme B. Impacts of CO_2 and H_2S on the risk of hydrate formation during pipeline transport of natural gas. Frontiers of Chemical Science and Engineering, 1-12 (2019). DOI: 10.1007/s11705-019-1795-2

[9] Makogon, Y. F.: Natural gas hydrates–A promising source of energy. Journal of Natural Gas Science & Engineering 2, 49-59 (2010). DOI: 10.1016/j.jngse.2009.12.004

[10] Woehler F. Krystallisirtes Schwefelwasserstoff-Hydrat. Justus Liebigs Annalen der Chemie 33, 125-126 (1840) Cross referenced from Hammerschmidt (1934)

[11] Chartsbin Website, Total Length of Pipelines for Transportation by Country, http://chartsbin.com/view/1322, last accessed 2017/01/16.

[12]] Li W, Gong J, Lü X, Zhao J, Feng Y, Yu D. A study of hydrate plug formation in a subsea natural gas pipeline using a novel high-pressure flow loop. Petroleum Science 10(1), 97-105 (2013). DOI: 10.1007/s12182-013-0255-8

[13] Aromada S A, Kvamme B. New approach for evaluating the risk of hydrate formation during transport of hydrocarbon hydrate formers of sI and sII. AIChE Journal 65(3), 1097-1110, (2019). DOI:_ 10.1002/aic.16493

[14] Kvamme B. Fundamentals of Natural Gas Hydrates and Practical Implications. Unpublished Work: PTEK 232, Course Material, Spring Semester 2017, Dept of Physics and Technology, University of Bergen, Norway, 2017.

[15] Kumar S. Gas Production Engineering. Gulf Publishing Company, Book Division, (1987).

[16] John V, Holder G. Hydrates of methane+ butane below the ice point. Journal of Chemical and Engineering Data 27, 18-21 (1982).

[17] Ng H-J, Robinson D B. Equilibrium-phase properties of the toluene-carbon dioxide system, Journal of Chemical and Engineering data 23, 325-327 (1978).

[18] Soave G. Equilibrium constants from a modified Redlich-Kwong equation of state. Chemical Engineering Science 27, 1197-1203, (1972).

[19] Kvamme B, Tanaka H: Thermodynamic stability of hydrates for ethane, ethylene, and carbon dioxide. The Journal of Physical Chemistry 99(18), 7114-7119 (1995).

[20] van der Waals J H, Platteeuw J C. Clathrate solutions. Advance Chemical Physics 2,1-57 (1959).

[21] Deaton W M, Frost Jr E M. Gas hydrate composition and equilibrium data. Oil & Gas Journal 45, 170-178(1946).

[22] Wilcox W I, Carson D B, Katz D L. Natural gas hydrates. Industrial & Engineering Chemistry 33(5), 662-665 (1941).

[23] Kvamme B, Aromada S A, Kuznetsova T, Gjerstad P B, Canonge P C, Zarifi M. Maximum tolerance for water content at various stages of a natuna production. Heat and Mass Transfer 1-21 (2018). DOI: 10.1007/s00231-018-2490-4

[24] Aromada S A, Kvamme B, Wei N, Saeidi N. Enthalpies of hydrate formation and dissociation from residual thermodynamics. *Energies*, 12(24), 4726 (2019).

Wildfire Spreading Simulator Using Fast Marching Algorithm

Juan Carballeira*, Carolina Nicolás,Santiago Garrido, Luis Moreno

Robotics Laboratory, Department of System Engineering and Automation, Carlos III University of Madrid, 28911 Madrid, Spain; *jcarball@pa.uc3m.es

SNE 31(3), 2021, 159-167, DOI: 10.11128/sne.31.tn.10577
Received: March 10, 2021 (Selected EUROSIM 2019 Postconf. Publ.), Revised: August 31, 2021; Accepted: September 2, 2021
SNE - Simulation Notes Europe, ARGESIM Publisher Vienna, ISSN Print 2305-9974, Online 2306-0271, www.sne-journal.org

Abstract. Programs that can predict wildfire behavior are a very useful tool in terms of extinguishing these fires more effectively. State of the art wildfire simulators present some drawbacks such as not being sufficiently user-friendly, being expensive, requiring great computational power or having poor graphical representation. This paper presents a prototype wildfire simulation app that uses Fast Marching (FM) as its core algorithm. The wildfire app is developed as a Matlab GUI. Said application shows the shape of the fire front at a given moment in time in a 3D map of the terrain affected by the fire. Any real life maps can be loaded to the application for wildfire prediction. The user can choose to vary parameters such as starting (ignition) and ending points, wind direction and speed and propagation time, and see its effect on fire propagation. Interface response to each change in the input is very fast, therefore proving the efficiency of the algorithm. Although a prototype, the wildfire basic app is superior to some state of the art simulators regarding certain important features. It can be concluded that Fast Marching is a valid core algorithm for a fire simulator. The way the app is programmed in Matlab confers it flexibility, enabling further specific changes that make it truly competitive against currently used wildfire simulators.

Introduction

Wildfires constitute a serious threat around the globe,of special importance in the Mediterranean area. Each year, a country, such as Spain, experiments terrible environmental, material and economic loses that have been estimated to be of 3000 euros per hm^2 by Aguilera [1]. In addition to these loses, wildfires cause numerous deaths, most of them fire fighting professionals trapped in the fire due to abrupt changes in fire trajectory. Fire trajectory prediction enables the fire fighting team to choose the critical spots in order to save resources and extinguish the fire more effectively. A crucial characteristic for a useful predictor is a quick and accurate response to changes in parameters affecting the fire such as the speed and direction of the wind. This characteristic can be achieved by using a very efficient prediction model or algorithm. The Fast Marching algorithm, developed by Osher and Sethian [2] and currently used for path planning applications, has proven to be a very efficient algorithm to solve the Eikonal wave equation.

Therefore, the purpose of this paper is to prove the viability of the FM algorithm as a core algorithm to a wildfire simulator. A prototype wildfire app is developed in Matlab Guided User Interface to this end. The final objective of the prototype is to show the possibility of a user-friendly, economical, very competitive simulator that responds very efficiently to changes in inputs affecting fire spread.

1 State of the Art Wildfire Simulators

The most relevant fire prediction simulators are FireStar, FireRS, Prometheus and Farsite.

1.1 FireStar

FireStar [3] , is a project providing wildfire prediction assistance for users in the Mediterranean area. Its main characteristic is that the prediction model used is entirely physical. It predicts fire spread by solving a series of differential equations based on mass, momentum and

energy conservation. Results regarding the effect of numerous wildfire related variables (such as temperature or gas velocity) are extremely precise. Its biggest flaw is that due to the big computational cost associated with solving these equations, it can only work in 1 and 2 dimensions. Building a 3D prediction simulator using a entirely physical model is a very impractical computational task.

1.2 FireRS

FireRS [4], stands for wildFIRE Remote Settings and is a massive still unfinished project that started in 2016 for wildfire prediction and monitoring. It is mainly funded by the European Regional Development Fund (ERDF), coordinated by the University of Vigo and the University of Oporto, and the Centre National de Reserche Scientifique as collaborator. Its 2 million budget is destined to provide a global information system with real time data regarding the fires, actuation protocols, GPS positioning, a fleet of autonomous UAVs, infrared sensors and wildfire prediction, among other tools.

1.3 Prometheus

Prometheus [5], is the most widely used wildfire predictor in Canada. It uses Huygens' principle, stating that light propagation front at a given instant contains the initial point of small propagations, and the envelope curve of those small propagations determines the shape of the propagation front on the next instant. Figure 1 graphically represents this phenomenon.

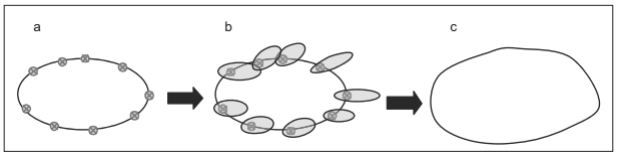

Figure 1: Huygens' principle.

Prometheus uses COM (Common Object Model) as programming tool, enabling the use of a higher level COM for computation and 5 lower level COMs related to variables that affect the fire spread (fuel, weather, etc.).

The user interface associated with Prometheus is Burn-P3 [6] Figure 2 represents the maps for the various possible inputs (the only required input is the information regarding fuels). The simulator returns a map and data regarding the probability of the wildfire reaching each specific zone of the considered terrain.

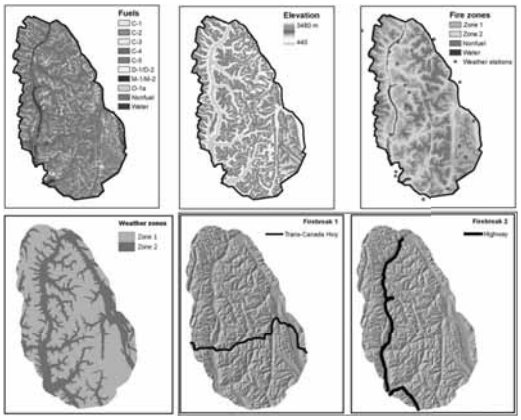

Figure 2: Burn-P3 inputs. Adapted from [**?**].

1.4 Farsite

Farsite, [7], is probably the best existing wildfire simulator. It also uses Huygens' principle in combination with Rothermel's surface model and Van Wagner's model.

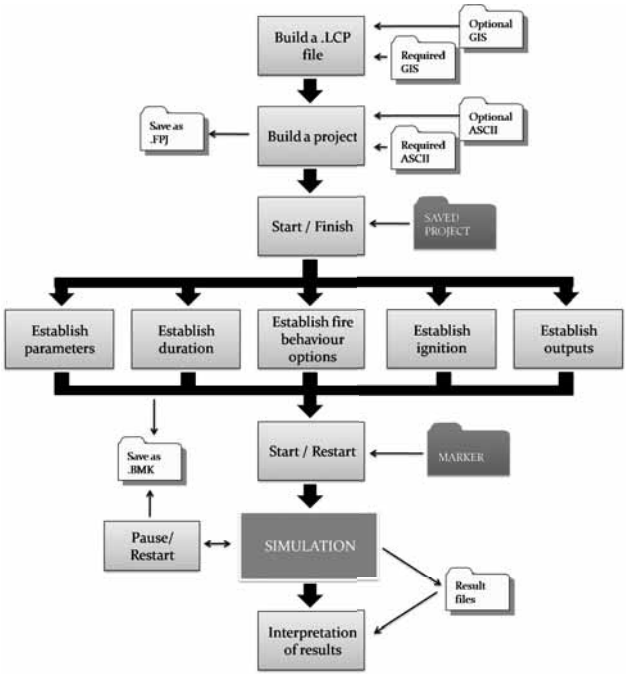

Figure 3: Farsite functioning scheme.

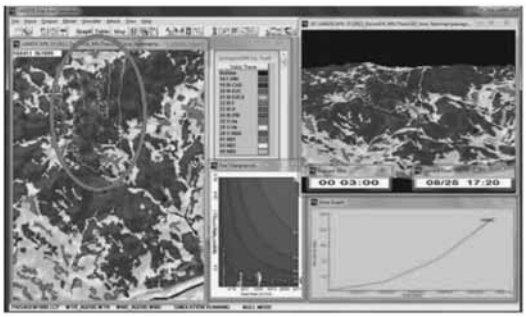

Figure 4: Farsite user's interface.

Figure 3 contains a diagram that shows the use procedure for Farsite. Actions on the program are represented as rectangles, inputs and outputs are represented as folders.

Figure 4 shows the interface of program for a given wild fire simulation. The wildfire spread is represented by thin white lines.

2 Methodology

Subsection 2.2 explains the fundamentals of the Fast Marching Algorithm, which is the core of the application. Subsection 2.1 covers the main development simulation and design aspects of the simulator and its main features.

2.1 Fast Marching Algorithm for wildfire prediction

The Fast Marching Algorithm [8], is a specific case of the Level Set method, initially designed to simulate the propagation of a wave in a discrete space. It does so by solving the Eikonal equation at every node of a discrete map.

This algorithm predicts the expansion of a wave given a velocity , cost or viscosity matrix. Its functioning can be intuitively understood by imagining how the wave front caused by a stone hitting water might be different if instead of water there was a mixture of liquids with different viscosities. In this analogy the viscosities of the liquids represent the different values of the cost matrix.

There are three significant matrices used in the algorithm:

- W matrix: Cost matrix. The value in each cell states the 'cost', or difficulty, of traveling to that node. It is the input to the algorithm.
- S matrix: Contains information about where the propagation front is at each moment. It determines weather a node is unknown (0), part of the front (1), or dead, which means that it was part of the front previously, but it is not anymore (-1).
- D matrix: Distance matrix. Each node contains, for the purpose of this application, information regarding how much time it has taken the front to reach said node. It can be considered as the final output of the algorithm.

Table 1 shows how the values of the matrices S and D would update with each iteration of the algorithm if the input matrix W was a 3x3 matrix of ones.

It.	**0**	**1**	**2**
S	$\begin{matrix}0&0&0\\0&0&0\\1&0&0\end{matrix}$	$\begin{matrix}1&0&0\\1&0&0\\-1&1&1\end{matrix}$	$\begin{matrix}-1&1&1\\1&0&0\\-1&1&1\end{matrix}$
D	$\begin{matrix}\infty&\infty&\infty\\\infty&\infty&\infty\\0&\infty&\infty\end{matrix}$	$\begin{matrix}1&\infty&\infty\\1&\infty&\infty\\0&1&1\end{matrix}$	$\begin{matrix}1&1.71&1.71\\1&\infty&\infty\\0&1&1\end{matrix}$

Table 1: Values for matrices S and D during each iteration for an example matrix W.

FM has been traditionally used for path planning in robotics. Nevertheless, the idea of fire spread behaving essentially like a wave where the values of the cost matrix represent the flammability of the terrain, presents the possibility of FM being a suitable algorithm for wildfire prediction. Another characteristic of the FM algorithm is that the propagation velocity is always considered positive, which matches with wildfire behavior.

The main advantage of FM is its computational speed and efficiency. Other fire spread prediction methods such as Huygens' principle (Farsite, Prometheus) are slower and less efficient computationally.

It is obvious that wildfire spread depends on factors other than the terrain flammability: wind, slope of the terrain, etc. These factors are vectorial. Vectorial fields can be included in the FM algorithm [9], by adding such vectorial fields to the D matrix (which is in fact a potential field created from scalar variables). By modeling

the influence of said factors into vectorial fields, these can be included in the algorithm. Figure 5 illustrates an example of how the propagation is affected by vector fields in different directions

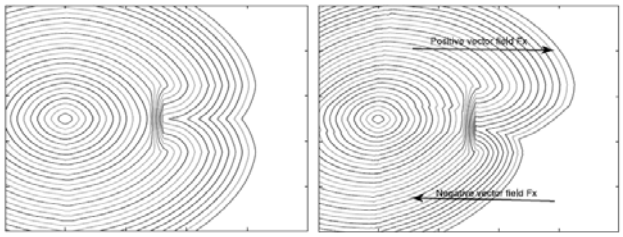

Figure 5: Effect of an external vectorial field to the FM algorithm. Adapted from [9].

2.2 Application design

Our wildfire prediction application is a simple Matlab graphical user interface (GUI). Its purpose is to show the propagation of a wildfire along a 3D map of the terrain over time in a very clear way. The main objective of this paper is to prove that FM is a viable option for a wildfire simulator. Another objective is for the user to be able to select and vary parameters that affect the fire spread.The main design aspects of the application are explained in this section.

2.2.1 Altitude and flamability maps

The application requires two maps as inputs (in matrix form) of the location where fire spread is simulated.

- Altitude matrix: *nxm* matrix. Required for the 3D representation of the spread. Each cell contains the altitude of that point in the map.

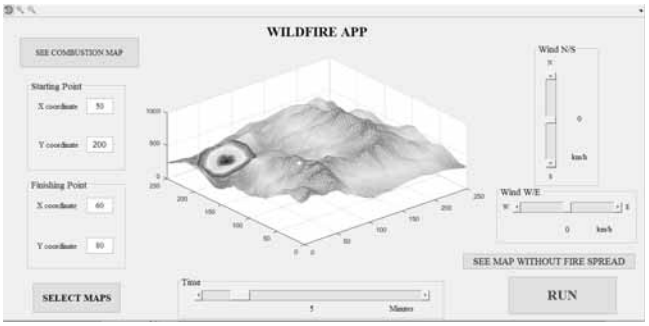

Figure 6: Screenshot of the wildfire prediction application.

- Flammability matrix: *nxm* matrix. FM algorithm requires a value ranging between 0 (not flammable) and 1 (extremely flammable) for each point of the map.

Any altitude and flammability maps can be used as long as they share the same dimensions. For a first test of the application, real maps from the LandFire website were used. Said website contains altitude and flammability maps of sites all along the USA territory. This maps, in .tiff format, are converted to Matlab matrices, resized and their values properly mapped before they can be used as inputs for the application.

2.2.2 Vectorial inputs: wind and terrain slope

Among the vectorial variables that might affect fire spread, two significant ones are taken into consideration in this application:

- Wind: Given that the maps considered for simulation represent a relatively small terrain, and for modeling simplicity, wind effect is considered constant in every point of the map. Additionally, also for simplicity reasons, only a bidimensional wind, parallel to the ground, is considered. The user can easily choose a wind input with any module and direction by adjusting the sliders for the N/S and W/E wind in the application. This is graphically represented in Figure 6.
- Terrain slope: Fire travels more easily in an upwards direction. Therefore, the slope or gradient of the terrain will have a positive vectorial effect on fire spread, similar to that of the wind. With the altitude matrix as an input it is easy to compute a 2D matrix with information about its gradient. This gradient matrix is used as a vectorial input to the FM algorithm, just as the wind was. This is graphically represented in Figure 7.

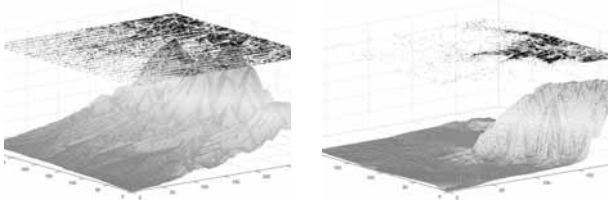

Figure 7: Gradients for two different altitude maps.

2.2.3 Graphical representation of fire spread

Once the FM algorithm is given all the inputs and executed, the next objective is to clearly represent the propagation of fire (D matrix) along the considered terrain. This representation must be consistent with the instant of the fire spread that the user wishes to see. Therefore, there are two main design aspects related to the representation of the fire spread that need to be understood:

- Contour matrix: In order to represent the matrix D as a propagating wave, it is transformed into contour levels with assistance of Matlab?s contour function. Every aspect regarding the graphical representation of the fire spread is related to a matrix known as the contour matrix. This matrix contains information regarding the number of contour levels (enough to make the propagation appear to be continuous), number of points in every level and 3D coordinates of such points. Figure 8 represents an example of a contour matrix of 3 levels for a better understanding.

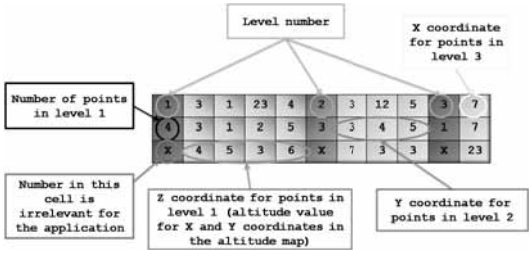

Figure 8: Example of a simple contour matrix.

- Time estimation: The simulator allows the user to see the fire spread at different snapshots of time. In order to offer this feature, an estimation of the total time taken by the wildfire to reach a certain final point is needed. This estimation is performed by computing a ratio between a rough estimation of the distance traveled by the wildfire and the average fire spread velocity.

The fire spread distance is calculated as the Euclidean distance between the initial and final points (in green in Figure 9). The velocity is estimated by performing the average in an estimated area of fire propagation (dark purple in Figure 9). The values of such area correspond to mapped values of the flammability matrix, where a 0.1 in the flammability matrix corresponds to a 1km/h fire spread velocity and a 0.9 in the flammability matrix corresponds to a 9km/h fire spread velocity. The mapping of the values is done accordingly with usual fire spread velocities as a function of terrain flammability. Additionally, the effect of the wind in fire spread velocity is taken into consideration, estimating an effect on velocity fire spread equal to wind velocity.

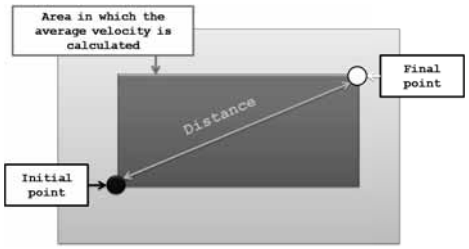

Figure 9: Distance and spread velocity representation.

2.2.4 GUI interface and its functionality

Even though the application is a viability trial for FM as a fire prediction algorithm, user-friendliness is strongly considered.

The simplicity of Matlab's GUI has helped the development of the main functionalities of a wildfire simulation application:

- Map selection: A pushbutton from the GUI ('SELECT MAPS') enables the user to upload the flammability and altitude matrices.
- Map display without propagation: A pushbutton from the GUI ('SEE MAP WITHOUT FIRE SPREAD') enables the user to visualize the 3D map for the region selected without the fire spread. The purpose of this is for the user to become familiar with the map, so the subsequent selection of the application parameters is easier.
- Starting and finishing points: The user can specify the coordinates of the fire ignition point and a finishing point (which will stop the simulation, once reached) in editable text boxes. The starting point is shown on the map in black and the finishing point in white.
- Time slider: The application estimates time it takes for the fire to reach the finishing point . For a better understanding of the fire spread, the user can view the propagation at any instant by using the 'Time' slider. The effect of the time slider is shown in Figure 10.

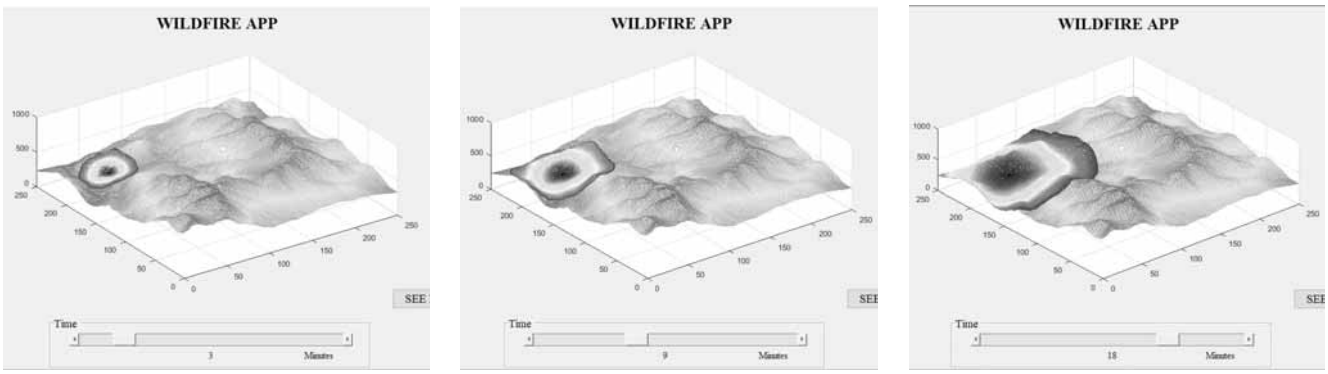

Figure 10: Simulation at different snapshots of time, in minutes.

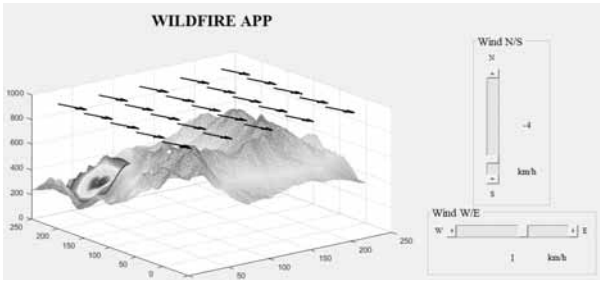

Figure 11: Display of the vectorial input related to the wind.

- Wind sliders: By selecting values in both of them, the user can choose how intense the wind is in each direction (North, South, East or West) and to provide an easier use, the direction of the wind is shown in the propagation map using black arrows. For a deeper understanding see Figure 11 .

- Flammability map visualization: The user might need a glimpse of the flammability map that has been used, so as to understand the propagation of fire. The push button ('SEE COMBUSTION MAP') pops up a window in which the flammability map is shown.

- Toolbar: The application includes a toolbar that enables the user to manipulate the maps (rotate, zoom in and out) for an optimal visualization.

- Run pushbutton: Starts the simulation. It must be pushed every time any changes in the inputs are made in order to see their effect.

3 Results

The results of different wildfire spread simulations are shown. The effect of the different variables that affect the fire spread are analyzed independently plus the results of the simulator in terms of computational efficiency are explained.

3.1 Effect of the flammability map

The flammability map determines fire spread, as it is an input for the FM algorithm. On the other hand, the altitude map is unrelated (except for the altitude gradient) to the algorithm, and it is only used to provide the user with a realistic view of the fire spread along the terrain. Therefore any combination of flammability and altitude maps can be used for the simulator. Figure 3.1 represents a commonly used altitude map, the Washington matrix, with a fictitious flammability map which is very flammable in every point except for a rectangular region.

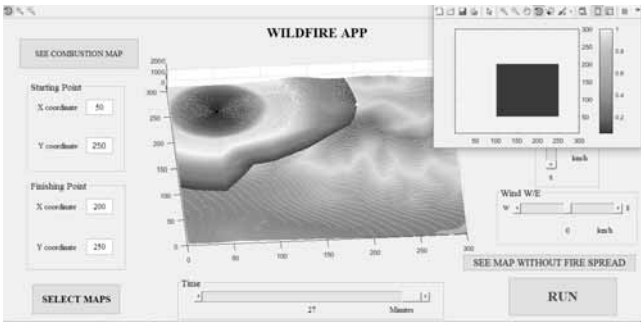

Figure 12: Washington matrix.

It can be easily observed that the fire spread avoids the region that is less flammable, creating an alternative path to that of the same altitude map and same inputs, but using a continuous flammability map.

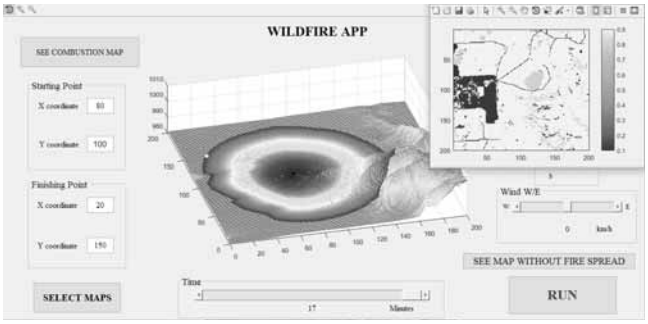

Figure 13: Real flammability and altitude maps.

Figure 13 represents the simulation results for a couple of real altitude and flammability maps.

3.2 Effect of the wind

The effect of the wind in the simulation is presented in Figure 14. For the same initial and final points in a given real life map, 3 different wind settings are configured, so as to appreciate the effect of the wind when every other variable is constant. It can also be noted from Figure 14 that some wind configurations speed the process of the wildfire spread reaching the final point and others slow it down. This affects the total time of fire spread in the time slider.

3.3 Computational efficiency of the simulator

In order to obtain results regarding the computational efficiency of the simulator the time required to run the main function of the application was computed. Said function includes both the FM algorithm and the representation of results, therefore, it is the core of the simulator. It runs every time the 'RUN' button is pressed in the GUI application and it requires the great majority of computational resources in the simulator. A brief study of the time needed to run the core function was performed for different maps (200x200 to 250x250) and different start and end points and wind settings, concluding that for no combination of inputs the function takes more than 10 seconds to run.

4 Discussion

The present section compares the state of the art wildfire simulators our wildfire app. The final goal is to prove that, although a basic, the wildfire app presents strong advantages compared to other simulators. This will prove the viability of FM as a wildfire prediction algorithm, and set a starting point for future work.

Our main purpose is to implement Fast Marching as a viable fire prediction algorithm in a user friendly wildfire simulator. As a prototype, there are a series of disadvantages to the use of the app with respect to the simulators presented in section :

- Very rough estimation of time, velocity and distance dimension correspondence. As introduced in section 2.2.3 Fast Marching is a mathematical algorithm, and so, correlations between wind velocity, time and fire spread velocity dimensions need to be thought outside from the algorithm itself. The estimations for this prototype are far less precise than those of simulators in section , but there is still room for improvement. It will probably be impossible to reach the precision of a physical model, such as the one used in FireStar, but with proper research work, levels of simulators such as Prometheus or Farsite could be reached.
- Fast Marching does not consider non positive velocity fields. If wind is not considered this is not a problem, but there could be a case in which a strong wind against the fire front direction could reverse the trajectory of the fire. If that were to happen the algorithm would collapse and so will the application, inducing a Matlab error that forces the application to be restarted. This is the greatest inconvenience when using FM algorithm for wildfire simulation. In order for the simulator to be functional for every case, the FM algorithm would need to be either modified for the specific case or the simulator would need to use an alternative algorithm or model for those very specific situations. Even if a less efficient model were used for those cases, as they are a small part compared to the total cases, the efficiency of the simulator would not decrease significantly.

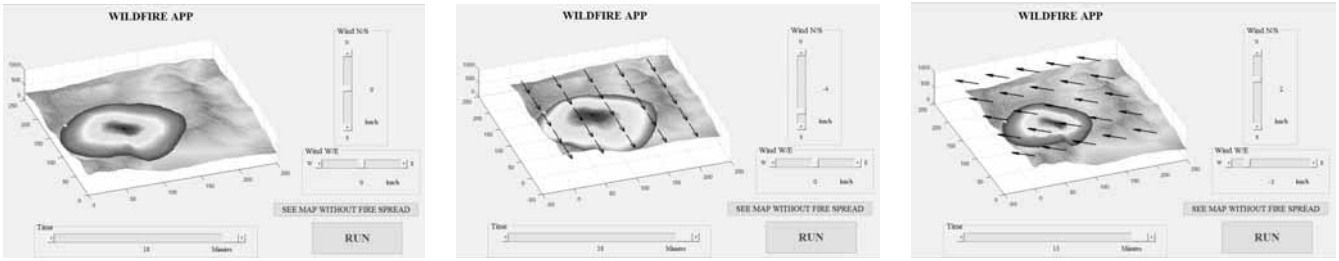

Figure 14: Wind effect on fire spread.

- The implementation of the wind as a vectorial input to the algorithm still needs to be perfected to represent the real effect of 3D real life wind. In addition, other meteorological inputs that might affect the fire spread such as air humidity should be included in further versions of the app in order to be more competitive with current simulators.

Nevertheless, this simple prototype does have a wide set of advantages over the commercial and currently used simulators:

- Higher efficiency than other simulators. Models using the Huygens' principle are far slower and less efficient than Fast Marching. It is easy to understand that the need to predict the trajectories of several points in the front and then calculating the envelope of those trajectories requires a significant amount of computational power. Needless to say that physical models, based on partial differential equation solving are also remarkably slower than Fast Marching.
- Its development is far more economical than the rest of simulators. As a visual comparison, the 2 million euro budget needed for the FireRS initiative can be contrasted with the wildfire app budget of 0 euros (provided a Matlab license is already owned). The wildfire app prototype has been developed essentially by one person, and subsequent improvements to the app can be probably conducted by small research team. This results in a big difference regarding simulators such as Prometheus or Farsite, that constitute big development projects, with their associated resources and personnel costs.
- User-friendly simulator, due to Matlab GUI interface. The user of this application does not need to have specific programming skills or specific wildfire propagation knowledge. This makes the simulator very accessible and attractive for use, since the organizations interested in using it would not need to invest in personnel training. The steps for the application prototype use can be easily explained in a one-page manual.

  Its structure of use is simple, as well user friendly. The only inputs that need to be imported are the combustion and elevation maps. Every other input (time, wind, starting points, etc.) can be selected in the application itself. No different formats, programming or simulating platforms need to be used. This is very different from the complex series of steps needed for a Prometheus or Farsite simulators (see Figure 3)

- The graphical representation of the fire spread is one of the strongest advantages of the wildfire app. The fire spread is presented in in a set of colours that makes it clearly distinguishable from the terrain map, and it also enables the user to see direction of front propagation (red most recent, blue least recent). This makes the wildfire app front representation superior to that of Farsite, as its fire front is presented with thin white lines, that cannot be traced clearly by the user (see Figure 4). The current real time propagation is represented, as opposed to the probability of the terrain being burned, which constitutes the output of the Prometheus simulator.

  Starting and finishing points are clearly traceable, enabling the user to easily familiarize with the coordinates of the map.

  The wildfire app has a properly working 3D representation format. The change from one map to another is done almost instantly. This 3D representation for mat is not supported by some of the current working simulators.

5 Conclusions

The objective of the research was to prove the viability of the Fast Marching algorithm to build a wildfire simulator. It can be concluded that such objective has been reached. The result is a wildfire app developed in the Matlab GUI?s environment. Said application shows the shape of the fire front at a certain moment in time in a 3D map of the terrain affected by the fire. Any real life maps can be loaded to the application for wildfire prediction. The user can choose to vary parameters such as ignition and ending points, wind direction and speed or propagation time and see its effect on fire propagation. Response to each change in the input is very fast, therefore proving the efficiency of the algorithm.

Regardless of the wildfire app being a basic prototype, it is superior to some state of the art simulators regarding certain important features.

It can be concluded that Fast Marching is indeed a valid core algorithm for a fire simulator. Moreover, the prototype of the wildfire app opens a line of research in perfecting this prototype and becoming a truly competitive tool against currently used wildfire simulators.

References

[1] Aguilera M. La cruz de los veranos: cada hectárea quemada cuesta 3.000 euros. El Economista. URL http://ecodiario.eleconomista.es/espana/noticias/53524/08/06/La-cruz-de-los-veranos-cada-hectarea-quemada-cuesta-3000-euros.html. 2006

[2] Osher S, Sethian JA. Fronts propagating with curvature- dependent speed: Algorithms based on hamilton-jacobi formula- tions. *Journal of Computational Physics*.1988; Vol. 79.

[3] Morvan D, Dupuy J, Rigolot E, Valette J. Firestar: A physically based model to study wildfire behaviour. Forest Ecology and Management. 2006.

[4] FireRS team, FireRS webpage.URL http://www.fire-rs.com 2017

[5] Tymstra C, Bryce R, Wotton B, Taylor S, Armitage O. Development and structure of prometheus: the canadian wildland fire growth simulation model. Forest Service. 2010.

[6] Parisien MA, Kafka VG, Hirsch KG, Todd JB, Lavoie SG, Maczek PD. Mapping wildfire susceptibility with the BURN-P3 simulation model. Nat. Resour. Can., Can. For. Serv., North. For. Cent., Edmonton, Alberta. Inf. Rep. NOR-X-405. 36 p. [URL http://cfs.nrcan.gc.ca/publications?id=25627]

[7] Finney MA. FARSITE: Fire Area Simulator-model development and evaluation . Res. Pap. RMRS-RP-4, Revised 2004, Ogden, UT: U.S. Department of Agriculture, Forest Service, Rocky Mountain Research Station. 47 p.

[8] Gómez JV. Fast marching methods in path and motion planning: Improvements and high-level applications. Ph.D. thesis, University Carlos III Madrid. 2015.

[9] Garrido S, Moreno L, Martín F, Álvarez D. Fast marching subjected to a vector field path planning method for mars rovers. *Expert Systems With Applications.* 2017

Towards Clothes Hanging via Cloth Simulation and Deep Convolutional Networks

David Estevez*, Juan G. Victores, Raul Fernandez-Fernandez, Carlos Balaguer

RoboticsLab, University Carlos III of Madrid, Calle Butarque 15, 28911 Madrid, Spain
*david.estevez@alumnos.uc3m.es

SNE 31(3), 2021, 169-176, DOI: 10.11128/sne.31.tn.10578
Received: March 10, 2021 (Selected EUROSIM 2019 Postconf. Publ.), Revised: Sept. 1, 2021; Accepted: September 3, 2021
SNE - Simulation Notes Europe, ARGESIM Publisher Vienna, ISSN Print 2305-9974, Online 2306-0271, www.sne-journal.org

Abstract. People spend several hours a week doing laundry, with hanging clothes being one of the laundry tasks to be performed. Nevertheless, deformable object manipulation still proves to be a challenge for most robotic systems, due to the extremely large number of internal degrees of freedom of a piece of clothing and its chaotic nature. This work presents a step towards automated robot clothes hanging by modeling the dynamics of the hanging task via deep convolutional models. Two models are developed to address two different problems: determining if the garment will hang or not (classification), and estimating the future garment location in space (regression). Both models have been trained with a synthetic dataset formed by 15k examples generated though a dynamic simulation of a deformable object. Experiments show that the deep convolutional models presented perform better than a human expert, and that future predictions are largely influenced by time, with uncertainty influencing directly the accuracy of the predictions.

Introduction

Domestic tasks are very time-consuming. In general, every single human would benefit from a complete automation of domestic tasks, as they are not only a nuisance, but they can be considered a form of unpaid labor. In addition, certain collectives, such as the elder and disabled people, could specially take advantage of domestic task automation, due to their lack of mobility. For these collectives, domestic tasks can become a daily struggle that may even require assistance from other people. To automate some of these tasks, such as washing or cooking, specific appliances have been developed that help us save time and effort. However, due to the large number of disparate tasks to be automated, it becomes impossible to own a specific machine for each task, as this would be both expensive and demand an unfeasible amount of space for installation. For these reasons, robots are key in automating domestic tasks in a viable and maintainable way.

Laundry tasks constitute one of the most prominent subsets of domestic tasks and, at the same time, one of the hardest to automate, as they involve working with textiles. Textile articles, such as garments, are intrinsically hard to perceive and manipulate due to, amongst other facts, their almost infinite number of internal degrees of freedom and possible configurations, as well as their deformable and chaotic nature, which is extremely difficult to predict. While there is extensive existing literature on the typical laundry pipeline, defined as unfolding, ironing and folding, few works exist that focus on other garment-related tasks such as bed making, dressing assistance or hanging garments.

Hanging garments is a task performed after garments are washed, and before the garments are unfolded and ironed, to have a perfectly dry clothing article. As with all garment-related tasks, automation of garment hanging is difficult because of several reasons:

- Garment manipulation requires a robotic system with proficient manipulation skills and enough dexterity to deal with thin textile materials.
- It requires a deep understanding of deformable objects intrinsic properties and the physics that govern their movements, which make their movements chaotic and difficult to predict.
- The high number of internal degrees of freedom, possible poses, and occlusions present on a garment in a real world scenario makes perceiving and modelling garments a challenging problem.

In this paper, we aim to make a contribution towards the goal of an automated robotic system able to do the laundry, specifically the hanging garments task. For that purpose, we present two different deep convolutional models that are able to predict the behavior of the garment about to be hanged, addressing two different problems: determining if a garment dropped onto a hanger will hang or not from a depth image of the garment just before it is released, and estimating the future location in space of a dropped garment onto a hanger. To train these models, a synthetic dataset has been created, including examples of both dropped garments that hanged and garments that fell to the floor.

1 State of the Art

The typical laundry pipeline, as defined in the literature, is composed of three different tasks: unfolding, ironing and folding. For unfolding, existing approaches use depth images of the garment to determine the most suitable grasp sequence for unfolding, using active random forests [3], upper layer detection via Canny Edge detector [18] or a garment-agnostic model-less approach [5]. Once the garment is unfolded, it has to be ironed before it can be folded and stored, so that no wrinkles are present in the garment when the owner is about to wear it. If the wrinkles are large and soft, pulling the edges of the garment is enough to remove them [17]. If the wrinkles are small and marked, the robot has to iron them. While some approaches target individual wrinkles in very controlled illumination conditions [9], other use a human-inspired ironing method based on force control and a garment surface analysis [6]. When all the wrinkles have been removed, the only remaining step is to fold the garment. For folding, some approaches rely on manipulation sequences that take the garment from a random initial state to the desired folded state using Hidden Markov Models (HMMs) [2] while others follow a perception-based approach use polygonal models to estimate the garment shape and folding sequence [16].

For every garment-related task, prediction of garment movement and state estimation are key abilities, specially when involving garment manipulation. Miller et al. [13] used parametrized shape models that are able to fit 2D views of already flattened garments to find the grasp points required to apply a given folding sequence. Cusumano-Towner et al. [2] applied an approach heavily based on manipulation. Their approach used a series of manipulation operations to estimate the state a garment with a Hidden Markov Model. The initial state might be unknown, but a known state is reached through manipulation. Bersch et al. [1] used fiducial markers stamped on a t-shirt to obtain a 3D reconstruction of the garment. Since the markers were unique for each point, the state of the garment can easily be estimated from them, allowing them to compute suitable grasp poses on the cloth, for later manipulation with a PR2 robot. Kita el al. [7] introduced a method to estimate the state of a garment through a 3D reconstruction of the garment from different viewpoints. A cylindrical Z buffering algorithm is then applied to the reconstructed point cloud and expanded to obtain a flattened representation of the garment. Though matching with a database of garments grasped from different garment points, the actual state of the garment can be estimated.

Willimon et al. [19] used energy minimization and graph cuts to estimate the configuration of cloth surfaces from 2D color images, with an automatic mesh generation algorithm that provides a triangular mesh encapsulating the cloth surface without predefined values. Li et al. [10] proposed a real-time state estimation algorithm based on a cylindrical descriptor used to match a given real-world observation with a garment pose database generated through physical simulation. This descriptor obtains a binary string representation by fitting the garment 3D point cloud in a cylinder divided into different sections, that are then used as an occupancy grid and unrolled into a 1D binary string. Mariolis et al. [11] use two stacked deep convolutional neural networks to estimate the state of a garment from a depth image of the garment being hanged by one point. The first convolutional network determines the garment category, which is used to select which of the convolutional networks that have been trained on that particular category has to be used to compute the current pose.

Although the literature has traditionally focused on the tasks in the laundry pipeline, recent works exist that discuss other tasks, such as clothing assistance [8], and bed making [15].

2 Dataset Generation

A Deep Convolutional Network is used to model the behavior of a free falling garment and to predict its final location. Deep neural networks employ a large amount of parameters that need to be trained, and therefore they require a very large amount of data for training and val-

idation. Ideally, the network has to be trained with data from the same domain as the application. That is, if the model is to be applied in a real world scenario, it should be trained with real world data. However, training data generation in the real world is very time demanding, as for each trial the robot has to be reset to its initial position, a garment has to be placed on its end-effector, and then the robot has to drop it so that the trajectory of the free falling garment can be recorded. Finally, the garment has to be picked up again from its final location to be set for the next trial. In addition, tracking the exact 3D position of the garment while falling is not trivial.

An alternative to using real world data is to train the model instead with simulated data. Since the characteristics of the simulated domain are very different from the real world domain (no noise, no lens distortion, different illumination conditions, uniform colors...), some modifications or special techniques are required to apply a model trained in the simulated domain to the real world. One of such techniques is domain randomization, that generates training data from a simulation using random colors, textures and illumination, so that the model is able to generalize and perform correctly independently of the domain.

In this work, simulation was used as the source of training examples to obtain a large training dataset. A piece of cloth is simulated in a virtual environment representing a simplified setup similar to the one in our lab, including a 1 m x 1 m hanger and the floor. (Figure 1). To simulate the garment dynamics and interaction with the lab environment, we use a spring-based model applied to the 3D mesh, as included in the Blender software package[`https://www.blender.org/`, last accessed: 08-06-2019].

For each of the trials, one vertex of the mesh is selected as hanging point, and then placed at a random initial location. The initial location is sampled from a normal distribution (with mean μ_{init} and standard deviation σ_{init}). To increase the chances of a garment being randomly hanged, the source distribution is centered around the hanger, and close to it. The simulation of the garment dynamics is then started so that the garment moves from its initial flat pose to the in-air hanging pose. The garment is left hanged a sufficient amount of time to reach a static state, as it will swing due to the inertia of this initial movement. Once the garment is static, a depth image showing the initial pose and location is stored. Using depth images instead of color images enables us to translate well between domains

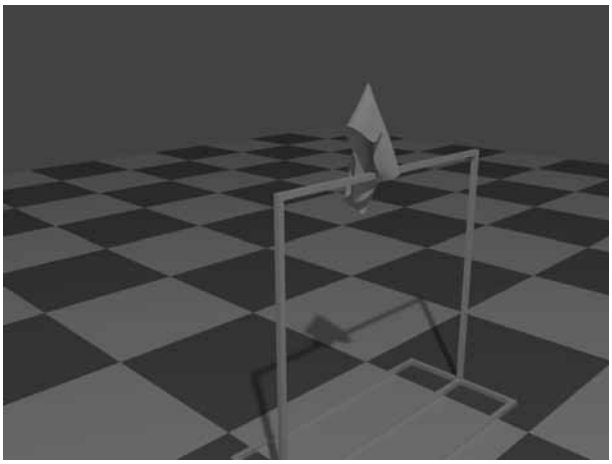

Figure 1: Simulated lab setup with hanging garment and hanger.

without the need for domain randomization, as depth images from the real sensor and virtual depth images are monochromatic and of very similar characteristics. Finally, the garment is dropped and the position of the center of mass of the falling garment is tracked for later analysis and to derive a ground truth binary label for classification.

As garments are dynamic systems displaying a chaotic behavior, the result of each trial is not deterministic and depends heavily on small changes of the initial conditions (location and pose) of the piece of cloth. For that reason, the resulting dataset is unbalanced, including a larger amount of samples in which the cloth did not hang.

3 Hanging Prediction

Once enough training data has been generated, it is used to train a model to predict the behavior of the free falling garment. Two different models have been trained and evaluated. The first one tries to estimate the location of the garment at a given simulation time step, usually the last one in the trajectory (i.e. the final location of the garment, either hanged or in the floor). The other one classifies the final outcome into two different categories: hanged or floor, depending on the expected outcome of dropping the garment. This section will describe each of them.

3.1 Regression

The objective of the regression model is to predict the exact location of a garment at a given simulation time step from a depth image showing the initial location and pose of the garment. In most of the cases, the most interesting time step from the perspective of hanging clothes is the last one, as it will determine whether the garment will hang or not when dropped from a given initial location. Due to the chaotic nature of the cloth dynamics, as time steps advance the uncertainty of the garment location increases, with the initial location being the easiest to predict, and the final location the most difficult.

For the model, a Deep Convolutional Network is used. Figure 2 shows the architecture of the network. The network is composed of 4 sets of convolutional layers, and 2 fully connected layers to compute the output. Sets 1 and 3 are built from 2 convolutional layers with 16 filters of size (3x3) and an Exponential Linear Unit (ELU) as the activation function, followed by a max-pooling layer of size (2x2) and stride 2. Sets 2 and 4 are composed of a single convolutional layer with 32 filters of size (3x3) and ELU as the activation function, followed by a max-pooling layer of size (2x2) and stride 2. The fully connected layers have 300 and 3 neurons, respectively. For the regression problem, we use ELU as activation function for the last layer, representing the predicted 3D coordinates (X, Y and Z) of the garment at a given time step. The total number of learnable parameters of this model is 2 100 707.

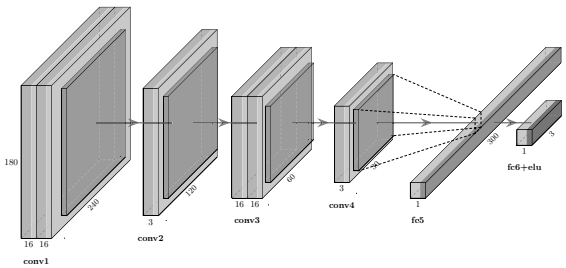

Figure 2: HANGnet architecture diagram.

The parameters were trained by optimizing a custom loss using an Adam stochastic optimizer. As the aim of the prediction is to hang garments, the most interesting information obtained from the prediction is the value of the Z coordinate. To emphasize in the importance of the Z coordinate, a custom loss function was developed:

$$Loss = \omega_x * (X - \hat{X})^2 + \omega_y * (Y - \hat{Y})^2 + \omega_z * (Z - \hat{Z})^2 \quad (1)$$

Where $\vec{X} = (X, Y, Z)$ are the actual coordinates of the point in the training example, $\vec{\hat{X}} = (\hat{X}, \hat{Y}, \hat{Z})$ are the predicted coordinates, and ω_x, ω_y and ω_z are hyperparameters expressing the relative importance of each of the coordinate components.

The performance of the network is reported in the Results section.

3.2 Classification

The classification problem is defined as predicting, from a depth image of its initial location and pose, whether a garment will hang or fall to the floor when dropped near a hanger.

The architecture of the Deep Convolutional Network used as model for the classification problem is very similar to the one used for the regression problem. Figure 3 depicts the architecture of the network. A total of 4 sets of convolutional layers, and 2 fully connected layers to compute the output are used. Sets 1 and 3 include 2 convolutional layers with 16 filters of size (3x3) and ELU as the activation function, followed by a max-pooling layer of size (2x2) and stride 2. Sets 2 and 4 are composed of a single convolutional layer with 32 filters of size (3x3) and ELU as the activation function, followed by a max-pooling layer of size (2x2) and stride 2. The fully connected layers have 300 and 1 neuron, respectively. As only one class is to be predicted, instead of a Softmax function, a Sigmoid activation function is applied to the output neuron to obtain the probability of the garment falling to the floor given a certain input depth image. When the output is above 0.5, the prediction is that the garment will fall, otherwise the prediction is that it will hang. The total number of learnable parameters of this model is 2 099 705.

The binary labels for each training sample can be obtained from the trajectory recorded at each simulated trial, by observing the Z coordinate of the last point of the trajectory (Z_{end}). Based on the final location of the center of mass, and considering a threshold T_{floor} one can compute the binary label $floor$ as:

$$floor = \begin{cases} 1, & \text{if } Z_{end} < T_{floor} \\ 0, & \text{otherwise} \end{cases} \quad (2)$$

The resulting labels are used as ground truth to train

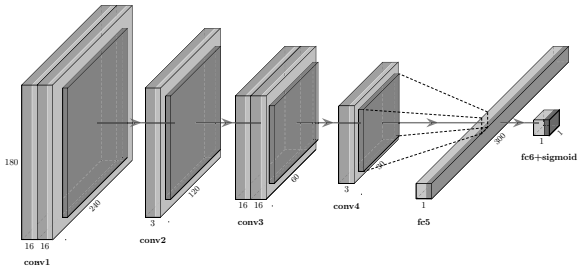

Figure 3: HANGnet_classify architecture diagram.

the classification network. For training, a Binary Cross Entropy loss is optimized by an Adam stochastic optimizer. This loss is weighted to account for the imbalance of the hanged/floor classes in the synthetic dataset.

4 Results

In this section we will discuss the training process of both models (regression and classification) as well as the results obtained with each of the models.

4.1 Regression

4.1.1 Setup

Following the simulation procedure described in section 2, a total of 15000 training examples were obtained. Each of these training examples is composed by a depth image of the virtual setup at the initial time step (after the garment has reach a stable pose) and the trajectory of the center of mass of the garment once it has been dropped. The initial position of the garment is sampled from a normal distribution with $\mu_{init} = (0, 0, 1.5)$ m and $\sigma_{init} = (0.01, 0.4, 0.2)$ m. A duration of 51 simulation time steps has been selected as a good compromise between computational cost and reaching a stable hanged/floor state in simulation. Before they are fed to the network for training, the depth images are cropped at 2 m to remove the empty background and then normalized in the 0 m to 2 m range.

As the samples were obtained randomly, not every single sample results in the garment being hanged. In fact, the ratio of garments hanged/not hanged is near 1:3, making the dataset imbalanced. In order to deal with the imbalance in the dataset, stratification was used to make the training/validation/test splits, so that each of the three sets has the same proportion of examples of each of the two classes. The stratified split was the following: 20% of the samples (3000) were used for testing and, from the 80% remaining, 20% (2400) were used for validation and 80% (9600) for training.

For training the regression model, an Adam stochastic optimizer was used, with a learning rate of 0.0001. The custom loss introduced in section 3.1 (Eq. 1) was used, with weights $\omega_x = 0.033$, $\omega_y = 0.033$ and $\omega_z = 0.33$. The model was trained for 10 epochs, with a batch size of 32.

4.1.2 Results

To study the effect of the time on the uncertainty of the prediction and, therefore, on the accuracy of the model, the network was trained to predict the location at different time steps. Figure 4 shows the increase of the Mean Squared Error (MSE) as time advances.

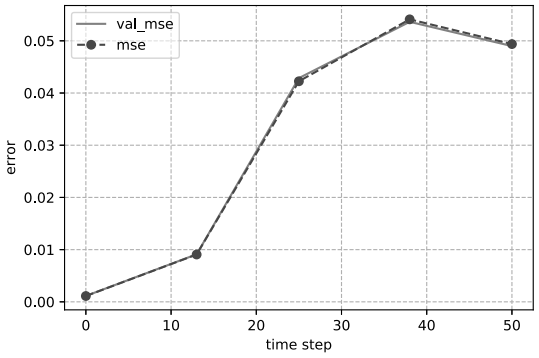

Figure 4: Mean Squared Error (MSE) and Validation MSE with respect to the time step.

In terms of coordinates, MSE was computed for each of the 3D components of the prediction (X, Y and Z). Figure 5 shows the MSE of each of the component, as well as the variation in error for each of them. It can be observed that the error increases from a few millimeters to several centimeters, and it is more dramatic in the case of the Z coordinate, which was an expected result, as the fact that the garment can remain randomly hanged or not hanged affects to the expected location in the Z axis.

4.2 Classification

4.2.1 Setup

For the classification model, the same dataset as the one described in section 4.1.1 was used, and the same

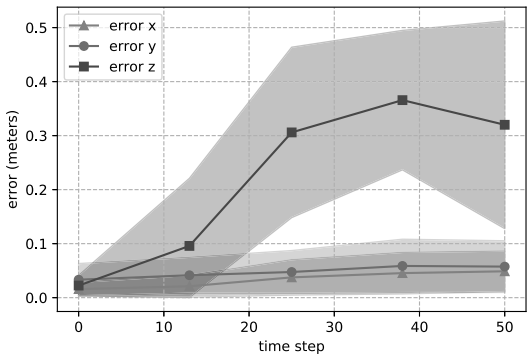

Figure 5: Mean Squared Error (MSE) of each of the 3 coordinates (X, Y, Z) with respect to the time step.

stratification techniques were use to deal with the imbalance of the dataset when performing the training/validation/test splits. As the output of the classification model is a single binary value representing the prediction of the network (0 if the garment with hang, or 0 if the garment will fall), the trajectory previously recorded in the dataset needs to be processed to obtain a binary label. For that purpose, eq. 2 was used, with a threshold value $T_{floor} = 0.81\,\text{m}$.

For training the classification model, an Adam stochastic optimizer was used, with a learning rate of 0.0001. In addition, L2 regularization was added to the model, with a regularization strength of 0.01 to improve the generalization capabilities of the network.

4.2.2 Human baseline

To evaluate the relevance of the results achieved, a human baseline was obtained by labelling a subset of 200 elements from the training set by hand, based only on the input data. In other words, a depth image was presented to a human expert for him to predict whether it will hang or fall. To improve the human perception of depth in the input depth image, the 8-bit greyscale image was transformed using a GIST stern[`https://www.ncl.ucar.edu/Document/Graphics/ColorTables/MPL_gist_stern.shtml`, last accessed: 08-06-2019] colormap for display.

4.2.3 Results

After training, several metrics were computed based on the 3000 element test set, as reported in table 1. A subset of 200 elements were randomly selected and used to compute a human baseline and compare it with the performance of the classification model. Table 2 shows the results of this analysis. Although the model has a lower recall for the hanged class than the human expert, it improves the performance of the human in all remaining metrics considered.

Table 1: Classification model, 3000 items.

Class	Precision	Recall	F1-score	# items
Hanged	0.51	0.32	0.39	819
Floor	0.78	0.88	0.83	2181

Table 2: Classification model vs Human baseline, 200 items.

Class	Precision	Recall	F1-score	# items
Hanged	0.60	0.39	0.47	54
Floor	0.80	0.90	0.85	146
Hanged	0.38	0.56	0.45	54
Floor	0.80	0.66	0.72	146

In addition, confusion matrices were computed to compare the performance of the model and the human expert in terms of false positives / false negatives. As shown in Figure 6, the classification model outperforms the human expert when predicting garments that fell to the floor, while having a similar performance when predicting garments that remained hanged.

5 Conclusions

In this work we propose two different deep convolutional models to predict the behavior of a piece of clothing when dropped onto a hanger. One of models is able to predict whether the garment will hang or fall, and the other estimates the future location of the garment after it is dropped. A synthetic dataset composed of 15 000 examples obtained via deformable object simulation is used to train both models. Experiments performed with the regression model demonstrate an influence of time in the accuracy of the predictions, as uncertainty in the position estimation increases with time. The classification model performance was compared to the baseline performance of a human expert, obtaining a slightly better performance.

Our future work will focus on the integration of both models (regression and classification) to increase the individual accuracy of each of them, as well as in the implementation of these models on one or several robotic

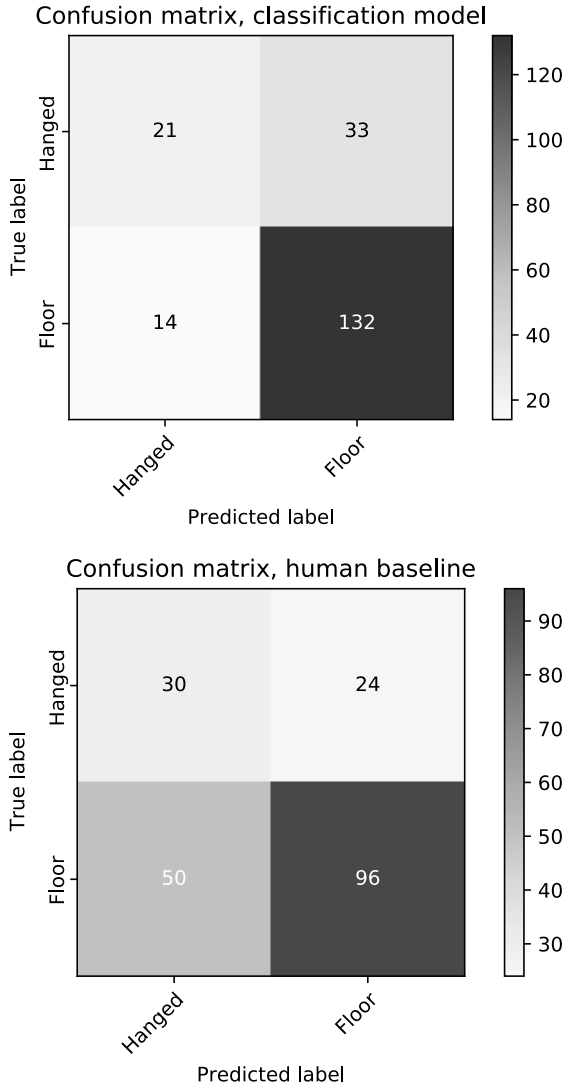

Figure 6: Confusion matrices for the classification model and human baseline.

platforms to obtain real world data and action, and further validate the idea behind this work.

Acknowledgement

This work was supported by RoboCity2030-III-CM project (S2013/MIT-2748), funded by Programas de Actividades I+D in Comunidad de Madrid and EU and by a FPU grant funded by Ministerio de Educación, Cultura y Deporte. We gratefully acknowledge the support of NVIDIA Corporation with the donation of the NVIDIA Titan X GPU used for this research.

References

[1] Bersch C, Pitzer B, Kammel S. Bimanual robotic cloth manipulation for laundry folding. In: IEEE International Conference on Intelligent Robots and Systems. pp. 1413–1419 (2011).

[2] Cusumano-Towner M, Singh A, Miller S, O'Brien JF, Abbeel P. Bringing clothing into desired configurations with limited perception. In: IEEE International Conference on Robotics and Automation (ICRA). pp. 3893–3900. IEEE (2011).

[3] Doumanoglou A, Kim Tk, Zhao X, Malassiotis S. Active Random Forests: An Application to Autonomous Unfolding of Clothes. In: European Conference on Computer Vision (ECCV). pp. 644–658. Springer International Publishing (2014).

[4] Elbrechter C, Haschke R, Ritter H. Folding Paper with Anthropomorphic Robot Hands using Real-Time Physics-Based Modeling. 2012 12th IEEE-RAS International Conference on Humanoid Robots (Humanoids 2012) pp. 210–215 (2012).

[5] Estevez D, Fernandez-Fernandez R, Victores JG, Balaguer C. Improving and Evaluating Robotic Garment Unfolding: A Garment-Agnostic Approach. In: IEEE International Conference on Autonomous Robot Systems and Competitions (ICARSC) (2017).

[6] Estevez D, Victores JG, Fernandez-Fernandez R, Balaguer C. Robotic Ironing with 3D Perception and Force/Torque Feedback in Household Environments. In: IEEE/RSJ International Conference on Intelligent Robots and Systems (IROS) (2017).

[7] Kita Y, Ueshiba T, Kanehiro F, Kita N. Recognizing clothing states using 3D data observed from multiple directions. In: International Conference on Humanoid Robots (Humanoids). pp. 227–233 (2013).

[8] Koganti N, Ngeo JG, Tomoya T, Ikeda K, Shibata T. Cloth dynamics modeling in latent spaces and its application to robotic clothing assistance. IEEE International Conference on Intelligent Robots and Systems **2015-Decem**, 3464–3469 (2015).

[9] Li Y, Hu X, Xu D, Yue Y, Grinspun E, Allen P. Multi-Sensor Surface Analysis for Robotic Ironing. In: IEEE International Conference on Robotics and Automation (ICRA). Stockholm (2016).

[10] Li Y, Wang Y, Case M, Chang Sf, Allen PK. Real-time Pose Estimation of Deformable Objects Using a Volumetric Approach. In: International Conference on Intelligent Robots and Systems (IROS). pp. 1046–1052. IEEE (2014).

[11] Mariolis I, Peleka G, Kargakos A, Malassiotis S. Pose and category recognition of highly deformable objects using deep learning. Proceedings of the 17th International Conference on Advanced Robotics, ICAR 2015 pp. 655–662 (2015).

[12] Matas J, James S, Davison AJ. Sim-to-Real Reinforcement Learning for Deformable Object Manipulation (CoRL) (2018).

[13] Miller S, Fritz M, Darrell T, Abbeel P. Parametrized shape models for clothing. In: International Conference on Robotics and Automation (ICRA). pp. 4861–4868 (2011).

[14] Schulman J, Lee A, Ho J, Abbeel P. Tracking deformable objects with point clouds. In: Proceedings - IEEE International Conference on Robotics and Automation. pp. 1130–1137. No. i, IEEE (2013).

[15] Seita D, Jamali N, Laskey M, Berenstein R, Tanwani AK, Baskaran P, Iba S, Canny J, Goldberg K. Robot Bed-Making: Deep Transfer Learning Using Depth Sensing of Deformable Fabric (2018).

[16] Stria J, Pruša D, Hlaváč V. Polygonal Models for Clothing. In: Advances in Autonomous Robotics Systems. vol. 8717, pp. 173–184 (2014).

[17] Sun L, Aragon-Camarasa G, Rogers S, Siebert JP. Accurate garment surface analysis using an active stereo robot head with application to dual-arm flattening. In: IEEE International Conference on Robotics and Automation (ICRA). vol. 2015-June, pp. 185–192. IEEE (2015).

[18] Triantafyllou D, Aspragathos NA. Upper layer extraction of a folded garment towards unfolding by a robot. In: Mechanisms and Machine Science, vol. 67, pp. 597–604 (2019).

[19] Willimon B, Walker I, Birchfield S. 3D Non-Rigid Deformable Surface Estimation Without Feature Correspondence. 2013 IEEE International Conference on Robotics and Automation pp. 646–651 (2013).

SNE Simulation News

EUROSIM Data and Quick Info


VESS – Virtual EUROSIM Seminar
Virtual Simulation Presentations, since June 2020 www.eurosim2023.eu



MATHMOD Vienna 2022
Feb. 16-18, 2022, Vienna, Austria www.mathmod.at
ASIM 2022 - 26.Symposium Simulation Technique
Feb. 14-16, 2022, Vienna, Austria www.asim-gi.org/asim2022


EUROSIM CONGRESS 2023
Spring/Autumn 2023, Amsterdam, The Netherlands www.eurosim2023.eu

Contents

Simulation Notes Europe SNE is the official membership journal of **EUROSIM** and distributed / available to members of the **EUROSIM Societies** as part of the membership benefits.

If you have any information, announcement, etc. you want to see published, please contact a member of the editorial board in your country or the editorial office. For scientific publications, please contact the EiC.

This *EUROSIM Data & Quick Info* compiles data from **EUROSIM** societies and groups: addresses, weblinks, and officers of societies with function and email, to be published regularly in **SNE** issues. This information is also published at **EUROSIM**'s website *www.eurosim.info*.

SNE Editorial Office /ARGESIM

→ *www.sne-journal.org, www.eurosim.info*
office@sne-journal.org, *eic@sne-journal.org*
✉ SNE Editorial Office
Johannes Tanzler (Layout, Organisation)
Irmgard Husinsky (Web, Electronic Publishing)
Felix Breitenecker EiC (Organisation, Authors)
ARGESIM/Math. Modelling & Simulation Group,
Inst. of Analysis and Scientific Computing, TU Wien
Wiedner Hauptstrasse 8-10, 1040 Vienna, Austria

EUROSIM Federation of European Simulation Societies

General Information. **EUROSIM**, the Federation of European Simulation Societies, was set up in 1989. The purpose of **EUROSIM** is to provide a European forum for simulation societies and groups to promote modelling and simulation in industry, research, and development – by publication and conferences. → *www.eurosim.info*

Member Societies. **EUROSIM** members may be national simulation societies and regional or international societies and groups dealing with modelling and simulation. At present **EUROSIM** has *Full Members* and *Observer Members* (*), and *Member Candidates* (**).

ASIM	Arbeitsgemeinschaft Simulation *Austria, Germany, Switzerland*
CEA-SMSG	Spanish Modelling and Simulation Group; *Spain*
CSSS	Czech and Slovak Simulation Society *Czech Republic, Slovak Republic*
DBSS	Dutch Benelux Simulation Society *Belgium, Netherlands*
KA-SIM	Kosovo Simulation Society, *Kosovo*
LIOPHANT	LIOPHANT Simulation Club; *Italy & International*
LSS	Latvian Simulation Society; *Latvia*
PSCS	Polish Society for Computer Simulation; *Poland*
NSSM	Russian National Simulation Society *Russian Federation*
SIMS	Simulation Society of Scandinavia *Denmark, Finland, Norway, Sweden*
SLOSIM	Slovenian Simulation Society; *Slovenia*
UKSIM	United Kingdom Simulation Society *UK, Ireland*
ALBSIM	Albanian Simulation Society*; *Albania*
ROMSIM	Romanian Society for Modelling and Simulation*; *Romania*
Societies in Re-Organisation:	
CROSSIM	*Croatian Society f. Simulation Modeling;* Croatia
FRANCOSIM	*Société Francophone de Simulation* *Belgium, France*
HSS	*Hungarian Simulation Society;* Hungary
ISCS	*Italian Society for Computer Simulation, Italy*

EUROSIM Board / Officers. **EUROSIM** is governed by a board consisting of one representative of each member society, and president, past president, and **SNE** representative. The President is nominated by the society organising the next **EUROSIM** Congress. Secretary, and Treasurer are elected out of members of the board.

President	M. Mujica Mota (DBSS), *m.mujica.mota@hva.nl*
Past President	Emilio Jiménez (CAE-SMSG), *emilio.jimenez@unirioja.es*
Secretary	Niki Popper, *niki.popper@dwh.at*
Treasurer	Felix Breitenecker (ASIM) *felix.breitenecker@tuwien.ac.at*
Webmaster	Irmgard Husinsky, *irmgard.husinsky@tuwien.ac.at*
SNE Editor	F. Breitenecker, *eic@sne-journal.org*

SNE – Simulation Notes Europe. **SNE** is **EUROSIM**'s scientific journal with peer reviewed contributions as well as a membership journal for **EUROSIM** with information from the societies. **EUROSIM** societies distribute **SNE** (electronic or printed) to their members as official membership journal. **SNE** Publishers are **EUROSIM**, **ARGESIM** and **ASIM**.

SNE Editor-in-Chief	Felix Breitenecker *eic@sne-journal.org*

→ *www.sne-journal.org,* *office@sne-journal.org*

EUROSIM Congress and Conferences.

Each year a major **EUROSIM** event takes place, the **EUROSIM CONGRESS** organised by a member society, **SIMS EUROSIM Conference**, and **MATHMOD Vienna Conference (ASIM)**.

EUROSIM Congress 2019, the *10th EUROSIM Congress*, was organised by **CEA-SMSG**, the Spanish Simulation Society, in La Rioja, Logroño, Spain, July 1-5, 2019;

Due to Covid-19 virus in 2020 no **EUROSIM** events take place. To bridge this gap, **EUROSIM** is organising the series **VESS - Virtual EUROSIM Simulation Seminar** – seminars by simulation professionalists (2 hours via web), in preparation for upcoming **EUROSIM** events. → ***www.eurosim2023.eu***

Next main event is **MATHMOD Vienna**. This triennial **EUROSIM Conference** is mainly organized by **ASIM**, the German simulation society, and **ARGESIM,** with main co-sponsor **IFAC**.

MATHMOD 2022, the *10th MATHMOD Vienna Conference on Mathematical Modelling* will take place in Vienna, Februray 16-18, 2022. → ***www.mathmod.at***

EUROSIM Congress 2023, the *11th EUROSIM Congress*, will be organised by **DBSS**, the Dutch Benelux simulation society, in Amsterdam, Spring/Autumn 2023.
→ ***www.eurosim2023.eu***

Furthermore, **EUROSIM Societies** organize also local conferences, and **EUROSIM** co-operates with the organizers of the **I3M Conference Series.**
→ ***www.liophant.org/conferences/***

EUROSIM Member Societies

ASIM
German Simulation Society
Arbeitsgemeinschaft Simulation

ASIM (Arbeitsgemeinschaft Simulation) is the association for simulation in the German speaking area, servicing mainly Germany, Switzerland and Austria. **ASIM** was founded in 1981 and has now about 400 individual members (including associated), and 90 institutional or industrial members.

→ *www.asim-gi.org* with members' area

info@asim-gi.org, admin@asim-gi.org

✉ ASIM – Inst. of Analysis and Scientific Computing
Vienna University of Technology (TU Wien)
Wiedner Hauptstraße 8-10, 1040 Vienna, Austria

ASIM Officers	
President	Felix Breitenecker *felix.breitenecker@tuwien.ac.at*
Vice presidents	Sigrid Wenzel, *s.wenzel@uni-kassel.de*
	T. Pawletta, *thorsten.pawletta@hs-wismar.de*
	A. Körner, *andreas.koerner@tuwien.ac.at*
Secretary	Ch. Deatcu, *christina.deatcu@hs-wismar.de*
	I. Husinsky, *Irmgard.husinsky@tuwien.ac.at*
Membership Affairs	S. Wenzel, *s.wenzel@uni-kassel.de*
	Ch. Deatcu, *christina.deatcu@hs-wismar.de*
	F. Breitenecker, *felix.breitenecker@tuwien.ac.at*
Repr. EUROSIM	F. Breitenecker, *felix.breitenecker@tuwien.ac.at*
	A. Körner, *andreas.koerner@tuwien.ac.at*
Internat. Affairs – GI Contact	O. Rose, *Oliver.Rose@tu-dresden.de*
	N. Popper, *niki.popper@dwh.at*
Editorial Board SNE	T. Pawletta, *thorsten.pawletta@hs-wismar.de*
	Ch. Deatcu, *christina.deatcu@hs-wismar.de*
Web EUROSIM	I. Husinsky, *Irmgard.husinsky@tuwien.ac.at*

Last data update *April 2020*

ASIM is organising / co-organising the following international conferences:

- **ASIM** Int. Conference 'Simulation in Production and Logistics' – biannual
- **ASIM** 'Symposium Simulation Technique' – biannual
- **MATHMOD** Int. Vienna Conference on Mathmatical Modelling – triennial

Furthermore, **ASIM** is co-sponsor of *WSC* - Winter Simulation Conference, of SCS conferences *SpringSim* and *SummerSim*, and of *I3M* and *Simutech* conference series.

ASIM Working Committees	
GMMS	Methods in Modelling and Simulation Th. Pawletta, *thorsten.pawletta@hs-wismar.de*
SUG	Simulation in Environmental Systems Jochen Wittmann, *wittmann@informatik.uni-hamburg.de*
STS	Simulation of Technical Systems Walter Commerell, *commerell@hs-ulm.de*
SPL	Simulation in Production and Logistics Sigrid Wenzel, *s.wenzel@uni-kassel.de*
EDU	Simulation in Education/Education in Simulation A. Körner, *andreas.koerner@tuwien.ac.at*
BIG DATA	Working Group Data-driven Simulation in Life Sciences; *niki.popper@dwh.at*
WORKING GROUPS	Simulation in Business Administration, in Traffic Systems, for Standardisation, etc.

CEA-SMSG – Spanish Modelling and Simulation Group

CEA is the Spanish Society on Automation and Control and it is the national member of IFAC (International Federation of Automatic Control) in Spain. Since 1968 **CEA-IFAC** looks after the development of the Automation in Spain, in its different issues: automatic control, robotics, *SIMULATION*, etc. The association is divided into national thematic groups, one of which is centered on Modeling, Simulation and Optimization, constituting the **CEA** Spanish Modeling and Simulation Group (**CEA-SMSG**). It looks after the development of the Modelling and Simulation (M&S) in Spain, working basically on all the issues concerning the use of M&S techniques as essential engineering tools for decision-making and optimization.

→ *http://www.ceautomatica.es/grupos/*

→ *emilio.jimenez@unirioja.es*
simulacion@cea-ifac.es

✉ CEA-SMSG / Emilio Jiménez, Department of Electrical Engineering, University of La Rioja, San José de Calasanz 31, 26004 Logroño (La Rioja), SPAIN

CEA - SMSG Officers	
President	Emilio Jiménez, *emilio.jimenez@unirioja.es*
Vice president	Juan Ignacio Latorre, *juanignacio.latorre@unavarra.es*
Repr. EUROSIM	Emilio Jiménez, *emilio.jimenez@unirioja.es*
Edit. Board SNE	Juan Ignacio Latorre, *juanignacio.latorre@unavarra.es*
Web EUROSIM	Mercedes Perez *mercedes.perez@unirioja.es*

Last data update February 2018

CSSS – Czech and Slovak Simulation Society

CSSS -The *Czech and Slovak Simulation Society* has about 150 members working in Czech and Slovak national scientific and technical societies (*Czech Society for Applied Cybernetics and Informatics*, *Slovak Society for Applied Cybernetics and Informatics*). **CSSS** main objectives are: development of education and training in the field of modelling and simulation, organising professional workshops and conferences, disseminating information about modelling and simulation activities in Europe. Since 1992, **CSSS** is full member of **EUROSIM**.

→ *www.fit.vutbr.cz/CSSS*

snorek@fel.cvut.cz

✉ CSSS / Miroslav Šnorek, CTU Prague
FEE, Dept. Computer Science and Engineering,
Karlovo nam. 13, 121 35 Praha 2, Czech Republic

CSSS Officers	
President	Miroslav Šnorek, *snorek@fel.cvut.cz*
Vice president	Mikuláš Alexík, *alexik@frtk.fri.utc.sk*
Scientific Secr.	A. Kavička, *Antonin.Kavicka@upce.cz*
Repr. EUROSIM	Miroslav Šnorek, *snorek@fel.cvut.cz*
Edit. Board SNE	Mikuláš Alexík, *alexik@frtk.fri.utc.sk*
Web EUROSIM	Petr Peringer, peringer@fit.vutbr.cz

Last data update December 2012

DBSS – Dutch Benelux Simulation Society

The *Dutch Benelux Simulation Society* (**DBSS**) was founded in July 1986 in order to create an organisation of simulation professionals within the Dutch language area. **DBSS** has actively promoted creation of similar organisations in other language areas. **DBSS** is a member of **EUROSIM** and works in close cooperation with its members and with affiliated societies.

→ *www.DutchBSS.org*

a.w.heemink@its.tudelft.nl

✉ DBSS / A. W. Heemink
Delft University of Technology, ITS - twi,
Mekelweg 4, 2628 CD Delft, The Netherlands

DBSS Officers	
President	M. Mujica Mota, *m.mujica.mota@hva.nl*
Vice president	A. Heemink, *a.w.heemink@its.tudelft.nl*
Treasurer	A. Heemink, *a.w.heemink@its.tudelft.nl*
Secretary	P. M. Scala, p.m.scala@hva.nl
Repr. EUROSIM	M. Mujica Mota, *m.mujica.mota@hva.nl*
Edit. SNE/Web	M. Mujica Mota, *m.mujica.mota@hva.nl*

Last data update June 2016

LIOPHANT Simulation

Liophant Simulation is a non-profit association born in order to be a trait-d'union among simulation developers and users; Liophant is devoted to promote and diffuse the simulation techniques and methodologies; the Association promotes exchange of students, sabbatical years, organization of International Conferences, courses and internships focused on M&S applications.

→ *www.liophant.org*

info@liophant.org

✉ LIOPHANT Simulation, c/o Agostino G. Bruzzone,
DIME, University of Genoa, Savona Campus
via Molinero 1, 17100 Savona (SV), Italy

LIOPHANT Officers	
President	A.G. Bruzzone, *agostino@itim.unige.it*
Director	E. Bocca, *enrico.bocca@liophant.org*
Secretary	A. Devoti, *devoti.a@iveco.com*
Treasurer	Marina Massei, *massei@itim.unige.it*
Repr. EUROSIM	A.G. Bruzzone, *agostino@itim.unige.it*
Deputy	F. Longo, *f.longo@unical.it*
Edit. Board SNE	F. Longo, *f.longo@unical.it*
Web EUROSIM	F. Longo, *f.longo@unical.it*

Last data update June 2016

LSS – Latvian Simulation Society

The Latvian Simulation Society (LSS) has been founded in 1990 as the first professional simulation organisation in the field of Modelling and simulation in the post-Soviet area. Its members represent the main simulation centres in Latvia, including both academic and industrial sectors.

→ *www.itl.rtu.lv/imb/*

Egils.Ginters@rtu.lv

✉ Prof. Egils Ginters, Kirshu Str.13A, Cesis LV-4101,
Latvia

LSS Officers	
President	Yuri Merkuryev, *merkur@itl.rtu.lv*
Vice President	Egils Ginters, *egils.ginters@rtu.lv*
Secretary	Artis Teilans, *artis.teilans@rta.lv*
Repr. EUROSIM	Egils Ginters, egils.ginters@rtu.lv
Deputy	Artis Teilans, *artis.teilans@rta.lv*
Edit. Board SNE	Juri Tolujew, *Juri.Tolujew@iff.fraunhofer.de*
Web EUROSIM	Vitaly Bolshakov, *vitalijs.bolsakovs@rtu.lv*

Last data update November 2020

KA-SIM Kosovo Simulation Society

Kosova Association for Modeling and Simulation (KA-SIM, founded in 2009), is part of Kosova Association of Control, Automation and Systems Engineering (KA-CASE). KA-CASE was registered in 2006 as non Profit Organization and since 2009 is National Member of IFAC – International Federation of Automatic Control. KA-SIM joined EUROSIM as Observer Member in 2011. In 2016, KA-SIM became full member.

KA-SIM has about 50 members, and is organizing the international conference series International Conference in Business, Technology and Innovation, in November, in Durrhes, Albania, and IFAC Simulation Workshops in Pristina.

→ *www.ubt-uni.net/ka-case*

ehajrizi@ubt-uni.net

✉ MOD&SIM KA-CASE; Att. Dr. Edmond Hajrizi
Univ. for Business and Technology (UBT)
Lagjja Kalabria p.n., 10000 Prishtina, Kosovo

KA-SIM Officers	
President	Edmond Hajrizi, *ehajrizi@ubt-uni.net*
Vice president	Muzafer Shala, *info@ka-sim.com*
Secretary	Lulzim Beqiri, *info@ka-sim.com*
Treasurer	Selman Berisha, *info@ka-sim.com*
Repr. EuroSim	Edmond Hajrizi, *ehajrizi@ubt-uni.net*
Deputy	Muzafer Shala, *info@ka-sim.com*
Edit. Board SNE	Edmond Hajrizi, *ehajrizi@ubt-uni.net*
Web EuroSim	Betim Gashi, *info@ka-sim.com*

Last data update December 2016

NSSM – National Society for Simulation Modelling (Russia)

NSSM - The Russian National Simulation Society (Национальное Общество Имитационного Моделирования – НОИМ) was officially registered in Russian Federation on February 11, 2011. In February 2012 NSS has been accepted as an observer member of **EUROSIM**, and in 2015 NSSM has become full member.

→ *www.simulation.su*

yusupov@iias.spb.su

✉ NSSM / R. M. Yusupov,
St. Petersburg Institute of Informatics and Automation RAS, 199178, St. Petersburg, 14th lin. V.O, 39

NSSM Officers	
President	R. M. Yusupov, *yusupov@iias.spb.su*
Chair Man. Board	A. Plotnikov, *plotnikov@sstc.spb.ru*
Secretary	M. Dolmatov, *dolmatov@simulation.su*
Repr. EuroSim	R.M. Yusupov, *yusupov@iias.spb.su* Y. Senichenkov, *senyb@dcn.icc.spbstu.ru*
Deputy	B. Sokolov, *sokol@iias.spb.su*
Edit. Board SNE	Y. Senichenkov, *senyb@mail.ru, senyb@dcn.icc.spbstu.ru*,

Last data update February 2018

PSCS – Polish Society for Computer Simulation

PSCS was founded in 1993 in Warsaw. PSCS is a scientific, non-profit association of members from universities, research institutes and industry in Poland with common interests in variety of methods of computer simulations and its applications. At present PSCS counts 257 members.

→ *www.eurosim.info*, www.ptsk.pl/

leon@ibib.waw.pl

✉ PSCS / Leon Bobrowski, c/o IBIB PAN,
ul. Trojdena 4 (p.416), 02-109 Warszawa, Poland

PSCS Officers	
President	Leon Bobrowski, *leon@ibib.waw.pl*
Vice president	Tadeusz Nowicki, *Tadeusz.Nowicki@wat.edu.pl*
Treasurer	Z. Sosnowski, *zenon@ii.pb.bialystok.pl*
Secretary	Zdzislaw Galkowski, *Zdzislaw.Galkowski@simr.pw.edu.pl*
Repr. EuroSim	Leon Bobrowski, *leon@ibib.waw.pl*
Deputy	Tadeusz Nowicki, *tadeusz.nowicki@wat.edu.pl*
Edit. Board SNE	Zenon Sosnowski, z.sosnowski@pb.ed.pl
Web EuroSim	Magdalena Topczewska *m.topczewska@pb.edu.pl*

Last data update December2013

SIMS – Scandinavian Simulation Society

SIMS is the *Scandinavian Simulation Society* with members from the five Nordic countries Denmark, Finland, Iceland, Norway and Sweden. The SIMS history goes back to 1959. SIMS practical matters are taken care of by the SIMS board consisting of two representatives from each Nordic country (Iceland one board member).

SIMS Structure. SIMS is organised as federation of regional societies. There are **FinSim** (Finnish Simulation Forum), **MoSis** (Society for Modelling and Simulation in Sweden), **DKSIM** (Dansk Simuleringsforening) and **NFA** (Norsk Forening for Automatisering).

→ *www.scansims.org*

bernt.lie@usn.no

✉ SIMS / Bernt Lie, Faculty of Technology, Univ.College of Southeast Norway, Department of Technology, Kjølnes ring 56, 3914 Porsgrunn, Norway

SIMS Officers	
President	Bernt Lie, *Bernt.Lie@usn.no*
Vice president	Erik Dahlquist, *erik.dahlquist@mdh.se*
Treasurer	Vadim Engelson, *vadime@mathcore.com*
Repr. EUROSIM	Esko Juuso, *esko.juuso@oulu.fi*
Edit. Board SNE	Esko Juuso, *esko.juuso@oulu.fi*
Web EUROSIM	Vadim Engelson, *vadime@mathcore.com*

Last data update February 2020

SLOSIM – Slovenian Society for Simulation and Modelling

SLOSIM - Slovenian Society for Simulation and Modelling was established in 1994 and became the full member of **EUROSIM** in 1996. Currently it has 90 members from both Slovenian universities, institutes, and industry. It promotes modelling and simulation approaches to problem solving in industrial as well as in academic environments by establishing communication and cooperation among corresponding teams.

→ www.slosim.si

slosim@fe.uni-lj.si

✉ SLOSIM / Vito Logar, Faculty of Electrical Engineering, University of Ljubljana, Tržaška 25, 1000 Ljubljana, Slovenia

SLOSIM Officers	
President	Vito Logar, *vito.logar@fe.uni-lj.si*
Vice president	Božidar Šarler, *bozidar.sarler@ung.si*
Secretary	Simon Tomažič, *simon.tomazic@fe.uni-lj.si*
Treasurer	Milan Simčič, *milan.simcic@fe.uni-lj.si*
Repr. EUROSIM	B. Zupančič, *borut.zupancic@fe.uni-lj.si*
Deputy	Vito Logar, *vito.logar@fe.uni-lj.si*
Edit. Board SNE	R. Karba, *rihard.karba@fe.uni-lj.si*
Web EUROSIM	Vito Logar, *vito.logar@fe.uni-lj.si*

Last data update December 2018

UKSIM - United Kingdom Simulation Society

The UK Simulation Society is very active in organizing conferences, meetings and workshops. UKSim holds its annual conference in the March-April period. In recent years the conference has always been held at Emmanuel College, Cambridge. The Asia Modelling and Simulation Section (AMSS) of UKSim holds 4-5 conferences per year including the EMS (European Modelling Symposium), an event mainly aimed at young researchers, organized each year by UKSim in different European cities. Membership of the UK Simulation Society is free to participants of any of our conferences and their co-authors.

→*uksim.info*

david.al-dabass@ntu.ac.uk

✉ **UKSIM / Prof. David Al-Dabass**
Computing & Informatics,
Nottingham Trent University
Clifton lane, Nottingham, NG11 8NS, United KingdomUKSIM Officers

President	David Al-Dabass, *david.al-dabass@ntu.ac.uk*
Secretary	T. Bashford, *tim.bashford@uwtsd.ac.uk*
Treasurer	D. Al-Dabass, *david.al-dabass@ntu.ac.uk*
Membership chair	G. Jenkins, *glenn.l.jenkins@smu.ac.uk*
Local/Venue chair	Richard Cant, *richard.cant@ntu.ac.uk*
Repr. EUROSIM	Dr Taha Osman, taha.osman@ntu.ac.uk
Deputy	T. Bashford, *tim.bashford@uwtsd.ac.uk*
Edit. Board SNE	D. Al-Dabass, *david.al-dabass@ntu.ac.uk*

Last data update March 2020

EUROSIM Observer Members

ROMSIM – Romanian Modelling and Simulation Society

ROMSIM has been founded in 1990 as a non-profit society, devoted to theoretical and applied aspects of modelling and simulation of systems. ROMSIM currently has about 100 members from Romania and Moldavia.

→ *www.eurosim.info/societies/romsim/*

florin_h2004@yahoo.com

✉ ROMSIM / Florin Hartescu,
National Institute for Research in Informatics, Averescu Av. 8 – 10, 011455 Bucharest, Romania

ROMSIM Officers	
President	N. N.
Vice president	Florin Hartescu, *florin_h2004@yahoo.com* Marius Radulescu, *mradulescu.csmro@yahoo.com*
Repr. EUROSIM	Marius Radulescu, *mradulescu.csmro@yahoo.com*
Deputy	Florin Hartescu, *florin_h2004@yahoo.com*
Edit. Board SNE	Constanta Zoe Radulescu, *zoe@ici.ro*
Web EUROSIM	Florin Hartescu, *florin_h2004@yahoo.com*

Last data update June 2019

ALBSIM – Albanian Simulation Society

The Albanian Simulation Society has been initiated at the Department of Statistics and Applied Informatics, Faculty of Economy at the University of Tirana, by Prof. Dr. Kozeta Sevrani.

The society is involved in different international and local simulation projects, and is engaged in the organisation of the conference series ISTI - Information Systems and Technology. In July 2019 the society was accepted as EUROSIM Observer Member.

→ *www.eurosim.info/societies/albsim/*

kozeta.sevrani@unitir.edu.al

✉ Albanian Simulation Goup, attn. Kozeta Sevrani
University of Tirana, Faculty of Economy
rr. Elbasanit, Tirana 355 Albania

Albanian Simulation Society- Officers	
Chairt	Kozeta Sevrani, *kozeta.sevrani@unitir.edu.al*
Repr. EUROSIM	Kozeta Sevrani, *kozeta.sevrani@unitir.edu.al*
Edit. Board SNE	Albana Gorishti, *albana.gorishti@unitir.edu.al* Majlinda Godolja, *majlinda.godolja@feut.edu.al*

Last data update July 2019

Societies in Re-Organisation / Former Societies

The following societies are at present inactive or under re-organisation:

- CROSSIM – *Croatian Society for Simulation Modelling*
  Contact: Tarzan Legović, *Tarzan.Legovic@irb.hr*
- FRANCOSIM – Société Francophone de Simulation
- HSS – Hungarian Simulation Society
- ISCS – Italian Society for Computer Simulation

The following societies have been formally terminated:

- MIMOS –Italian Modeling & Simulation Association; terminated end of 2020.

Association Simulation News

ARGESIM is a non-profit association generally aiming for dissemination of information on system simulation – from research via development to applications of system simulation. **ARGESIM** is closely co-operating with **EUROSIM**, the Federation of European Simulation Societies, and with **ASIM**, the German Simulation Society. **ARGESIM** is an 'outsourced' activity from the *Mathematical Modelling and Simulation Group* of TU Wien, there is also close co-operation with TU Wien (organisationally and personally).

→ *www.argesim.org*

→ *office@argesim.org*

→ ARGESIM/Math. Modelling & Simulation Group,
Inst. of Analysis and Scientific Computing, TU Wien
Wiedner Hauptstrasse 8-10, 1040 Vienna, Austria
Attn. Prof. Dr. Felix Breitenecker

ARGESIM is following its aims and scope by the following activities and projects:

- Publication of the scientific journal **SNE** – *Simulation Notes Europe* (membership journal of **EUROSIM**, the *Federation of European Simulation Societies*) – *www.sne-journal.org*
- Organisation and Publication of the **ARGESIM Benchmarks** for *Modelling Approaches and Simulation Implementations*
- Publication of the series **ARGESIM Reports** for monographs in system simulation, and proceedings of simulation conferences and workshops
- Publication of the special series **FBS Simulation** – Advances in Simulation / Fortschrittsberichte Simulation - monographs in co-operation with ASIM, the German Simulation Society
- Support of the Conference Series **MATHMOD Vienna** (triennial, in co-operation with **EUROSIM**, **ASIM**, and **TU Wien**) – www.mathmod.at
- Administration of **ASIM** (German Simulation Society) and administrative support for **EUROSIM** *www.eurosim.info*
- Simulation activities for TU Wien

ARGESIM is a registered non-profit association and a registered publisher: **ARGESIM Publisher Vienna**, root ISBN 978-3-901608-xx-y, root DOI 10.11128/z…zz.zz. Publication is open for **ASIM** and for **EUROSIM Member Societies**.

SNE – Simulation Notes Europe

The scientific journal **SNE** – *Simulation Notes Europe* provides an international, high-quality forum for presentation of new ideas and approaches in simulation – from modelling to experiment analysis, from implementation to verification, from validation to identification, from numerics to visualisation – in context of the simulation process. **SNE** puts special emphasis on the overall view in simulation, and on comparative investigations.
Furthermore, **SNE** welcomes contributions on education in/for/with simulation.

SNE is also the forum for the **ARGESIM Benchmarks** on *Modelling Approaches and Simulation Implemen-tations* publishing benchmarks definitions, solutions, reports and studies – including model sources via web.

→ *www.sne-journal.org,*

→ *office@sne-journal.org*, *eic@sne-journal.org*

→ SNE Editorial Office
ARGESIM/Math. Modelling & Simulation Group,
Inst. of Analysis and Scientific Computing, TU Wien
Wiedner Hauptstrasse 8-10, 1040 Vienna, Austria
EiC Prof. Dr. Felix Breitenecker

SNE, primarily an electronic journal, follows an open access strategy, with free download in basic layout. **SNE** is the official membership journal of **EUROSIM**, the *Federation of European Simulation Societies*. Members of **EUROSIM Societies** are entitled to download **SNE** in high-quality, and to access additional sources of benchmark publications, model sources, etc. On the other hand, **SNE** offers **EUROSIM Societies** a publication forum for post-conference publication of the society's international conferences, and the possibility to compile thematic or event-based **SNE Special Issues**.

Simulationists are invited to submit contributions of any type – *Technical Note*, *Short Note*, *Project Note*, *Educational Note*, *Benchmark Note*, etc. via **SNE**'s website:

MATHMOD 2022 Vienna

10th Vienna International Conference on Mathematical Modelling
February 16-18, 2022

The scope of *MATHMOD 2022* covers theoretic and applied aspects of various types of mathematical modelling (e.g., equations of various types, automata, Petri nets, bond graphs, qualitative and fuzzy models, machine learning) for systems of dynamic nature (deterministic, stochastic, continuous, discrete or hybrid with respect to time).

The *topics* to be discussed include e.g.

- modelling theory; first-principles, identification, optimization, order reduction and validation
- automation of modelling and software tools
- computer based modelling, modelling for/by simulation, co-simulation, modelling standards
- qualitative, modular, interdisciplinary modelling
- comparison of methods for modelling, alternative modelling methods (CAS, fuzzy, NN, QSS, etc.)
- machine learning and artificial intelligence for modelling
- model analysis and calibration, effects of modelling errors on overall performance of an engineering system
- applications in the field of engineering systems and in natural sciences
- applications in environmental systems, biotechnology, etc.
- applications in operation research, logistics and planning
- applications in medicine, physiology, health care and health systems
- education in/for/with modelling
- modelling aspects in scientific computing
- modelling for control and real-time applications
- machine learning, data analytics, big data

TYPES OF CONTRIBUTIONS

MATHMOD 2022 invites to submit contributions of following types:

- *MATHMOD Full Contribution*
  6 pages, full paper peer review;
  publication in *MATHMOD 2022 Full Contribution Proceedings* at IFAC-PapersOnLine
  (MATHMOD Volume ISBN and individual paper DOI);
  oral presentation in thematic sessions or minisymposia
- *MATHMOD Discussion Contribution*
  2 pages extended abstract, abstract review;
  publication in *MATHMOD 2022 Discussion Contribution Proceedings* in ARGESIM Report
  (electronic; MATHMOD Volume ISBN and individual paper DOI)
  short oral presentation with poster display or oral presentation in minisymposium

MATHMOD MINISYMPOSIA

Established scientists and engineers in mathematical modelling are encouraged to organise MATHMOD Minisymposia by inviting contributions to a special topic of interest (Full Contributions or Discussion Contributions). Details for organisation of minisymposia can be found at the MATHMOD website **www.mathmod.at**.

CONFERENCE PUBLICATIONS

The MATHMOD Conference Proceedings (Full Contributions) are published in the IFAC-PapersOnLine series hosted at the ScienceDirect web service. A MATHMOD Abstract Preprint Volume with abstracts of all contribution types will be available electronically at the conference. Furthermore, following the IFAC copyright regulations, suitably adapted versions of MATHMOD Contributions which contain sufficiently new material may be submitted to the Journal of Mathematical and Computer Modelling of Dynamical Systems (MCMDS), published by Taylor and Francis.

MATHMOD 2022 Office
Gußhausstraße 27-29
TU Wien / Inst. 376
1040 Vienna, Austria
Email: mathmod@acin.tuwien.ac.at
Phone: +43 1 58801-376239
www.mathmod.at

Schedule for EUROSIM Conferences and Congress

EUROSIM societies organise virtual conferences 2020 – 2021, and from 2022, the simulation community hopes to meet again at conferences as they used to be: Face-to-Face conferences.

The **EUROSIM Board** and **DBSS** started in June 2020 **VESS** – the **Virtual EUROSIM Seminar**, a series of online presentations discussing trends in modelling and simulation. These international online simulation seminars – monthly or bi-monthly – are open to everybody, via Zoom, lasting 60 minutes (45 minutes presentations, 15 minutes Q & A).
Information and informal registration via website **www.eurosim2023.eu**

The First **SIMS EUROSIM Conference** on Modelling and Simulation, **SIMS EUROSIM 2021** takes place in Oulu, Finland, September 21-23, 2021. The 62nd International Conference of Scandinavian Simulation Society, SIMS 2021, is embedded with **SIMS EUROSIM 2021**. The **SIMS EUROSIM** conference will be organized every third year by **SIMS** and **EUROSIM**. The background of this conference series is in the 60-years history of Scandinavian Simulation Society, **SIMS**.
SIMS EUROSIM 2021 will be organised as virtual conference – info **www.scansims.org**

MATHMOD organizers continue the conference series one year later, with **10th MATHMOD 2022**, February 16-18, 2022, as *F2F* event. **MATHMOD 2022**, one of **EUROSIM**'s main events, provides a forum for professionals, researchers, and experts in the field of theoretic and applied aspects of mathematical modelling for systems of dynamic nature.
The scope of the **MATHMOD 2022** conference covers theoretic and applied aspects of various types of mathematical modelling (equations of various types, automata, Petri nets, bond graphs, qualitative and fuzzy models) for systems of dynamic nature (deterministic, stochastic, continuous, discrete or hybrid) – info and details **www.mathmod.at**

ASIM - the German / Austrian / Swiss simulation society – is organising the **26th Symposium Simulation Technique** – **ASIM 2022** at TU Vienna, February 14-16, just before **MATHMOD 2022**. ASIM hopes for a German/English-based event as it used to be before – with personal contacts, and in synergy with **MATHMOD 2022**. – info **www.asim-gi.org/asim2022**

EUROSIM 2023, the **11th EUROSIM Congress**, will take place in Amsterdam, The Netherlands, Spring/Autumn 2023. It will be organized by the Dutch Benelux Simulation Society (www.dutchbss.org) supported mainly by their corporate members like TU Delft, Amsterdam University of Applied Sciences, EUROCONTROL and IGAMT (www.igamt.eu).
Due to the growth of Simulation and its relationship with other analytical techniques like Big Data, AI, Machine Learning, Large Scale Simulation and others, the event will be structured, for the first time, in dedicated tracks focused on different areas and applications of Simulation ranging from aviation to health care and humanitarian activities.
Please follow the news and activities towards the **EUROSIM 2023** at **www.eurosim2023.eu**

www.tuverlag.at
ISBN 978-3-903311-17-6